Phenyl dialkynylcarbinols, a Bioinspired Series of Synthetic Antitumor Acetylenic Lipids

Margaux Bossuat, Pauline Rullière, Nadège Preuilh, Antonio Peixoto, Etienne Joly, Jean-Guillaume Gomez, Maroua Bourkhis, Frédéric Rodriguez, Fernanda Gonçalves, Isabelle Fabing, et al.

Phenyl diAlkynylCarbinols (PACs), a bioinspired series of synthetic antitumor acetylenic lipids

Margaux Bossuat,[§,#,¶] Pauline Rullière,[§,†] Nadège Preuilh,[¶] Antonio Peixoto,[¶] Etienne Joly,[¶] Jean-Guillaume Gomez,[§] Maroua Bourkhis,[§,¥] Frédéric Rodriguez,[§] Fernanda Gonçalves,[§] Isabelle Fabing,[§] Hafida Gaspard,[§] Vania Bernardes-Génisson,[#] Valérie Maraval,[#] Stéphanie Ballereau,[§] Remi Chauvin,[*,#] Sébastien Britton,[*,¶] Yves Génisson[*,§]

[§] Laboratoire de Synthèse et Physico-Chimie de Molécules d'Intérêt Biologique (SPCMIB), UMR 5068, CNRS, Université Paul Sabatier-Toulouse III, F-31062, Toulouse, France

[#] LCC-CNRS, Université de Toulouse, CNRS UPR 8241, UPS, F-31077, Toulouse, France

[¶] Institut de Pharmacologie et de Biologie Structurale (IPBS), Université de Toulouse, CNRS, Université Toulouse III - Paul Sabatier (UT3), Toulouse, F-31044, France

ABSTRACT: A series of 25 chiral anti-cancer Lipidic AlkynylCarbinols (LACs) was devised by introducing an (hetero)aromatic ring between the aliphatic chain and the dialkynylcarbinol warhead. The resulting Phenyl-diAlkynylCarbinols (PACs) exhibit enhanced stability, while retaining cytotoxicity against HCT116 and U2OS cell lines with IC_{50} down to 40 nM for resolved eutomers. A clickable probe allowed confirming the PACs prodrug behavior: upon enantiospecific bio-oxidation of the carbinol by the HSD17B11 Short-chain Dehydrogenase/Reductase (SDR), the resulting ynones covalently modify cellular proteins, leading to endoplasmic reticulum stress, ubiquitin-proteasome system inhibition and apoptosis. Insights into the design of LAC prodrugs specifically bioactivated by HSD17B11 *vs.* its paralogue HSD17B13 were obtained. The HSD17B11/HSD17B13-dependent cytotoxicity of PACs was exploited to develop a cellular assay to identify specific inhibitors of these enzymes. A docking study was performed with the HSD17B11 AlphaFold model providing molecular basis of the SDR substrates mimicry by PACs. The safety profile of a representative PAC was established in mice.

INTRODUCTION

Naturally occurring acetylenic lipids, sometimes referred to as polyacetylene or polyyne natural products, are a unique source of inspiration for the development of novel pharmacologically relevant compounds.[1,2,3,4] This large family of secondary metabolites mainly originates from marine sponges, with strongylodiols, lembehynes and durynes being the most studied chemical series (Fig. 1).[5] Closely related natural products were also isolated from plants, such as falcarindiol (Fig. 1).[6,7] These acetylenic lipids were reported to display a wide range of biological activities, and for most of them a significant cytotoxicity against cancer cells.[8,9,10,11] They are structurally characterized by the presence of at least one alkynyl carbinol unit along a linear aliphatic skeleton (Fig. 1). This chiral propargylic alcohol, most frequently located at the extremity of the lipophilic backbone, represents the key element of a wide range of pharmacophoric moieties.

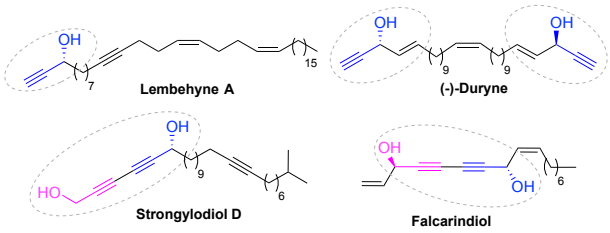

Figure 1. Examples of naturally occurring acetylenic lipids extracted from marine sponges or plants.

Following the systematic structural modulation of a prototypical lipidic alkynylcarbinol (LAC) (Fig. 2), it was previously shown that subtle modifications of the molecule can dramatically impact its cytotoxicity.[12,13,14,15,16,17,18,19,20] In particular, the absolute configuration and the steric and/or electronic environment of the chiral carbinol center are determining factors, as highlighted by the increased potency of the DiAlkynylCarbinol (DAC) series (Fig. 2). Structural evolution of synthetic LACs led to an overall 1000-fold increase in toxicity against HCT116 colon cancer cells compared to the natural product of reference (**Fig. 2**).[21] In-depth study of their mechanism of action also provided rational for these structure-activity trends. It was evidenced that LACs act as prodrugs, the secondary dialkynylcarbinol center being enantiospecifically oxidized by enzymes of the short-chain dehydrogen-

ase/reductase (SDR) family, in particular HSD17B11 (aka SDR16C2, PAN1B, DHRS8 or retSDR2) (**Fig.** 2).[22,23] The resulting dialkynylketones (DACones) were shown to behave as reactive Michael acceptors, irreversibly modifying a set of cellular proteins through addition of cysteine and lysine side chain residues. This process, called lipoxidation (i.e. covalent modification by a reactive lipid-like entity),[24] leads to the inhibition of the ubiquitin-proteasome system, triggering the unfolded protein response and an endoplasmic reticulum stress, ultimately leading to apoptotic cell death.

The most active LACs known to date belong to the Butadiynyl AlkynylCarbinol (BAC) series in which the dialkynylcarbinol warhead is bonded with an acetylenic unit formally resulting from a double dehydrogenation of the lipidic chain of a parent DAC.[17] Such a modification induces both proximal backbone rigidification and π-electronic conjugation of the internal triple bond. These effects are expected to favor the oxidative bioactivation of the carbinol center, but also decrease the overall stability of BACs in comparison to the parent DACs. On these bases, it was envisioned to replace the extra-triple bond - a reactive formal "two-membered" aromatic ring[25] - by a more stable aromatic ring, such as a phenylene ring. While offering an opportunity to enhance both the intrinsic stability and the susceptibility to HSD17B11-mediated bioactivation, this modification was thought to improve drug-likeness and introduce new prospects for further structural evolution. Opportunities supporting the development of such Phenyl diAlkynylCarbinols (PACs) include: (i) a modular synthetic access based on well-established Pd(0)-catalyzed coupling procedures; (ii) an easy modulation of the PAC geometry by varying the phenyl ring substitution pattern; (iii) a fine-tuning of the pharmacophore electronic properties by means of the phenyl ring decoration or its replacement by diverse heteroaromatic nuclei. We report here the implementation of this strategy regarding the design, synthesis and biological evaluation of the first series of PAC derivatives.

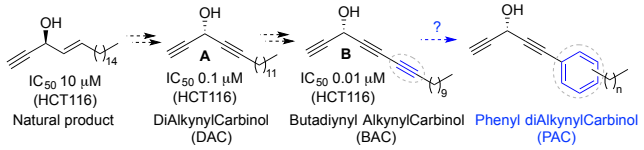

Figure 2. Structure-activity relationship of LACs for anti-cancer cytotoxicity from a natural reference representative to the designed PAC series.

RESULTS AND DISCUSSION

Chemical synthesis of racemic PACs

A general access to PACs was devised according to the general retrosynthetic plan depicted in **Scheme 1**. A key issue was the late elaboration of the pharmacophoric dialkynylcarbinol unit by addition of a metal acetylide onto an ynal. Two alternative disconnections a and b were envisioned. Access to both precursors was in turn planned by means of a common disconnection c corresponding to a Sonogashira coupling with either a trialkylsilyl-protected acetylene or propargylic alcohol. The corresponding synthetic routes **A** and **B** share common aryl halide precursors, which are either commercially available or described in the literature. Their preparation, relying on the introduction of the lipophilic chain onto a halogenated aromatic building block, was accomplished using known methods (see SI). Both alternative sequences **A** and **B** offer opportunities for asymmetric synthesis by means of the previously developed modified Carreira protocol for the enantioselective addition of TMS acetylene onto a functionalized ynal.[26,27,12,13,14,15,16,17]

Scheme 1. Retrosynthetic analysis of targeted PAC derivatives.

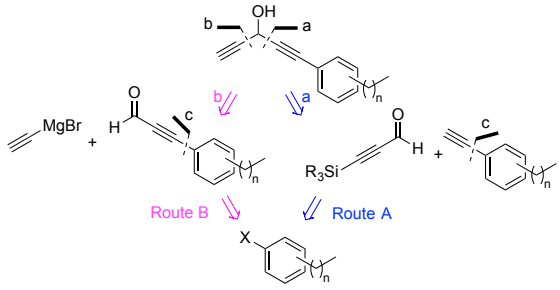

Route A

To first assess the feasibility of route A, the model compound **5.8a** with a phenyl ring *para*-substituted by *n*-octyl chain was targeted (Scheme 2). Sonogashira coupling of bromide **1.8a** with TMS-acetylene proceeded gently using the standard catalytic system $Pd(PPh_3)_2Cl_2$/CuI in Et_3N. It was followed by proto-desilylation with K_2CO_3 in MeOH. Final assembly of the dialkynylcarbinol unit was realized by addition of the lithium acetylide of **3.8a** onto TMS-protected propynal. Smooth deprotection of the terminal ethynyl group by K_2CO_3 in MeOH delivered the first PAC target **5.8a**. Previous studies of LAC derivatives pointed out a marked influence of the length of the lipidic backbone on cytotoxicity.[21] The same sequence was thus also used for the preparation of homologues **5.6a**, **5.9a**, **5.10a** and **5.12a** embedding a 6 to 12 carbon atoms long aliphatic chain (**Scheme 2**).

Scheme 2. Synthesis of undecorated and fluorinated *para*-alkyl-substituted PACs *via* route A[a]

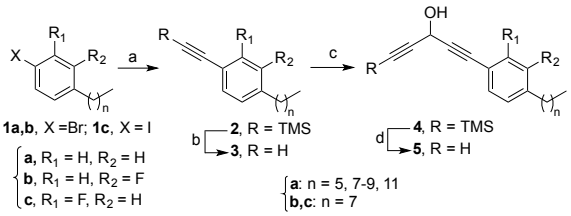

[a]Reagents and conditions: a) TMS-acetylene, CuI, $Pd(PPh_3)_2Cl_2$, Et_3N, 80 °C (**2.6a** (n = 5), 82%; **2.8a** (n = 7), 84%; **2.8b** (n = 7), 91%; **2.8c** (n = 7), 80%; **2.9a** (n = 8), 30%; **2.10a** (n = 9), 71%; **2.12a** (n = 11), 57%; b) K_2CO_3, MeOH, RT (**3.6a** (n = 5), 82%; **3.8a** (n = 7), quant.; **3.8b** (n = 7), 38%; **3.8c** (n = 7), 96%; **3.9a** (n = 8), 98%; **3.10a** (n = 9), 95%; **3.12a** (n = 11), 68%; c) *n*-BuLi, THF, TMS-propynal, - 78 °C to RT (**4.6a** (n = 5), 71%; **4.8a** (n = 7), 58%; **4.8b** (n = 7), quant.; **4.8c** (n = 7), 62%; **4.9a** (n = 8), 95%; **4.10a** (n = 9), 56%; **4.12a** (n = 11), 58%; d) K_2CO_3, MeOH, RT (**5.6a** (n = 5), 71%; **5.8a** (n = 7), 72%; **5.8b** (n = 7), 50%; **5.8c** (n = 7), 56%; **5.9a** (n = 8), 60%; **5.10a** (n = 9), 79%; **5.12a** (n = 11), 66%.

The route **A** (**Scheme 1**) was then tested for the preparation of PACs embedding a decorated phenyl ring. Aiming at adjusting the oxidation potential of the secondary carbinol center and optimizing the compound biodisponibility,[28,29] introduction of a fluorine atom was first applied in the case of an 8 carbon atoms aliphatic chain. The reaction sequence proved flexible enough to deliver both the *ortho*- and *meta*-fluorinated isomers from the properly substituted phenyl halide precursors (**Scheme 2**). The *meta*-fluorinated PAC **5.8b** was first accessed from the alkylbromofluorobenzene precursor **1.8b**. The *ortho*-fluorinated analogue **5.8c** was prepared using the same reaction sequence starting from the alkyliodofluorobenzene **1.8c**.

An alternative approach to modulate the electronic density of the phenyl ring was explored with the preparation of *para*-alkoxy PAC derivatives (**Scheme 3**). Compounds **10a,b** were obtained by means of a slight adaptation of route **A**. Two phenyl halide precursors **6a** and **6b** bearing respectively an *n*-heptyl or a diethylene glycol ethyl ether appendage were selected. The PACs **10a,b** were obtained via the Sonogashira coupling of **6a,b** with TMS-acetylene and late construction of the dialkynylcarbinol unit by addition of the lithium salt of **8a,b** onto TMS-protected propynal.

Scheme 3. Synthesis of *para*-alkoxy-substituted PACs *via* route A[a]

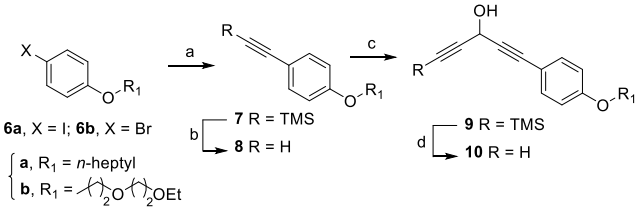

[a]Reagents and conditions: a) TMS-acetylene, CuI, $Pd(PPh_3)_2Cl_2$, Et_3N, 80 °C (**7a**, 90%; **7b**, 46%); b) K_2CO_3, MeOH, RT (**8a**, 84%; **8b**, 83%); c) *n*-BuLi, THF, TMS-propynal, - 78 °C to RT (**9a**, 27%; **9b**, 56%); d) K_2CO_3, MeOH, RT (**10a**, 41%; **10b**, 28%).

We then applied the reaction sequence **A** to the preparation of the *meta*-alkyl-substituted PACs **15.6**, **15.9** and **15.10** with 6, 9 and 10 carbon atom-long aliphatic chain, respectively, from suitably *meta*-substituted phenyl halide precursors **11** (**Scheme 4**).

The versatility of the route **A** was further explored with the preparation of PAC analogues embedding other aromatic rings than phenyl. A naphthyl derivative bearing a representative *n*-octyl chain was first envisioned. The reaction sequence proved to be efficient in delivering the target PAC **20** from alkylbromonaphthalene **16** (**Scheme 5**).

Scheme 4. Synthesis of *meta*-alkyl-substituted PACs *via* route A[a]

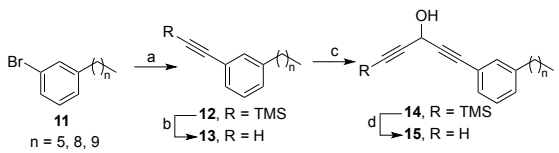

[a]Reagents and conditions: a) TMS-acetylene, CuI, $Pd(PPh_3)_2Cl_2$, Et_3N, 80 °C (**12.6** (n = 5), 72%; **12.9** (n = 8), quant.; **12.10** (n = 9), 71%); b) K_2CO_3, MeOH, RT (**13.6** (n = 5), 81%; **13.9** (n = 8), quant.; **13.10** (n = 9), 85%); c) *n*-BuLi, THF, TMS-propynal, - 78 °C to RT (**14.6** (n = 5), 81%; **14.9** (n = 8), 55%; **14.10** (n = 9), 62%); d) K_2CO_3, MeOH, RT (**15.6** (n = 5), 36%; **15.9** (n = 8), 25%; **15.10** (n = 9), 55%).

Scheme 5. Synthesis of a 2,6-naphthyl PAC analogue 20 *via* route A[a]

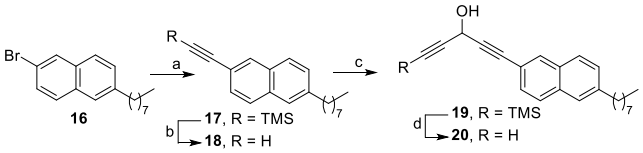

[a]Reagents and conditions: a) TMS-acetylene, CuI, $Pd(PPh_3)_2Cl_2$, Et_3N, 80 °C (**17**, 85%); b) K_2CO_3, MeOH, RT (**18**, 98%); c) *n*-BuLi, THF, TMS-propynal, - 78 °C to RT (**19**, quant.); d) K_2CO_3, MeOH, RT (**20**, 37%).

The principle of route **A** was finally applied to the preparation of heteroaromatic PAC analogues from commercially available 2-alkyl thiophene precursors (**Scheme 6**). This aromatic nucleus was selected so as to finely modulate the electronic properties of the dialkynylcarbinol pharmacophoric unit through the participation of the sulfur atom to the conjugated system via its +M effect. Thiophene derivatives **25.10** and **25.12**, bearing a decyl and a dodecyl chain, respectively, were prepared. Sonogashira coupling from 2-alkyl-5-bromothiophenes **21** under previously employed conditions was used as an entry to route **A**.

Scheme 6. Synthesis of 2,5-thienyl PAC analogues 25 *via* route A[a]

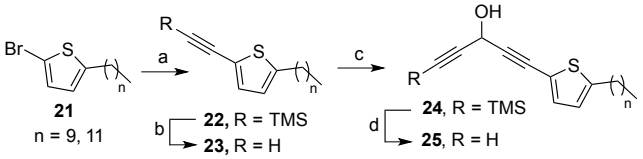

[a]Reagents and conditions: a) TMS-acetylene, CuI, $Pd(PPh_3)_2Cl_2$, Et_3N, 80 °C (**22.10** (n = 9), 94%; **22.12** (n = 11), 74%); b) K_2CO_3, MeOH, RT (**23.10** (n = 9), **23.12** (n = 11), quant.); c) *n*-BuLi, THF, TMS-propynal, - 78 °C to RT (**24.10** (n = 9), **24.12** (n = 11), 89%); d) K_2CO_3, MeOH, RT (**25.10** (n = 9), 21% (over 3 steps); **25.12** (n = 11), 58%).

Route B

In order to widen the scope of PAC derivatives, we then studied the implementation of synthetic pathway **B** (Scheme 1). This route advantageously avoids the final TMS deprotection step, thanks to the late addition of ethynyl Grignard onto a lipidic aromatic ynal directly giving the unprotected dialkynylcarbinol unit. Key to this sequence is the Sonogashira coupling of the aryl bromide precursor with unprotected propargylic alcohol. The catalytic system based on Na_2PdCl_4, PIntB and CuI in TMEDA/water was found to perform well.[30,31] We first validated this 3-step sequence with the prep-

aration of the unsubstituted reference PAC **5.8** bearing an octyl chain (**Scheme 7**). Route **B** thus competes well with the 4-step sequence **A** for the synthesis of **5.8a**, both in terms of number of steps and in terms of overall yield (42% for route **B** *vs.* 35% for route **A**).

Scheme 7. Synthesis of undecorated and fluorinated *para*-alkyl-substituted PACs *via* route B[a]

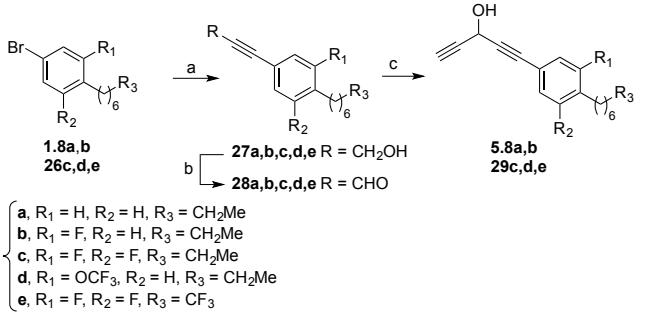

[a]Reagents and conditions: a) propargylic alcohol, Na_2PdCl_4, PIntB, CuI, TMEDA, H_2O, 70 to 80 °C (**27a**, 61%; **27b**, 66%; **27c**, 76%; **27d**, 50%; **27e**, 68%); b) DMP, DCM, RT (**28a**, quant.; **28b**, 82%; **28c**, quant.; **28d**, 85%; **28e**, 78%); c) HC≡CMgBr, THF, 0 °C to RT (**5.8a**, 70%; **5.8b**, 69%; **29c**, 48%; **29d**, 80%; **29e**, 52%). TMEDA: *N*,*N*,*N*′,*N*′-Tetramethylethylenediamine. PIntB: *N*-Phenyl-2-(di-*t*-butyl-phosphino)indole. DMP: Dess-Martin periodinane.

The flexibility of route **B** was then further demonstrated with the preparation of PAC derivatives fluorinated either on the phenyl ring or both on the phenyl ring and on the terminal position of the aliphatic chain. Regarding the phenyl ring substitution, the *meta*-fluorinated derivative **5.8b,** the *meta*-difluorinated product **29c** and the *meta*-trifluoromethoxylated analogue **29d** were readily secured *via* this reaction sequence. Regarding the fluorination of the lipophilic skeleton, the terminal CF_3 group was considered as a bioisostere of an ethyl radical.[32] By comparison to **29c**, the one-carbon shorter derivative **29e** was thus efficiently prepared from the precursor **26e**.

Similarly, two fluorinated *para*-alkoxy-substituted PACs were targeted *via* route **B** (**Scheme 8**). Sonogashira coupling of the aryl bromide precursors **30a,b** with propargylic alcohol proved to be straightforward using a standard catalytic system, $Pd(OAc)_2/PPh_3$ in Et_3N. The resulting primary alcohols **31a,b** were smoothly converted into the targeted PAC analogues **33a,b**. Finally, the CF_2-embedding analogue **33c**, regarded as a bioisostere of the *para*-alkoxy PAC **10a** (**Scheme 3**), was prepared through a 3-step sequence from the aryl bromide precursor **30c** (**Scheme 8**).[33]

Route **B** was also applied to the synthesis of heteroaryl PAC analogues. For comparison with the thiophene **25.10** (**Scheme 6**), the furan analogue **37** bearing a C10 alkyl chain was targeted. It is worth noting that notopolyenol A, a related furan-containing acetylenic lipid with cytotoxic activity, was recently isolated from a traditional Chinese herb.[34] Starting from the 2-bromo-5-alkyl-furan **34**, synthesized using a recently described methodology,[35] the 3-step synthetic sequence **B** readily delivered the targeted furyl PAC analogue **37** (**Scheme 9**).

Scheme 8. Synthesis of undecorated and fluorinated *para*-alkyl- and *para*-alkoxy-substituted PACs *via* route B[a]

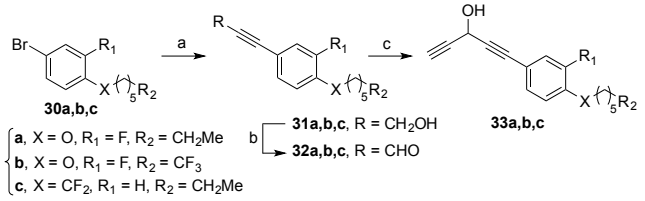

[a]Reagents and conditions: a) propargylic alcohol, $Pd(OAc)_2$, PPh_3, CuI, Et_3N, 65 °C (**31a**, 66%; **31b**; 60%; **31c**, 80%); b) DMP, DCM, RT (**32a**, 74%; **32b**, 53%; **32c**, 55%); C) HC≡CMgBr, THF, 0 °C to RT (**33a**, 48%; **33b**, 33%; **33c**, 55%). DMP: Dess-Martin periodinane.

Scheme 9. Synthesis of 2,5-furyl PAC analogue 37 *via* route B[a]

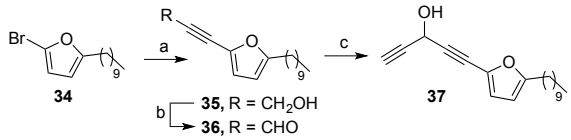

[a]Reagents and conditions*:* a) propargylic alcohol, Na_2PdCl_4, PIntB, CuI, TMEDA, H_2O, 70 to 80 °C (**35**, 25%); b) DMP, DCM, RT (**36**, 73%); c) HC≡CMgBr, THF, 0 °C to RT (**37**, 47%). DMP: Dess-Martin periodinane. PIntB: *N*-Phenyl-2-(di-*t*-butyl-phosphino)indole.

To broaden the variability around the heteroaromatic nucleus, we also synthesized a regioisomer of furan **37**, in which the dialkynylcarbinol unit is shifted from the C-5 to the C-4 furan position. The 2-iodo-4-alkyl-furan precursor **38**, obtained according to the same methodology,[35] was transformed into the furyl PAC analogue **41** in 3 steps (**Scheme 10**). In this case, the standard catalytic system made of $Pd(PPh_3)_2Cl_2$ and CuI in Et_3N proved to be efficient for the Sonogashira coupling of **38** with propargylic alcohol.

Scheme 10. Synthesis of 2,4-furyl PAC analogue 41 *via* route B[a]

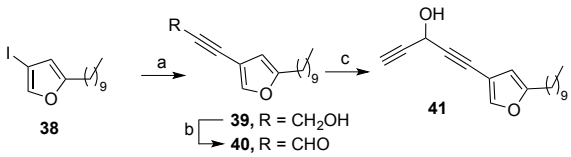

[a]Reagents and conditions: a) propargylic alcohol, $Pd(PPh_3)_2Cl_2$, CuI, Et_3N, 50 °C (**39**, 80%); b) DMP, DCM, RT (**40**, 92%); c) HC≡CMgBr, THF, 0 °C to RT (**41**, 47%). DMP: Dess-Martin periodinane.

Access to enantiomerically enriched PAC derivatives

Our previous work showed the critical importance of the absolute configuration of the carbinol center on the cytotoxicity of LACs. A strong eudismic ratio favoring the enantiomeric series opposite to that most frequently encountered in naturally occurring LACs was notably observed.[21] The preparation of the representative PAC **5.8a** under scalemic form was then studied by implementing the Carreira's method for enantiose-

lective alkynylation of aldehydes modified for ynals (**Scheme 11**).[12,13,14,15,16,17,26] While both disconnections a or b (Scheme 1) were potentially compatible with this method, it was previously shown that these two retrosynthetic options were not equivalent in terms of yields and enantiomeric excess.[21] The eutomeric (*S*)-enantiomer of **5.8a** was first targeted through the disconnection a. Alkyne **3.8a** was reacted in DCM with TMS-propynal in the presence of $Zn(OTf)_2$ and (-)-*N*-methyl ephedrine ((-)-NME) as a chiral inductor. The expected carbinol (*R*)-**4.8a**, isolated in 74% yield, was then smoothly desilylated to give the targeted (*S*)-**5.8a** with 57% e.e., as measured by chiral chromatography analysis (the change of absolute configuration between **4.8a** and **5.8a** is due to an inversion of the Cahn-Ingold-Prelog priority of the carbinol substituents). The (*S*) absolute configuration was assigned to the dextrorotatory enantiomer of **5.8a** on the basis of our previous work.[21] Employing the (+)-NME, the levorotatory enantiomer (*R*)-**5.8a** was generated in similar yield and enantiomeric excess via (*S*)-**4.8a** (see SI). The modified Carreira procedure was then challenged with the disconnection b. The use of (+)-NME as chiral inductor was this time required to generate the (*S*)-enantiomer of **5.8a**. Aldehyde **28a** was thus reacted with TMS-acetylene under otherwise identical conditions to give the silylated intermediate **4.8a** in 41% yield. The latter was deprotected to yield the expected PAC (*S*)-**5.8a** in 88% e.e.

The relative performance of the modified Carreira procedure according to either disconnection a or b thus indicates that an appreciable enantiomeric excess is attainable, but at the detriment of the yield (74% yield/57% e.e. *vs.* 41% yield/88% e.e.). In addition, scaling-up of the experimental procedure to gram-scale led to erratic variations of both yield and enantiomeric excess. Access to enantiopure samples of **5.8a** by means of a chiral resolution of a racemic mixture was thus considered. Upon extensive optimization, we were able to produce hundreds of mgs of both enantiomers of **5.8a** with e.e. > 99% by semi-preparative supercritical fluid chromatography on a Chiralpak IB column (5 µm (20 x 250 mm) column, 90:10 $ScCO_2$/MeCN, 40 mL/min, 150 bar, 37 °C). In an effort to expand the scope of this approach, we also managed to resolve a racemic sample of **29c** at a semi-preparative scale on a Chiralpak IG column (5 µm (20 x 250 mm) column, 85:15 $ScCO_2$/MeCN, 40 mL/min, 100 bar, 25 °C) to obtain both enantiomers with e.e. > 99%. On the basis of our previous work, the (*S*) absolute configuration was assigned to the dextrorotatory enantiomer of **29c**, and, conversely, the levorotatory sample was considered to be (*R*)-configured.[21]

Access to an alkyne-tagged clickable PAC probe

We previously developed the ω-alkyne derivative of a cytotoxic DAC and used this clickable probe for *in cellulo* imaging and chemoproteomics target identification.[22] Similar strategies were used to study the mechanism of action of falcarinol[36] and callyspongynic acid.[37] In order to access related tools in the PAC series, the clickable analogue of PAC **5a** (**Scheme 2**) bearing an alkyne tag at the terminal position of the aliphatic chain was targeted. Route **A** was first envisioned (**Scheme 12**) from the corresponding aryl halide. Implementation of disconnection a at the penultimate stage of the synthesis required a selective deprotection of the phenyl acetylene moiety in the presence of the silyl-protected alkyne tag present at the terminus of the aliphatic chain. TMS and TIPS were thus selected as orthogonal silyl-protecting groups of the two terminal alkynes (**Scheme 12**).

Scheme 11. Asymmetric synthesis of enantioenriched PAC 5.8a via routes A and B[a]

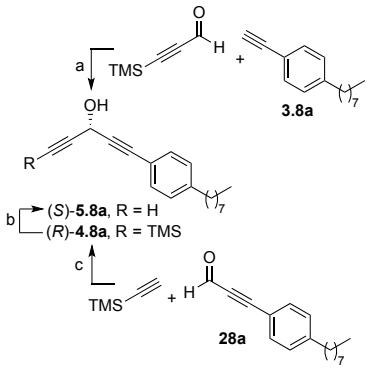

[a]Reagents and conditions: a) $Zn(OTf)_2$, (-)-NME, DCM, RT ((*R*)-**4.8a**, 74% yield, 57% e.e.); b) K_2CO_3, MeOH, RT ((*S*)-**5.8a**, 62-67% yield, 57-88% e.e); c) $Zn(OTf)_2$, (+)-NME, DCM, RT ((*R*)-**4.8a**, 41% yield, 88% e.e.). NME: *N*-methyl ephedrine.

Scheme 12. Retrosynthetic analysis of the targeted clickable PAC probe

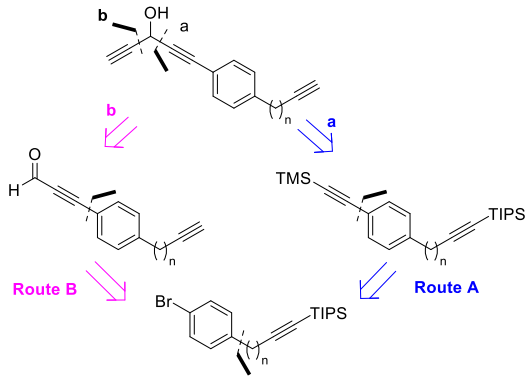

The orthogonally diprotected diyne **43** was smoothly obtained from the properly functionalized aryl bromide **42** (**Scheme 13**).[38] Selective deprotection of the TMS group delivered the terminal alkyne **44** which, upon lithiation, was added onto TMS-protected propynal to afford the diprotected form **45** of the targeted probe **46**. However, whereas treatment with TBAF at low temperature resulted in the smooth cleavage of the TMS group (according to the NMR analysis of the crude mixture), attempts to remove the TIPS-protecting group of the terminal alkyne failed, resulting in the decomposition of the expected product **46**.

Scheme 13. Attempted synthesis of the clickable probe 46 by route A[a]

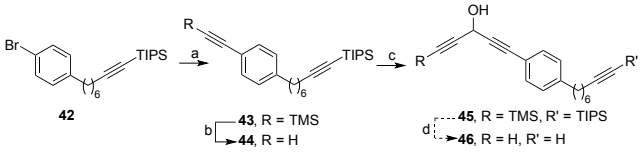

[a]Reagents and conditions: a) TMS-acetylene, CuI, $Pd(PPh_3)_2Cl_2$, Et_3N, 80 °C (**43**, quant.); b) K_2CO_3, MeOH, RT (**44**, 87%); c) *n*-BuLi, THF, TMS-propynal, - 78 °C to RT (**45**, 47%); d) TBAF, THF, - 30 °C to RT.

The alternative route **B** was thus attempted to prepare the clickable probe **46** from the same TIPS-protected precursor **42** (**Scheme 14**). Installation of the key dialkynylcarbinol moiety through disconnection b, corresponding to the final addition of ethynyl Grignard reagent onto an ynal, would allow to anticipate the cleavage of the TIPS group at an earlier stage of the sequence.

Scheme 14. Synthesis of the clickable probe 46 by route B[a]

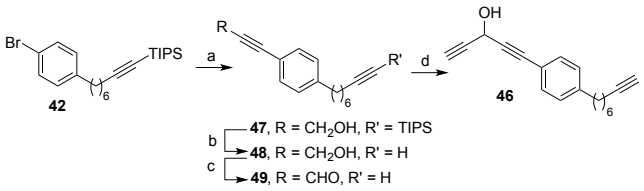

[a]Reagents and conditions: a) propargylic alcohol, Na_2PdCl_4, PIntB, CuI, TMEDA, H_2O, 70 to 80 °C (**47**, 62%); b) TBAF, THF, 0 °C to RT (**48**, 79%); c) DMP, DCM, RT (**49**, 92%); d) HC≡CMgBr, THF, 0 °C to RT (**46**, 55%). DMP: Dess-Martin periodinane. PIntB: *N*-Phenyl-2-(di-*t*-butyl-phosphino)indole.

Sonogashira coupling of aryl bromide **42** with propargylic alcohol gave the primary alkynylcarbinol **47** in 62% yield (**Scheme 14**). Smooth desilylation of **47** with TBAF, followed by Dess-Martin periodinane-mediated oxidation of the primary propargylic carbinol center afforded the expected ynal **49**. Final addition of ethynyl magnesium bromide to the latter directly delivered the targeted PAC probe **46**. The chiral chromatographic resolution of the racemic mixture of **46** proved arduous but few mgs of enantioenriched (*S*)-**46** (95% e.e.) and (*R*)-**46** (60% e.e.) were obtained by semi-preparative fluid chromatography on a Chiralpak IA column (5 µm (20 x 250 mm) column, 90:10 to 85:15 heptane/isopropanol, 14 mL/min). As mentioned above, the absolute configuration of both enantiomers of **46** was assigned on the basis of the sign of their optical rotation and corroborated by their biological activity profile.[21]

Biological evaluations of PAC derivatives

Stability assay in growth media of representative LACs

We first assessed our starting hypothesis according to which the replacement of the internal triple bond of BACs by a *para*-phenylene ring would lead to a gain in stability of the corresponding PACs. Racemic samples of the representative DAC **A**, BAC **B** (**Fig. 1**) and PAC **5.8a** (**Scheme 2**) were subjected to a stability assay in which the molecules were incubated at 37 °C during different times at twice the final concentration in complete culture medium before being added to the cells. As can be seen from **Table 1**, a 5-fold increase in IC_{50} was observed after 8 h for the BAC **B**, whereas the IC_{50} of the corresponding **5.8a** was increased by 1.6 times only. The latter also proved to be even slightly more stable than the parent DAC **A** (2.1 increase in IC_{50} after 8 h), substantiating the added value of the PAC series.

Table 1. Stability data for representative LACs[a]

Incubation time	Fold increase in DAC **A** IC_{50}	Fold increase in BAC **B** IC_{50}	Fold increase in PAC **5.8a** IC_{50}
0 h	1	1	1
1 h	1.1	1.2	1.1
2 h	1.2	1.3	1.2
4 h	1.4	2.2	1.3
8 h	2.1	4.9	1.6

[a]DAC **A**, BAC **B** and PAC **5.8a** were incubated in growth media at 37 °C for the indicated time before evaluation of their cytotoxic activity against HCT116. The table reports the fold increase in IC_{50} observed after different incubation times.

Cell viability assay of PAC derivatives

Having in hands a large number of PAC derivatives, their systematic biological evaluation was carried out in order to draw the first structure-activity relationships. Cytotoxicity against the HCT116 cancer cell line was selected as a reference data allowing direct comparison of the new PAC compounds with previously reported synthetic LACs (**Table 2**). We first assessed the effect of racemic samples on cell viability. As a reference, IC_{50} of toxicity in the submicromolar range are typically observed for the most potent compounds like the DAC **A** and the BAC **B**, both possessing a C17 skeleton (**Table 2**, entries 1 and 2).[21]

The influence of the chain length was first evaluated in the *para*-substituted PACs which are geometrically related to the BAC series of reference. The PACs **5.8a** to **5.10a** carrying a C8 to C10 aliphatic appendage, respectively displayed an IC_{50} of 0.15 µM (**Table 2**, entries 4-6), which is equivalent to that of the DAC **A** (entry 1, IC_{50} 0.18 µM) and close to that of the reference BAC **B** (entry 2, IC_{50} 0.05 µM). A drop in activity was observed when decreasing or increasing the chain length by only 2 to 3 carbons in **5.6a** (entry 3, IC_{50} 0.6 µM *vs.* entry 4, IC_{50} 0.15 µM) or **5.12a** (entry 7, IC_{50} 0.4 µM *vs.* entry 6, IC_{50} 0.15 µM). An aliphatic chain length of 8 carbon atoms as in **5.8a** was thus found to confer the optimal potency for a minimized lipophilicity. Finally, the racemic clickable derivative **46** bearing a C8 ω-alkyne lipidic tail displayed an IC_{50} of 0.45 µM (entry 25). This result indicates a limited influence of the terminal alkyne tag on the cytotoxicity, an observation in favor of the use of the derivative **46** as a cellular probe.

Table 2. HCT116 cell viability data for racemic DAC and BAC reference compounds vs PACs

Entry	Compound	IC_{50} (μM)	Entry	Compound	IC_{50} (μM)
1	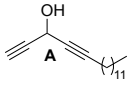	0.18	14	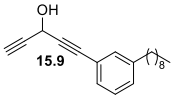	5
2	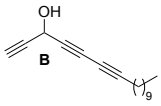	0.05	15	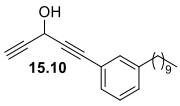	2.5
3	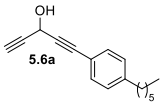	0.6	16	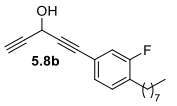	0.17
4	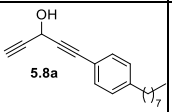	0.15	17	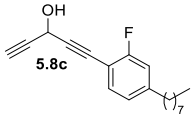	0.6
5	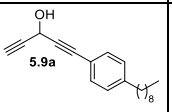	0.15	18	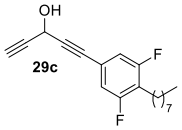	0.14
6	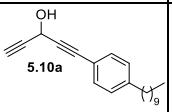	0.15	19	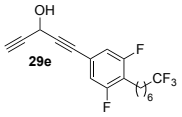	0.17
7	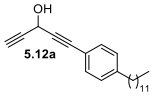	0.4	20	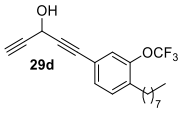	1.9
8	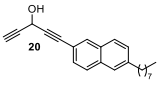	0.5	21	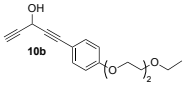	5
9	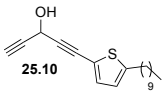	0.2	22	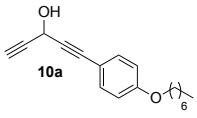	0.25
10	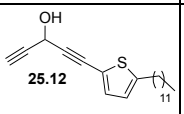	0.4	23	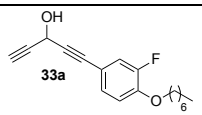	0.36
11	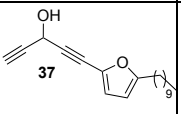	0.14	24	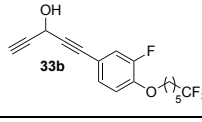	0.24
12	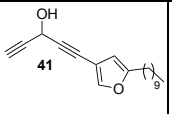	0.12	25	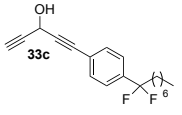	0.09
13	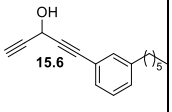	10	26	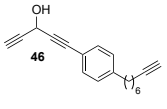	0.45

A quick look at the *meta*-substituted PAC analogues indicates that this substitution pattern is less favorable to cytotoxicity than the *para*-substitution pattern, with IC_{50} raising to the low micromolar range (entries 13-15). Yet, a clear effect of the chain length was observed within the *meta*-substituted series since compound **15.10** revealed to be 4 times more potent than its homologue **15.6** bearing an aliphatic chain truncated by 4 carbons (entry 15, IC_{50} 2.5 μM *vs.* entry 13, IC_{50} 10 μM).

Interestingly, a recent structure-activity relationship study showed that compound **47** (**Figure 3**), a very close analogue of **15.10** lacking the internal alkyne unit, was 3 orders of magnitude less cytotoxic (IC_{50} 152 μM against non-small cell lung carcinoma U-1810 cell line).[39] This data corroborates our preliminary results showing that related simple phenyl alkynylcarbinols **48** and **49** (**Figure 3**) were significantly less potent than their PAC congeners. These observations thus substantiate the relevance of the phenyl dialkynylcarbinol moiety of PACs, both in the *meta*- and *para*-substituted series.

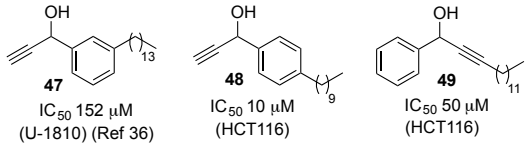

Figure 3. Examples of phenyl alkynylcarbinols taken from the literature (**47**)[39] or our own preliminary results (**48**, **49**).

We then focused on the *para*-substituted PACs possessing a C8 aliphatic chain to study the influence of the phenyl ring decoration. Introduction of a strongly electron-withdrawing substituent such as a fluorine is expected to deactivate the PAC carbinol center toward oxidative bioactivation. It may however also favorably influence the bioavailability by preventing unwanted metabolization. Comparison of the PACs **5.8b** and **5.8c** indicates an influence of the localization of the fluorine atom in favor of the *meta* position with regard to the dialkynylcarbinol unit (**Table 2**, entry 16, IC_{50} 0.17 μM *vs.* entry 17, IC_{50} 0.6 μM). This could be correlated to a less pronounced -I effect of the fluorine, due to a more distant position, leading to a less deactivated carbinol center than in the *ortho*-derivative **5.8c**. The analogue **29c**, fluorinated in both *meta* positions, retained the level of activity of the unsubstituted PAC **5.8a** (entry 18, IC_{50} 0.14 μM *vs.* entry 4, IC_{50} 0.15 μM), while presenting an electron-impoverished phenylene core potentially more stable *in vivo*. Replacement of the octyl chain by a heptyl chain trifluorinated at the terminal position led to an equivalent level of toxicity for **29e** (entry 19, IC_{50} 0.17 μM). In contrast, the OCF_3 group, known to confer a strong lipophilicity, had a negative effect on cytotoxicity when present in the same *meta* position (entry 20, IC_{50} 1.9 μM). This observation might be explained by specific steric factors associated with the conformational behavior of this group.[40]

The effect of other oxygenated substituents in the *para* position was explored with the PACs **10a** and **10b** in which the aliphatic chain is either connected as an ether, or replaced by a PEG fragment (**Scheme 3** and **8**). Whereas the PEG chain in **10b** led to a loss of activity (**Table 2**, entry 21, IC_{50} 5.0 μM), the PAC analogue **10a** bearing a heptyloxy chain retained an appreciable level of cytotoxicity (entry 22, IC_{50} 0.25 μM) as compared to its analogue **5.8a** embedding an octyl chain (entry 4, IC_{50} 0.15 μM), thus opening further prospects. Whereas

fluorination at the *meta* position of the phenylene ring in the PAC **33a** led to a slight decrease in activity (entry 23, IC_{50} 0.36 μM), the presence in **33b** of an hexyloxy chain trifluorinated at its extremity tended to restore the cytotoxicity (entry 24, IC_{50} 0.24 μM). Finally, replacement of the ether oxygen atom of **10a** by the bioisosteric CF_2 group led to a level of cytotoxicity for **33c** (entry 25, IC_{50} 0.09 μM) outperforming that of the parent compound **5.8a** bearing a plain octyl chain (entry 4, IC_{50} 0.15 μM).

We also assessed the cytotoxicity of PAC analogues containing an aromatic ring other than a phenylene. The 2,6-naphthylene derivative bearing an octyl chain **20** displayed a more than 3 times lower activity compared to its *para*-phenylene-based congener **5.10a** with a decyl chain (**Table 2**, entry 8, IC_{50} 0.5 μM *vs.* entry 6, IC_{50} 0.15 μM), suggesting an unfavorable impact of extended structural rigidification. Thienyl and furyl PAC derivatives were also evaluated as representative heteroaromatic analogues. Comparative evaluation of the sulfur-containing compounds **25.10** and **25.12** indicated that the submicromolar IC_{50} was 2 times lower for a C10 rather than a C12 lipophilic chain (entry 9, IC_{50} 0.2 μM *vs.* entry 10, IC_{50} 0.4 μM). The corresponding furan-based PAC derivative with a decyl chain displayed a slightly stronger cytotoxicity, with a IC_{50} of 0.14-0.12 μM for the 2,5- or 2,4-substituted derivatives **37** or **41** (entries 11, 12).

Enantioenriched samples of PAC **5.8a** (e.e. > 99%, issued from chiral SCF chromatography) were also evaluated against HCT116 cells (**Table 3**). The eutomeric dextrorotatory (*S*)-**5.8a** displayed an IC_{50} of 0.09 μM, which is equal to that of the reference DAC **A** (entry 1, IC_{50} 0.09 μM) and comparable to that of the related BAC **B** (entry 2, IC_{50} 0.012 μM). An IC_{50} of 10 μM was observed for the distomeric levorotatory enantiomer (*R*)-**5.8a**, corresponding to an eudismic ratio (IC_{50} eutomer/IC_{50} distomer) of 0.004. This low ratio value highlights the critical impact of the carbinol center absolute configuration on the cytotoxicity of PACs. The same trend was observed with the enantiomeric pair of **29c** and **33c** (**Table 3**). Of note, for the latter, the (*S*)-configured eutomer displayed a IC_{50} as low as 42 nM. These data are in full agreement with our previous results on non-aromatic DAC derivatives (see for instance entry 1, IC_{50} 0.09 μM *vs.* entry 8, IC_{50} 3 μM and entry 2, IC_{50} 0.012 μM *vs.* entry 9, IC_{50} 0.3 μM).[21] A similar gap in cytotoxicity in favor of the synthetic (*S*)-configured carbinol compared to the naturally occurring (*R*) enantiomer has been observed for several acetylenic lipids issued from plants.[34,41,42] These observations suggest that the recently uncovered enantiospecific bioactivation mechanism of DACs may be shared by different types of LACs.[22] A similar gap in cytotoxicity was observed between the two partially resolved samples of clickable PACs (*S*)- and (*R*)-**46** (entry 7, IC_{50} 0.28 μM *vs.* entry 14, IC_{50} 1.8 μM), further confirming the relevance of **46** as a cellular probe. This overall trend is in full agreement with the recently reported mode of action showing a HSD17B11-mediated oxidative enantiospecific bioactivation of synthetic LACs acting as prodrugs.[22]

To test whether the mechanism of action of these novel entities is shared with the parent DACs, the cytotoxic activity of **5.8a** and the related clickable analogues **46** was investigated on the U2OS human osteosarcoma cell line, either WT or inactivated for HSD17B11 using CRISPR/Cas9 (KO HSD17B11) (**Table 4**). U2OS cells were chosen because we have previously established that osteosarcoma cell lines display an acute sensitivity to (*S*)-DACs which was strongly reduced by HSD17B11 inactivation.[22] The ratio of the IC_{50} of cytotoxicity against the KO cells over the one against the WT cells, *i.e.* the resistance factor, allows assessing the selectivity index for HSD17B11 (**Table 4**).

Table 3. HCT116 cell viability data for enantioenriched DACs A and C, BAC B reference compounds vs PACs

	Compound	IC_{50} (μM)		Compound	IC_{50} (μM)
1	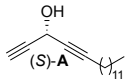 (*S*)-**A**	0.09	8	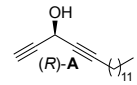 (*R*)-**A**	3
2	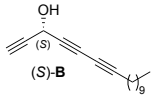 (*S*)-**B**	0.012	9	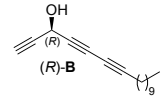 (*R*)-**B**	0.3
3	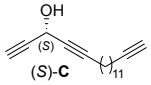 (*S*)-**C**	0.3	10	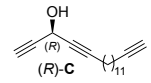 (*R*)-**C**	> 50
4	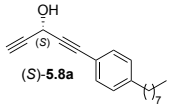 (*S*)-**5.8a**	0.09	11	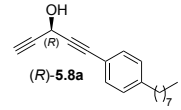 (*R*)-**5.8a**	10
5	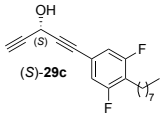 (*S*)-**29c**	0.09	12	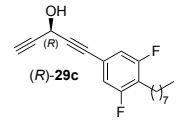 (*R*)-**29c**	≥ 5
6	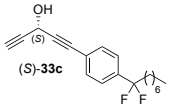 (*S*)-**33c**	0.042	13	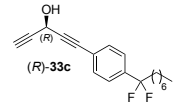 (*R*)-**33c**	≥ 5
7	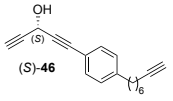 (*S*)-**46**	0.28	14	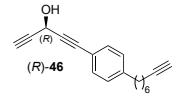 (*R*)-**46**	1.8

First, we validated that (*S*)-**5.8a** displays a greater cytotoxicity towards U2OS than HCT116 (40 nM *vs.* 90 nM), showing that osteosarcoma cells are also more sensitive to PACs. In addition, the inactivation of HSD17B11 in U2OS conferred them a strong resistance to (*S*)-**5.8a**, with an IC_{50} increased by ~200 times. This is close to the resistance conferred to (*S*)-DAC **A** by HSD17B11 inactivation (~250 times) but higher than that observed with (*S*)-BAC **B** (96 times), suggesting that the greater activity of (*S*)-BAC **B** is at the expense of a reduced stability in biological media (**Table 1**) and a lower selectivity towards HSD17B11 for its bioactivation.

We also compared the activity of (*S*)-**46** and (*R*)-**46** on these cells and confirmed that these clickable analogues retain the behavior of their parent molecules: (*S*)-**46** was more cytotoxic towards U2OS than HCT116, while (*R*)-**46** was ~12 times less active. More importantly, inactivating HSD17B11 also conferred a strong resistance to (*S*)-**46**. Altogether, these data support the notion that (*S*)-PACs and the related clickable analogue (*S*)-**46** are prodrugs enantiospecifically bioactivated by HSD17B11-catalysed oxidation into cytotoxic DACones species.

Table 4. Cell Viability Data for DAC and BAC Reference Compounds vs PACs on WT and KO HSD17B11 U2OS

Entry	Compound	IC_{50} (μM)		Resistance factor conferred by HSD17B11 inactivation
		U2OS	U2OS KO HSD17B11	
1	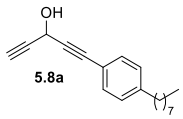 **5.8a**	0.08	>5	n.d.
2	(*S*)-DAC **A**	0.024	6.06	253
3	(*S*)-BAC **B**	0.014	1.35	96
4	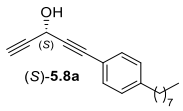 (*S*)-**5.8a**	0.04	8.56	214
5	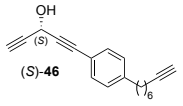 (*S*)-**46**	0.17	>5	n.d.
6	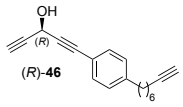 (*R*)-**46**	1.09	>5	n.d.

The HSD17B13 (aka SCDR9 or SDR16C3) SDR is the closest human protein to and the paralogue of HSD17B11 (63.3 % of sequence identity between them) with which it shares a similar subcellular localization.[43] Since the (*S*)-DAC **A** can also be bioactivated by HSD17B13,[22] albeit to a lower extent, we wanted to assess whether PACs would exhibit an enhanced selectivity towards HSD17B11 as compared to HSD17B13. For this, U2OS KO HSD17B11 osteosarcoma cells, which do not express HSD17B13, were stably complemented with HSD17B11-GFP or HSD17B13-GFP.[22] These two cell lines were used to monitor the cytotoxicity of selected LACs, with the ratio between the IC_{50} on HSD17B13 and HSD17B11 complemented U2OS providing a selectivity index (**Table 5**).

The data indicate that HSD17B13 displays an enantiospecific bioactivation in favor of the (*S*)- series, consistent with what was previously found for HSD17B11 (**Table 5**) (entry 1 *vs.* entry 2). The (*S*)-PAC **5.8a** presents a selectivity for HSD17B13 comparable to that of the (*S*)-DAC **A** but higher than that of its (*S*)-BAC **B** congener (entry 4 *vs.* entry 1 or entry 3), confirming the interest of the PAC series. The effect of PAC structural variation was also studied with a panel of analogues (**Table 5**). These data showed that even small structural modifications can have a strong impact on the selectivity profile with **29d** being the most selective (SI~9.2) of all tested compounds. In addition, **33c** combines the strongest cytotoxicity in this series with one of the highest selectivity (SI~6). Overall, these trends highlight how PAC compounds with an enhanced selectivity towards HSD17B11 can be developed through subtle structural modulations by taking advantage of differences between the substrate binding sites.

Table 5. Cell Viability Data for DAC and BAC Reference Compounds vs PACs on U2OS KO HSD17B11 Stably Complemented with HSD17B11-GFP or HSD17B13-GFP

Entry	Compound	IC_{50} (μM)		SI
		U2OS KO HSD17B11 +		
		HSD17B11	HSD17B13	
1	(*S*)-DAC **A**	0.015	0.047	3.1
2	(*R*)-DAC **A**	>4	>4	n.d.
3	(*S*)-BAC **B**	0.015	0.025	1.6
4	(*S*)-**5.8a**	0.017	0.048	2.9
5	**10b**	0.353	0.637	1.8
6	**33b**	0.046	0.087	1.9
7	**25.10**	0.052	0.109	2.1
8	**33a**	0.039	0.088	2.3
9	**46**	0.054	0.127	2.4
10	**10a**	0.039	0.097	2.5
11	**37**	0.026	0.081	3.1
12	**5.8b**	0.044	0.139	3.2
13	**29e**	0.045	0.152	3.4
14	**15.9**	0.127	0.495	3.9
15	**20**	0.076	0.298	3.9
16	**33c**	0.018	0.109	6.0
17	**5.8c**	0.048	0.330	6.8
18	**29d**	0.093	0.852	9.2

Use of (S)-PACs as probes to identify and characterize HSD17B11 or HSD17B13 inhibitors.

Having shown that (*S*)-PACs can be bioactivated by both HSD17B11 and HSD17B13, we explored the possibility of identifying and characterizing inhibitors of these enzymes by using the (*S*)-PAC SDR-dependent cytotoxicity as a readout of the cellular HSD17B11/HSD17B13 catalytic activity. When incubated with cells at 1 μM for 72 h, the PAC (*S*)-**5.8a** reduces the cellular viability of U2OS KO HSD17B11 complemented by HSD17B11 or HSD17B13 down to ≈ 0 %, while it has only a small effect on the control cells (GFP complemented, 90-92 % viability). In these conditions, we used the recently described selective HSD17B13 inhibitor BI-3231 available thanks to the opnMe platform,[44] to establish at which concentration it was able to inhibit the HSD17B11 and HSD17B13-dependent (*S*)-**5.8a** cytotoxic activity (**Figure 4A,B**). Computing from the measured viability the % of HSD17B11 or HSD17B13 bioactivating activity at increasing inhibitor concentrations led us to establish in U2OS a cellular IC_{50} of 117 nM for BI-3231 against HSD17B13 and of > 10 μM against HSD17B11. These data validate BI-3231 as a selective and potent HSD17B13 inhibitor and exemplify how (*S*)-PACs along with engineered cell models can be used to identify and characterize HSD17B11 and HSD17B13 inhibitors.

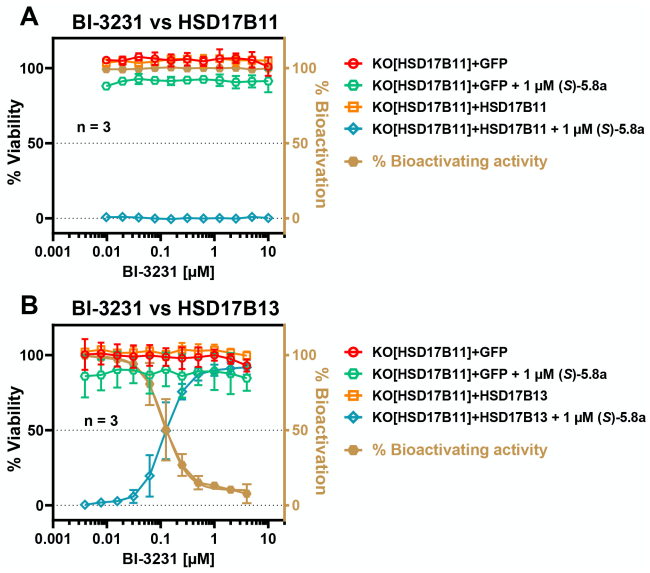

Figure 4. Using the PAC (*S*)-5.8a to identify HSD17B11/HSD17B13 specific inhibitors. U2OS KO for HSD17B11 and complemented with GFP (as a control), HSD17B11 (A) or HSD17B13 (B) were pre-incubated 1 h with the indicated concentration of BI-3231 before being cotreated for 72 h with 1 µM (*S*)-**5.8a**, a concentration which induces 100% cell death in HSD17B11 or HSD17B13-complemented cells. At the end of treatment, the viability was measured and used to compute HSD17B11/HSD17B13 cellular activity. The data correspond to three independent experiments.

Mechanistic study of PAC derivatives

We used the validated enantiomerically enriched clickable probe (*S*)-**46** to assess whether bioactivated (*S*)-PACs form Michael adducts with proteins in treated cells as previously demonstrated for (*S*)-DACs.[22] U2OS cells were treated with PACs (*S*)-**46** and (*S*)-**5.8a** as indicated, total cell extracts were collected using the strong ionic detergent sodium dodecyl sulfate (SDS), on which the copper-catalyzed azide-alkyne cycloaddition (CuAAC) to an azido-AlexaFluor647 fluorophore was performed. Heating the extracts at 95 °C in Laemmli loading buffer containing SDS and dithiothreitol (DTT), followed by migration in denaturing SDS-PAGE conditions, was used to disrupt the non-covalent interactions. Scanning the gel for the AlexaFluor647 fluorescence was subsequently used to reveal the proteins covalently modified by the clickable PAC (**Figure 5**). A set of fluorescently labeled proteins was detected in (*S*)-**46** treated extracts. This substantiates the hypothesis that (*S*)-PACs are bioactivated by HSD17B11 into protein-reactive phenyl-dialkynylketones (PACones) which subsequently undergo Michael addition of nucleophilic residues from a subset of proteins. No staining was observed with the non-clickable reference PAC (*S*)-**5.8a**. This observation supports the notion that the terminal alkyne of the dialkynylcarbinol warhead is engaged in the reaction with proteins, and therefore no longer available for the CuAAC reaction, the unbound PAC being lost during the SDS-PAGE procedure.

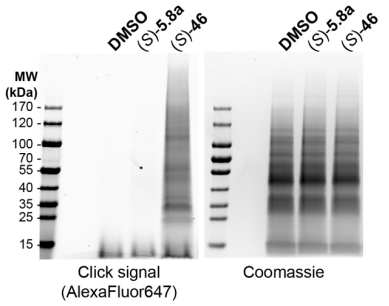

Figure 5. A (*S*)-PAC covalently modifies a set of proteins in cells. U2OS cells were treated for 2 h with 2 µM of the indicated molecules before being lysed. CuAAC was used to label the modified proteins with an azido-AlexaFluor647 fluorophore which could be detected in gel after separation by denaturing SDS-PAGE (left panel). After scanning the fluorescence, total proteins were visualized using Coomassie staining (right panel). The size of the protein ladders is indicated in kDa on the left.

The modification of a protein by a reactive lipidic entity is called lipoxidation.[24] Lipoxidation of a protein can modify its activity, its interactions with cellular components and its subcellular localization, for example by inducing its association to cellular membranes. Taking advantage of the clickable bioactive PAC (*S*)-**46**, we monitored if PAC-modified proteins presented an enrichment at membranes. For this, cells were treated with (*S*)-**46**, fixed, permeabilized and labeled using *in situ* CuAAC with an azido-AlexaFluor488 fluorophore. As shown in **Figure 6**, the non-clickable PAC (*S*)-**5.8a** did not display any staining, in agreement with the terminal alkyne of the alkynylcarbinol warhead being engaged in the reaction with proteins and with the PAC not covalently associated to proteins being washed away during the staining procedure. In contrast, the clickable PAC (*S*)-**46** displayed staining patterns related to the ones observed with the clickable DAC (*S*)-**C** and evocative of the nucleus and the endoplasmic reticulum (ER) membranes.[22] This is in line with the lipidic nature of PACs and with the localization of the bioactivating enzyme HSD17B11 at the ER and in lipid droplets.[45] A signal close to the background was observed in U2OS WT treated with (*R*)-**46** and in U2OS inactivated for HSD17B11 treated with (*S*)-**46**, supporting the notion that the staining observed with (*S*)-**46** is the readout of the stereospecific bioactivation mediated by HSD17B11 of (*S*)-PACs into protein-reactive DACones.

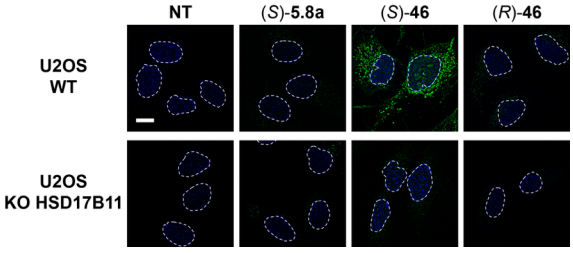

Figure 6. (*S*)-PAC-modified proteins are enriched at cellular membranes. U2OS cells, wild-type (WT) or inactivated for HSD17B11 using CRISPR/Cas9 (KO HSD17B11), were treated for 2 h with 1 µM of the indicated molecule before being fixed with paraformaldehyde and permeabilized. The modified proteins were detected using *in situ* click reaction with an azido-AlexaFluor488. The nuclear area stained with DAPI (blue) are delineated by white dashed lines. The AlexaFluor488 click staining is shown in green. The white scale bar corresponds to 10 µm.

Since DAC- and PAC-modified proteins being enriched at cellular membranes including the ER, U2OS in which the ER and mitochondrial compartments are labelled with fluorescent proteins were used to monitor through live imaging how these cell compartments are impacted by PACs (**Figure 7A**). This revealed that the PAC (*S*)-**5.8a** induces, as early as 4 h, the formation of multiple small and few large vacuoles originating from the ER. ER vacuolization is a hallmark of ER-stress, which is typically induced by the accumulation of improperly folded proteins in this compartment. The mitochondria, which is composed of an elongated network in normal conditions, was also altered by treatment by PAC (*S*)-**5.8a**, quickly losing its elongated structure (**Figure 7A**, also see **Video 1**). ER-derived vacuoles, which could also be seen in phase contrast microscopy (**Figure 7B**), preceded cell death which displayed apoptotic features such as cell shrinkage and fragmentation of the cell into multiple bodies (**Figure 7A&B**).

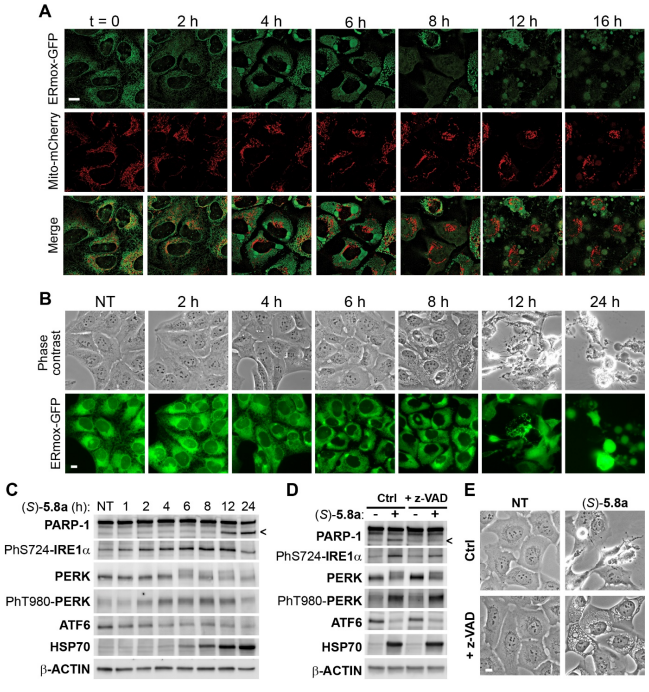

Figure 7. The PAC (*S*)-5.8a induces ER-stress and UPR activation followed by apoptotic cell death. A. U2OS cells stably co-expressing an ER-retained green-fluorescent protein variant (ER-moxGFP) and mitochondria-targeted mCherry fluorescent protein (Mito-mCherry) were treated for the indicated time with 1 µM (S)-5.8a and the mitochondria and ER compartments were monitored through live imaging on a 3D-SIM super-resolution microscope. **B.** U2OS cells stably expressing ER-moxGFP were treated for the indicated time with 1 µM PAC (*S*)-**5.8a** and their morphology was monitored through phase contrast and the ER compartment through GFP fluorescence. **C.** U2OS cells were treated with 1 µM (*S*)-**5.8a** for the indicated time and whole cell extracts were prepared and analyzed by immunoblotting to monitor UPR and apoptosis markers. **D.** U2OS cells were treated for 12 h with 1 µM (*S*)-**5.8a** in presence of the caspases inhibitor z-VAD-fmk, as indicated, and whole cell extracts prepared and analyzed as in C. **E.** U2OS cells were treated as in D and their morphology was monitored through phase contrast. The arrows on the panel C & D indicate the position of the caspase-dependent PARP-1 cleavage fragment. The white scale bars on the pictures correspond to 10 µm.

The accumulation of unfolded proteins within the ER activates three ER-resident signal transducers, which represent the three components of the Unfolded Protein Response (UPR): the IRE1α kinase/endoribonuclease (which autophosphorylates on S724), the PERK kinase (which autophosphorylates on T980) and the ATF6 transcription factor (which is cleaved into a transcriptionally active, short-lived fragment). The UPR aims at restoring ER protein homeostasis by reducing the influx of proteins into the ER and by enhancing the activity of ER protein quality control mechanisms, for example by increasing HSP70 chaperone expression.[46,47] In agreement with PAC (*S*)-**5.8a** triggering unfolded proteins accumulation and UPR activation, we observed that it induced the activation of the three UPR arms, as revealed by the rapid (between 2 to 6 h of treatment) increased autophosphorylation of IRE1α (S724) and PERK (T980) and a decrease of full-length ATF6, preceding a strong accumulation of the chaperone HSP70. Ultimately, (*S*)-**5.8a** treatment resulted in apoptosis, as marked by PARP-1 cleavage (**Figure 7C,D**), in a caspase inhibitor (z-VAD-fmk)-sensitive manner (**Figure 7D**). Caspase inhibition blocked cell death but not the vacuolization process nor the activation of the UPR (**Figure 7D,E**), supporting that ER-stress is upstream of apoptosis induction.

Acute ER-stress can result in the inhibition of the ubiquitin-proteasome system (UPS), most likely by depleting the free ubiquitin pool.[48] In agreement, we observed that treatment of U2OS cells stably expressing the UPS substrate Ub-G76V-YFP with the PAC (*S*)-**5.8a** induced the accumulation of the substrate similarly to the proteasome inhibitor bortezomib (**Figure 8A&B**). This opens prospects for PACs, considering that UPS addiction represents a targetable vulnerability in some cancers, such as multiple myeloma and mantle cell lymphoma.[49]

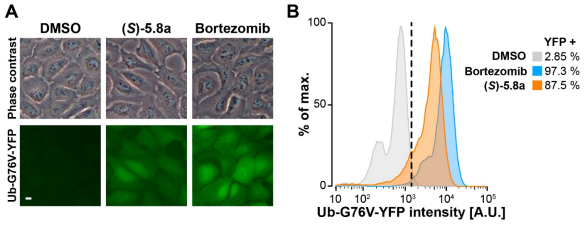

Figure 8. The PAC (*S*)-5.8a inhibits the Ubiquitin-Proteasome System (UPS). U2OS cells stably expressing the UPS substrate Ub-G76V-YFP[50] were treated for 4 h with 50 nM of proteasome inhibitor bortezomib or 1 µM of PAC (*S*)-**5.8a**. Accumulation of the UPS substrate resulting from the UPS inhibition was monitored through fluorescence microscopy (**A**) and flow cytometry (**B**). The white scale bar on the panel A corresponds to 10 µm.

Altogether these data support that PACs are enantiospecifically bioactivated into protein-reactive species which accumulate at cell membranes, including at the ER, and result into an ER-stress and UPS inhibition, triggering apoptotic cell death.

In silico docking study of PAC derivatives in HSD17B11

We undertook a molecular modelling study in order to get insights into the PACs recognition at the active site of HSD17B11, their main bioactivation enzyme. Structural analysis showed that 1YB1b,[51] the only PDB crystal structure of human HSD17B11 currently available, possesses a truncated

and misfolded structure unsuited for docking studies (see SI). As an alternative, we considered the corresponding AlphaFold[52] predicted structure, AF-Q8NBQ5-F1.[53] This model structure was found to display an appropriate degree of confidence in the proximal ligand-cofactor interaction zone of the binding site. It notably shows the presence at relevant positions of conserved catalytic site residues such as TYR185 and SER172. Structural alignments further allowed consistent insertion of the NAD+ cofactor from the human HSD17B1 PDB structure 1FDVa, a representative 17ß/1 HSD.[54] The AlphaFold model was thus submitted to a flexible docking protocol aiming at translating at a molecular level the specificity profile of LACs as enzymatic substrates.

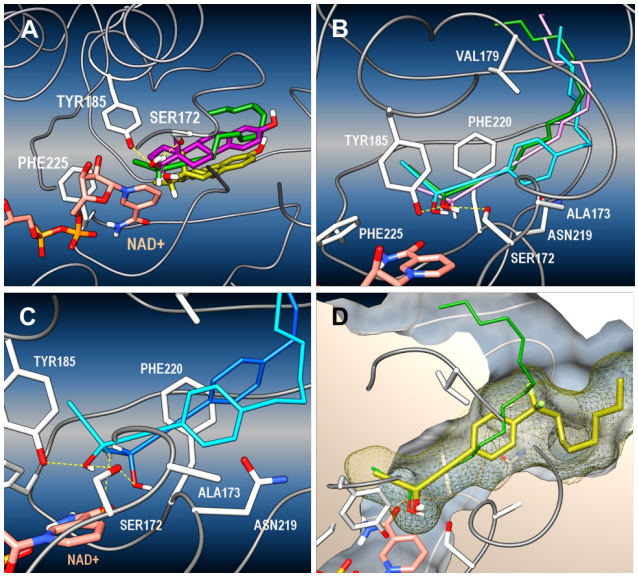

Figure 9. Docking of substrate molecules into human HSD17B11 AlphaFold Q8NBQ5 **model. A** - Comparison of crystallographic estradiol (**EST**) of 1A27a (yellow) with optimized docked poses of **EST** (pink) and (*S*)-**A** (green) in AF-Q8NBQ5 (grey ribbons) in complex with NAD+ (salmon) from the aligned 1FDVa HSD17B1 structure. For (*S*)-**A**, the oxygen-oxygen distances (yellow dashed lines) are of 2.43 Å with TYR185 (white stick) and 3.22 Å with SER172 (white sticks). **B** - Optimized poses of (*S*)-**A** (green), (S)-**5.8a** (blue) and (*S*)-**B** (light pink) in AF-Q8NBQ5 (ribbons), NAD+ from 1FDVa is shown at bottom left (salmon). For (*S*)-**A**, the oxygen-oxygen distances are of 2.47 Å with TYR185 and 3.04 Å with SER172. **C** - Optimized poses of compounds (*S*)-**5.8a** (light blue) and (*R*)-**5.8b** (dark blue) in AF-Q8NBQ5 (ribbons), NAD+ from 1FDVa is shown at bottom left (salmon). For (*S*)-**5.8a**, the distance from the carbinol hydrogen to NAD+ carbon at the position 4 of the pyridinium nucleus is of 3.36 Å; the oxygen-oxygen distances are of 2.40 Å with TYR185 and 3.59 Å with SER172. For (*R*)-**5.8a**, the oxygen-oxygen distance is of 2.84 Å with SER172. **D** - Optimized pose of (*S*)-**A** (green) with the optimized pose of (*S*)-**33c** (yellow, mesh: ligand surface) in AF-Q8NBQ5 (ribbons, clipped molecular surface), NAD+ from 1FDVa is shown at bottom left (salmon).

First, the binding of the reference DAC (*S*)-**A** was compared to that of 17 β-estradiol (**EST**), a relevant HSD17B11 substrate.[55] The calculated ligand poses were compared to the lowest energy docked conformation of **EST**. The relevance of this calculated **EST** poses is substantiated by its strong conformity with the crystallographic positioning of **EST** from PDB entry 1A27a,[56] an HSD of reference used in the initial structural analysis (see SI) (**Figure 9A**). Selected docking poses of (*S*)-**A** and **EST** shares two critical substrate binding features. First, the hydroxyl group is hydrogen-bonded with the catalytic residues TYR185 and SER172. Second, the hydrogen atom of the chiral alkynylcarbinol center points down toward the nicotinamide core of the NAD+ cofactor. In addition, the first half of the LAC backbone overlaps the steroidal framework of **EST**, while the extremity of the flexible aliphatic chain is curved out of the catalytic site. This initial set of data obtained with (*S*)-**A** gave the first molecular basis of the endogenous HSD substrate mimicry by synthetic LACs.

Then, we compared the calculated binding mode of the prototypical PAC (*S*)-**5.8a** with both that of the DAC (*S*)-**A** and the BAC (*S*)-**B** (**Figure 9B**). Lowest energy docked poses of the three series of compounds show very limited conformational fluctuations of the dialkynylcarbinol warhead. The overall positioning of the proximal region of the LAC backbone, formally substituting the tetracyclic core of **EST**, was also convergent. On the other hand, the fluctuations of the distal lipidic chain cover a large conformational space within the binding cavity (see SI). In addition to the two characteristic carbinol binding features noted earlier, the external alkyne groups establish Pi-Alkyl interactions with surrounding residues, typically TYR185, LEU182, VAL124, PHE220, ILEU226. Pi-Alkyl interactions are also found between PHE220 and the internal alkyne group, sometimes completed by Pi-Alkyl interactions with ALA173 and VAL179. This second set of results reinforced the relevance of the chemical filiation between the (*S*)-**DAC**, (*S*)-**BAC** and (*S*)-**PAC** series as HSD substrates. We further challenged our docking protocol in the AlphaFold Q8NBQ5 model of HSD17B11 with two additional examples. The enantiospecificity of the LAC bioactivation being a hallmark of their cellular mechanism of action, we comparatively docked both enantiomers of the PAC **5.8a** (**Figure 9C**). In its lowest energy pose, the distomeric (*R*)-**5.8a** loses the key hydroxyl group hydrogen bonds with TYR185, while sharing the same envelop as the compound of reference (*S*)-**A**. Most significantly the hydrogen of the chiral carbinol center now points in the direction opposite to the NAD+ pyridinium nucleus, in agreement with the notion that the weakly active (*R*)-**5.8a** would be a poor HSD17B11 substrate. Compound (*S*)-**33c** was finally selected as the most potent compound so far in the PAC series, although the correlation between the cytotoxicity of a LAC derivative and its propensity to act as an HSD substrate may be only partial. The most energetically favorable docked pose of (*S*)-**33c** displays a highly similar space arrangement of the dialkynylcarbinol warhead compared to the unsubstituted DAC of reference (*S*)-**A** (**Figure 9D**). Although the gem-difluoro moiety may locally restrain the lipidic skeleton conformation, the bending forward of the aliphatic chain illustrates a set of orientations also observed with other LACs (see SI). It is interesting to note that the CF_2 group of (*S*)-**33c** is located in the same binding subsite as the 3-OH of **EST**, suggesting that it might, to some extent, mimic the hydroxyl group on the A ring of the endogenous steroidal substrate (see SI). However, the limited reliability of AlphaFold structure in this region of the binding cavity does not allow to substantiate any stabilizing interaction with the fluorine atoms.

Pharmacokinetics studies in CD1-mice

To prepare future *in vivo* investigations of the anticancer efficacy of the PAC series, we focused on (*S*)-**5.8a**, chosen as the prototype, and evaluated its solubility in a suitable formulation, its pharmacokinetics through different delivery routes and its toxicity when performing chronic administration.

First, we established for (*S*)-**5.8a** a maximum solubility of 10.7 ± 0.6 mM in an injection solution based on 10% polyethoxylated castor oil (aka Kolliphor EL or Cremophor EL) in water (for oral route) or saline (for injections), a formulation suitable for hydrophobic molecules.

Then, four delivery routes in female CD-1 mice, intravenous (IV), intraperitoneal (IP), subcutaneous (SC) and *per os* (PO), were tested and the plasmatic concentration of (*S*)-**5.8a** was monitored (**Table 6**). The IV injection provided the measurement of (*S*)-**5.8a** plasmatic half-life which we established at 40 ± 2 min. The maximum exposure was achieved with the IV injection as compared to the IP > SC > PO routes. The bioavailability was low using the PO route. A local, non-dolorous and reversible edema was observed with the SC and IP injection. For comparison, the pharmacokinetic parameters were also measured in male CD-1 mice after IV and PO administration (**Table 7**). This revealed a slightly higher clearance in male, resulting in a lower exposure. However, small experimental variations in the collection of the 5 min time points could account for this difference.

Table 6: Pharmacokinetics parameters determined in adult female CD-1 mice.

Female	IV	per os	IP	SC
Cmax (µM)	17	0.2	1.2	0.2
t1/2 (min)	40 ± 2	33 ± 2	58 ± 14	147 ± 230
Tmax (min)		5	5	60
Cl IV (ml/min/kg)	47 ± 6			
Cl/F (ml/min/kg)		1 456 ± 236	414 ± 135	675 ± 232
Vz IV (mL/kg)	2 759 ± 479			
Vss IV (mL/kg)	1 497 ± 376			
Vz/F (mL/kg)		69 435 ± 16 430	34 354 ± 19 610	143 391 ± 78 637
AUC (min.ng/mL)	105 614 ± 13 275	3 433 ± 556	12 086 ± 3 930	7 409 ± 2 549
F (%) = bioavailab.		3.3 ± 0.9	26 ± 14	16 ± 9

Cmax: maximum plasmatic concentration observed; t1/2: plasmatic half-life; Tmax: time to reach the Cmax; Cl IV and Cl/F: Clearance; Vz IV and Vz/F: distribution volume in the elimination phase; Vss IV: distribution volume in the equilibrium phase; AUC: Area Under the Curve = exposure; F%: bioavailability.

Finally, we assessed the toxicity of (*S*)-**5.8a** in mice using three IV injections per week at 3 escalating doses, 2, 5 and 10 mg/kg. During the first ten days, no sign of toxicity or pain was observed at all three concentrations, indicating that (*S*)-**5.8a** does not display acute toxicity up to 10 mg/kg. Reversible tail swelling was observed in some mice, with the occurrence of this event increasing with the dose. For the 2 and 5 mg/kg groups, the mice bodyweight remained stable during the course of the study (**Figure 10**). In contrast, in the 10 mg/kg concentration group, the mice bodyweight started to decrease at day 10, quickly declining down to –18% by day 15, reaching the ethical endpoint. Furthermore, at day 15 in that group, the animal's general state of health was deteriorated, with a shaggy coat (5/6 mice), diarrhea (2/6 mice) and one mice found dead. Necropsies in that group did not reveal signs of organ damage but most mice had empty stomach (4/6) providing an explanation for the loss in bodyweight. These analyses support that 5 mg/kg is the maximum tolerated dose for repeated IV administration the frequency of which should be decreased to twice a week to account for the observed tail swelling. Altogether these data pave the ways for the *in vivo* exploration of the PAC series antitumor activities.

Table 7: Pharmacokinetics parameters determined in adult male CD-1 mice.

Male	IV	per os
Cmax (µM)	7	0.26
t1/2 (min)	54 ± 5	38 ± 4
Tmax (min)		15
Cl IV (ml/min/kg)	108 ± 24	
Cl/F (ml/min/kg)		1 759 ± 415
Vz IV (mL/kg)	8 401 ± 2 695	
Vss IV (mL/kg)	3 987 ± 1 757	
Vz/F (mL/kg)		97 204 ± 31 901
AUC (min.ng/mL)	46 345 ± 10 215	2 843 ± 671
F (%) = bioavailab.		6.1 ± 2.8

Cmax: maximum plasmatic concentration observed; t1/2: plasmatic half-life; Tmax: time to reach the Cmax; Cl IV and Cl/F: Clearance; Vz IV and Vz/F: distribution volume in the elimination phase; Vss IV: distribution volume in the equilibrium phase; AUC: Area Under the Curve = exposure; F%: bioavailability.

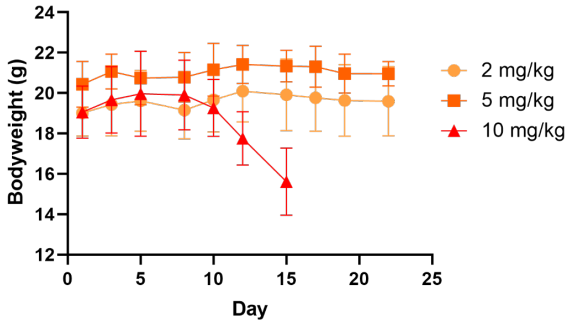

Figure 10: Mouse bodyweight evolution upon chronic treatment with (*S*)-5.8a. Balb/c mice were randomized into 3 groups of 6 mice which received (*S*)-**5.8a** by IV administration 3 times a week at the indicated dosage. The mice bodyweight was monitored as indicated.

CONCLUSION

We herein introduced new aromatic derivatives of bioinspired cytotoxic lipidic alkynylcarbinols (LACs). The so-called Phenyl diAlkynylCarbinols (PACs) series was devised to combine increased stability and structural flexibility compared to the earlier generations of synthetic LACs. Two concise synthetic routes were implemented based on alternative retrosynthetic analyses of the phenylene-conjugated dialkynylcarbinol warhead. A total of 25 different PAC derivatives, varying from both the aromatic core and the lipophilic chain, were thus generated as racemic samples. With the view to identifying the PAC cellular target, the clickable probe **46** bearing an alkyne tag at the terminal position of the aliphatic chain was also secured. A selected set of PACs was also prepared under enantioenriched form. An enantioselective route making use of a modified Carreira procedure was implemented, while a more reliable chiral preparative supercritical fluid chromatographic resolution afforded samples in up to 99% e.e. Biological evaluations showcased the pharmacological promises of the PAC series against cancer cells. Preliminary studies in racemic series showed that the representative PAC **5.8a** is indeed intrinsically more stable than its non-aromatic DiAlkynylCarbinol (DAC) **A** and Butadiynyl AlkynylCarbinol (BAC) **B** counterparts, while being more susceptible to HSD17B11-mediated bioactivation than the most active to date BAC **B** derivative in U2OS cells. Selectivity toward bioactivation by HSD17B11 *vs.* its paralogue HSD17B13 could also be advantageously tuned thanks to the structural flexibility offered by PACs. The bioactivation of some PACs by both HSD17B11 and HSD17B13 represents a valuable tool to translate the cellular catalytic activity of these enzymes into cytotoxicity which is easy to monitor. As a proof-of-concept (POC), this simple readout was used here to characterize the recently developed HSD17B13 selective inhibitor BI-3231.[44] These POC data support the notion that PACs represent valuable probes to identify and characterize inhibitors of HSD17B11 and HSD17B13 and evaluate their selectivity. Genome-wide association studies identified HSD17B13 as an attractive therapeutic target in the context of non-alcoholic fatty liver disease (NAFLD)[57] and our approach opens the prospects of simplifying the screen for novel selective HSD17B13 inhibitors. Cell viability assays against HCT116 cells with racemic samples provided structure-activity relationship trends which should be useful for further developments. The PAC **5.8a** embedding a phenylene core *para*-substituted with an 8 carbon long aliphatic chain was identified as a prototypical scaffold. Fluorine or oxygen substitutions were well tolerated, both on the aromatic core and the aliphatic chain. PACs analogues with a heteroaromatic nucleus in place of the phenylene ring were also explored, the bioinspired furan derivatives **37** being one of the most efficient compounds in this series. IC_{50} between 90-150 nM were typically observed in HCT116 cells. Study of enantioenriched PAC samples confirmed the high gap in activity between both enantiomers in favor of the (*S*)-configured eutomeric series, with IC_{50} down to 40 nM for (*S*)-**5.8a** in the more sensitive U2OS cells. Protein modification and cell imaging experiments were further carried out in either WT or KO HSD17B11 U2OS cancer cells with the clickable probe (*S*)-**46**. All the collected data substantiate the key notion that PAC derivatives are prodrugs enantiospecifically bioactivated by HSD17B11 into protein-reactive species. Modification of multiple proteins in HSD17B11 vicinity triggers an acute ER-stress, UPR activation and UPS inhibition leading to cell death by apoptosis. A docking study in the AlphaFold model of HSD17B11 was undertaken to translate at a molecular level the enantiospecific behavior of LACs as HSD substrates. The first insights into the endogenous substrate mimicry by synthetic LACs were obtained, further substantiating the chemical filiation between (*S*)-**DACs**, (*S*)-**BACs** and (*S*)-**PACs**. The *in vivo* profile of (*S*)-**5.8a**, chosen as the prototype of the PAC series, was investigated, revealing a 40 min plasmatic half-life. This is short but comparable to some chemotherapeutic agents, such as azacytidine or bortezomib.[58,59] Exploring the anticancer activity of the PAC series might require increasing this parameter to achieve longer and higher exposure. Some of the fluorinated analogues developed within this work could address this need by reducing metabolization. Different routes for administration were tested, identifying the IV injection as the best route in terms of drug exposure. (*S*)-**5.8a** was well tolerated up to 5 mg/kg with repeated IV administration but the mechanism behind the reversible tail swelling (IV) or the local edema (IP and SC route) deserves further investigations. Altogether this work provides evidence that the herein introduced PAC series offers a promising direction to evolve bioinspired synthetic LAC compounds into novel anticancer agents.

EXPERIMENTAL SECTION

Chemical synthesis

All reagents were obtained from commercial suppliers and used without any further purification. If not specified, reactions were run under nitrogen atmosphere in oven-dried glassware. Standard inert atmosphere techniques were used in handling all air and moisture sensitive reagents. Toluene, dichloromethane (DCM), tetrahydrofuran (THF), dimethylformamide (DMF) and diethyl ether were obtained by filtration through a drying column on a filtration system. Thin-layer chromatography (TLC) analyses were performed on precoated, aluminum-backed silica gel (Merck 60 F254). Visualization of the developed chromatogram was performed by UV light (254 nm) and using 10% phosphomolybdic acid in EtOH, or aqueous potassium permanganate (KMnO4) stain. All compounds were analyzed by HPLC using a BEH Shield RP18 1.7µm (2.1x100mm) column, eluted with H_2O/CH_3CN, 0.1% HCOOH (100:0 to 0:100, 0.4 mL/min) with UV detection at 254 nm. Purity was >95%. Flash chromatography columns were performed using flash silica gel (SDS 35-70 µm). Nuclear magnetic resonance spectra were recorded on a Bruker Advance 300 or 400 or 500 MHz spectrometer. Chemical shifts for 1H NMR spectra are given in parts per million (ppm) with the residual solvent resonance as the reference $CHCl_3$ (δ = 7.26 ppm). Data are reported as follows: chemical shift, multiplicity (ps = pseudo, s = singlet, d = doublet, t = triplet, q = quartet, quint = quintet, m = multiplet and br = broad), coupling constant in Hz and integration. Chemical shifts for ^{13}C NMR spectra are given in ppm using the central peak of $CDCl_3$ (δ = 77.16 ppm) as the reference. All ^{13}C NMR spectra were obtained with complete proton decoupling. Infrared analyses were run on a Thermo-Nicolet Diamond ATR (4 cm^{-1} of resolution, 16 scans) equipped with a DTGS detector and are reported in reciprocal centimeters (cm^{-1}). High-resolution mass spectrometry (HRMS) was performed on a Thermo-Finnigan MAT 95 XL instrument. Mass spectrometry m/z values are given in Dalton units. Optical rotations were measured on a Jasco P-2000 polarimeter. $[\alpha]_D$ values are given in $deg.dm^{-1}.cm^3.g^{-1}$.

Route A:

General procedure for the synthesis of intermediates 2.6a-2.12a, 2.8b-c, 7a-b, 12.6-12.10, 17, 22.10 and 22.12. In a nitrogen-flushed two-necked flask equipped with a stirring bar, a reflux condenser and a rubber septum were introduced $Pd(PPh_3)_2Cl_2$ (5 mol%) and copper(I) iodide (5 mol%). The flask was flushed with nitrogen, then, freshly distilled and degassed Et_3N (0.7 M) was added followed by aryl bromide. Trimethylsilylacetylene (1.2 equiv.) was then slowly added dropwise and the solution was stirred at 80 °C for 15 h. After cooling to rt, the reaction mixture was quenched with aqueous HCl solution (1M) and extracted 3x with diethyl ether. The combined organic layers were dried over $MgSO_4$, filtered and concentrated under reduced pressure. The crude product was purified by flash column chromatography (silica gel) to afford the target silylated alkyne.

((4-Hexylphenyl)ethynyl)trimethylsilane (2.6a). The crude mixture was purified by flash column chromatography using up to 10% diethyl ether in pentane. The silylated alkyne **2.6a** (1.03 g, 82% yield) was isolated as a colourless oil. All analyses agreed with data reported in the literature.[61]

((4-Octylphenyl)ethynyl)trimethylsilane (2.8a). The crude mixture was purified by flash column chromatography using 100% pentane. The silylated alkyne **2.8a** (561 mg, 84% yield) was isolated as a yellow oil. All analyses agreed with data reported in the literature.[60]

((4-Nonylphenyl)ethynyl)trimethylsilane (2.9a). The crude mixture was purified by flash column chromatography using 100% pentane. The silylated alkyne **2.9a** (270 mg, 30% yield) was isolated as a yellow oil. **^{1}H NMR** (300 MHz, $CDCl_3$) δ (ppm) 7.37 (d, J = 8.3 Hz, 2H), 7.10 (d, J = 8.3 Hz, 2H), 2.58 (ps t, J = 7.7 Hz, 2H), 1.68 – 1.36 (m, 2H), 1.37 – 1.13 (m, 12H), 0.88 (t, J = 6.7 Hz, 3H), 0.24 (s, 9H). **^{13}C NMR** (75 MHz, $CDCl_3$) δ (ppm) 143.8, 132.0, 128.5, 120.4, 105.6, 93.4, 36.0, 32.0, 31.4, 29.7, 29.6, 29.5, 29.3, 22.8, 14.3, 0.2. **HRMS** (DCI-CH_4) *m/z*: calcd for $C_{20}H_{33}Si$ $[M+H]^+$: 301.2352, found: 301.2338. **FTIR** (cm^{-1}) (neat): 2954, 2919, 2854, 2161, 1507, 1251, 868, 838,759.

((4-Decylphenyl)ethynyl)trimethylsilane (2.10a). The crude mixture was purified by flash column chromatography using 100% pentane. The silylated alkyne **2.10a** (223 mg, 71% yield) was isolated as a yellow oil. All analyses agreed with data reported in the literature.[61]

((4-Dodecylphenyl)ethynyl)trimethylsilane (2.12a). The crude mixture was purified by flash column chromatography using 100% pentane. The silylated alkyne **2.12a** (1.57 g, 57% yield) was isolated as a yellow oil. All analyses agreed with data reported in the literature.[62]

((3-Fluoro-4-octylphenyl)ethynyl)trimethylsilane (2.8b). The crude mixture was purified by flash column chromatography using 100% pentane. The silylated alkyne **2.8b** (387 mg, 91% yield) was isolated as a brown oil. **^{1}H NMR** (300 MHz, $CDCl_3$) δ (ppm) 7.19 – 7.04 (m, 3H), 2.61 (ps t, J = 7.7 Hz, 2H), 1.63 – 1.49 (m, 2H), 1.35 – 1.15 (m, 10H), 0.88 (t, J = 6.7 Hz, 3H), 0.24 (s, 9H). **^{13}C NMR** (75 MHz, $CDCl_3$) δ (ppm) 160.6 (d, J = 245.4 Hz), 130.9 (d, J = 16.4 Hz), 130.6 (d, J = 6.0 Hz), 127.8 (d, J = 3.3 Hz), 122.2 (d, J = 9.5 Hz), 118.6 (d, J = 24.2 Hz), 104.1 (d, J = 2.9 Hz), 94.5, 32.0, 30.1, 29.5, 29.4, 29.4, 29.1 (d, J = 2.0 Hz), 22.8, 14.2, 0.1. **^{19}F NMR** (282 MHz, $CDCl_3$) δ (ppm) -118.8 (dd, J = 10.0, 7.7 Hz). **HRMS** (DCI-CH_4) *m/z*: calcd for $C_{19}H_{30}FSi$ $[M+H]^+$: 304.2101, found: 305.2091. **FTIR** (cm^{-1}) (neat): 2958, 2926, 2854, 2154, 2072, 1250, 843.

((2-Fluoro-4-octylphenyl)ethynyl)trimethylsilane (2.8c). The crude mixture was purified by flash column chromatography using 100% pentane. The silylated alkyne **2.8c** (242 mg, 80% yield) was isolated as a slightly yellow liquid. **^{1}H NMR** (300 MHz, $CDCl_3$) δ (ppm) 7.33 (t, J = 7.7 Hz, 1H), 6.91 – 6.82 (m, 2H), 2.58 (t, J = 7.7 Hz, 2H), 1.64 – 1.50 (m, 2H), 1.36 – 1.19 (m, 10H), 0.88 (t, J = 6.7 Hz, 3H), 0.26 (s, 9H). **^{13}C NMR** (75 MHz, $CDCl_3$) δ (ppm) 163.0 (d, J = 251.5 Hz), 146.4 (d, J = 7.4 Hz), 133.5 (d, J = 1.7 Hz), 124.0 (d, J = 3.1 Hz), 115.3 (d, J = 20.6 Hz), 108.8 (d, J = 15.9 Hz), 99.1 (d, J = 3.0 Hz), 98.3, 35.7 (d, J = 1.4 Hz), 31.9, 30.9, 29.4, 29.2, 29.1, 22.7, 14.1, -0.1. **^{19}F NMR** (282 MHz, $CDCl_3$) δ (ppm) -110.6 (dd, J = 10.5, 7.1 Hz). **HRMS** (DCI-CH_4) *m/z*: calcd for $C_{19}H_{30}FSi$ $[M+H]^+$: 305.2101, found: 305.2090. **FTIR** (cm^{-1}) (neat): 2957, 2927, 2856, 2162, 1250, 862, 843, 760.

((4-(Heptyloxy)phenyl)ethynyl)trimethylsilane (7a). The crude mixture was purified by flash column chromatography using 100% pentane. The silylated alkyne **7a** (2.07 mg, 90% yield) was isolated as a slightly yellow liquid. All analyses agreed with data reported in the literature.[63]

((4-(2-(2-ethoxyethoxy)ethoxy)phenyl)ethynyl)trimethylsilane (7b). The crude mixture was purified by flash column chromatography using up to 70% diethyl ether in pentane. The silylated alkyne **7b** (582 mg, 46% yield) was isolated as a colourless oil. **^{1}H NMR** (300 MHz, $CDCl_3$) δ (ppm) 7.40 – 7.37 (m, 2H), 6.84 – 6.81 (m, 2H), 4.13 (t, J = 4.7 Hz, 2H), 3.85 (t, J = 5.0 Hz, 2H), 3.72 – 3.70 (m, 2H), 3.62 – 3.60 (m, 2H), 3.53 (q, J = 7.1 Hz, 2H), 1.21 (t, J = 7.0 Hz, 3H), 0.22 (s, 9H). **^{13}C NMR** (75 MHz, $CDCl_3$) δ (ppm) 159.1, 133.6, 114.6, 105.3, 92.6, 71.1, 70.0, 69.8, 67.6, 66.8, 53.6, 15.3, 0.17. **HRMS** (DCI-CH_4) *m/z*: calcd for $C_{17}H_{27}O_3Si$ $[M+H]^+$: 307.1718, found: 307.1729. **FTIR** (cm^{-1}) (neat): 2955, 2923, 2866, 2155, 1604, 1506, 1247, 1111, 863, 838, 760.

((3-Hexylphenyl)ethynyl)trimethylsilane (12.6). The crude mixture was purified by flash column chromatography using up to 10% diethyl ether in pentane. The silylated alkyne **12.6** (700 mg, 72% yield) was isolated as a colourless oil. **^{1}H NMR** (300 MHz, $CDCl_3$) δ (ppm) 7.32 – 7.25 (m, 2H), 7.19 (td, J = 7.4, 0.9 Hz, 1H), 7.12 (dt, J = 7.6, 1.7 Hz, 1H), 2.55 (t, J = 7.5 Hz, 2H), 1.75 – 1.53 (m, 2H), 1.35 – 1.22 (m, 6H), 0.88 (t, J = 6.6 Hz, 3H), 0.24 (s, 9H). **^{13}C NMR** (75 MHz, $CDCl_3$) δ (ppm) 143.1, 132.1, 129.4, 129.0, 128.2, 123.0, 105.6, 93.6, 35.8, 31.8, 31.4, 29.1, 22.7, 14.2, 0.2. **HRMS** (DCI-CH_4) *m/z*: calcd for $C_{17}H_{27}Si$ $[M+H]^+$: 259.1886, found: 259.1882. **FTIR** (cm^{-1}) (neat): 2957, 2927, 2856, 2156, 1249, 841, 792, 759, 694, 433, 419, 408.

((3-Nonylphenyl)ethynyl)trimethylsilane (12.9). The crude mixture was purified by flash column chromatography using up to 10% diethyl ether in pentane. The silylated alkyne **12.9** (557 mg, quantitative yield) was isolated as a slightly yellow oil. **^{1}H NMR** (300 MHz, $CDCl_3$) δ (ppm) 7.32 – 7.24 (m, 2H), 7.23 – 7.08 (m, 2H), 2.56 (t, J = 7.6 Hz, 2H), 1.68 – 1.53 (m, 2H), 1.36 – 1.21 (m, 12H), 0.88 (t, J = 6.7 Hz, 3H), 0.25 (s, 9H). **^{13}C NMR** (75 MHz, $CDCl_3$) δ (ppm) 143.1, 132.1, 129.4, 129.0, 128.2, 123.0, 105.6, 93.7, 35.9, 32.0, 31.5, 29.7, 29.6, 29.5, 29.4, 22.8, 14.3, 0.2.

((3-Decylphenyl)ethynyl)trimethylsilane(12.10). The crude mixture was purified by flash column chromatography using up to 10% diethyl ether in pentane. The silylated alkyne **12.10** (488 mg, 71% yield) was isolated as a colourless oil. All analyses agreed with data reported in the literature.[64]

Trimethyl((6-octylnaphthalen-2-yl)ethynyl)silane (17). The crude mixture was purified by flash column chromatography using 100% pentane. The silylated alkyne **17** (280 mg, 85% yield) was isolated as a yellow solid. **^{1}H NMR** (300 MHz, $CDCl_3$) δ (ppm) 7.96 (s, 1H), 7.69 (dd, J = 8.5, 3.4 Hz, 2H), 7.56 (s, 1H), 7.47 (dd, J = 8.5, 1.6 Hz, 1H), 7.33 (dd, J = 8.4, 1.7 Hz, 1H), 2.75 (t, J = 7.8 Hz, 2H), 1.69 (quint, J = 7.5 Hz, 2H), 1.42 – 1.20 (m, 10H), 0.88 (t, J = 6.7 Hz, 3H), 0.28 (s, 9H). **^{13}C NMR** (75 MHz, $CDCl_3$) δ (ppm) 141.8, 133.3, 131.9, 131.5, 128.7, 128.3, 127. 8, 127.5, 126.3, 119.6, 105.9, 94.2, 36.3, 32.0, 31.4, 29.6, 29.5, 29.4, 22.8, 14.3, 0.2. **HRMS** (DCI-CH_4) *m/z*: calcd for $C_{23}H_{33}Si$ $[M+H]^+$: 337.2354, found: 337.2352. **FTIR** (cm^{-1}) (neat): 2961, 2924, 2853, 2154, 1249, 859, 759, 640, 474.

((5-Decylthiophen-2-yl)ethynyl)trimethylsilane (22.10). The crude mixture was purified by flash column chromatography using 100% pentane. The silylated alkyne **22.10** (495 mg, 94% yield) was isolated as a brown oil. **^{1}H NMR** (300 MHz, $CDCl_3$) δ (ppm) 7.04 (d, J = 3.6 Hz, 1H), 6.60 (d, J = 3.6 Hz, 1H), 2.75 (ps t, J = 7.5 Hz, 2H), 1.74 – 1.56 (m, 2H), 1.40 – 1.14 (m, 14H), 0.88 (t, J = 6.7 Hz, 3H), 0.23 (s, 9H). **FTIR** (cm^{-1}) (neat): 2958, 2924, 2854, 2145, 2068, 1249, 856, 842.

((5-Dodecylthiophen-2-yl)ethynyl)trimethylsilane (22.12). The crude mixture was purified by flash column chromatography using

100% pentane. The silylated alkyne **22.12** (312 mg, 74% yield) was isolated as a brown oil. **^{1}H NMR** (300 MHz, $CDCl_3$) δ (ppm) 7.04 (d, J = 3.6 Hz, 1H), 6.60 (d, J = 3.6 Hz, 1H), 2.76 (ps t, J = 7.5 Hz, 2H), 1.64 (dt, J = 14.7, 7.5 Hz, 2H), 1.37 – 1.19 (m, 18H), 0.88 (t, J = 6.7 Hz, 3H), 0.23 (s, 9H). **^{13}C NMR** (75 MHz, $CDCl_3$) δ (ppm) 148.6, 135.4, 132.8, 124.1, 98.3, 32.1, 31.7, 30.3, 29.8, 29.8, 29.7, 29.5, 29.5, 29.1, 22.8, 14.3, 0.1. **HRMS** (DCI-CH_4) *m/z*: calcd for $C_{21}H_{37}SSi$ $[M+H]^+$: 349.2385, found: 349.2385. **FTIR** (cm^{-1}) (neat): 2956, 2924, 2853, 2145, 1249, 857, 843.

General procedure for the synthesis of intermediates 3.6a-3.12a, 3.8b-c, 8a-b, 13.6-13.10, 18, 23.10 and 23.12. A solution of the silylated alkyne in MeOH (0.06 M) containing K_2CO_3 (0.2 equiv.) was stirred at RT overnight. DCM and water were added and extraction was realized with DCM (3x). The combined organic layers were dried over $MgSO_4$, filtered and concentrated under reduced pressure. The crude product was purified by flash column chromatography (silica gel) with 100% pentane to afford the target terminal alkyne.

1-Ethynyl-4-hexylbenzene (3.6a). The crude mixture was purified by flash column chromatography using up to 10% diethyl ether in pentane. The product **3.6a** (397 mg, 82% yield) was isolated as a yellow oil. All analyses agreed with data reported in the literature.[61]

1-Ethynyl-4-octylbenzene (3.8a). The crude mixture was purified by flash column chromatography using 100% pentane. The terminal alkyne **3.8a** (423 mg, quantitative yield) was isolated as a yellow oil. All analyses agreed with data reported in the literature.[60]

1-Ethynyl-4-nonylbenzene (3.9a). The crude mixture was purified by flash column chromatography using 100% pentane. The terminal free alkyne **3.9a** (202 mg, 98% yield) was isolated as a bright yellow oil. **^{1}H NMR** (300 MHz, $CDCl_3$) δ (ppm) 7.40 (d, J = 8.2 Hz, 2H), 7.13 (d, J = 8.4 Hz, 2H), 3.03 (s, 1H), 2.60 (ps t, J = 7.8 Hz, 2H), 1.72 – 1.44 (m, 2H), 1.36 – 1.11 (m, 12H), 0.88 (t, J = 6.7 Hz, 3H). **^{13}C NMR** (75 MHz, $CDCl_3$) δ (ppm) 144.2, 132.2, 128.6, 119.3, 76.6, 36.0, 32.0, 31.4, 29.7, 29.6, 29.5, 29.4, 22.8, 14.3. **HRMS** (DCI-CH_4) *m/z*: calcd for $C_{17}H_{25}$ $[M+H]^+$: 229.1956, found: 229.1955. **FTIR** (cm^{-1}) (neat): 3303, 2955, 2925, 2854, 2105, 1508, 1466, 840, 821.

1-Ethynyl-4-decylbenzene (3.10a). The crude mixture was purified by flash column chromatography using 100% pentane. The terminal free alkyne **3.10a** (37 mg, 95%) was isolated as a yellow oil. All analyses agreed with data reported in the literature.[61]

1-Ethynyl-4-dodecylbenzene (3.12a): The crude mixture was purified by flash column chromatography using 100% pentane. The terminal free alkyne **3.12a** (40 mg, 68%) was isolated as a yellow oil. All analyses agreed with data reported in the literature.[62]

4-Ethynyl-2-fluoro-1-octylbenzene (3.8b). The crude mixture was purified by flash column chromatography using 100% pentane. The terminal free alkyne **3.8b** (44 mg, 38% yield) was isolated as a yellow oil. **^{1}H NMR** (300 MHz, $CDCl_3$) δ (ppm) 7.22 – 7.07 (m, 3H), 3.05 (s, 1H), 2.62 (t, J = 7.7 Hz, 2H), 1.65 – 1.53 (m, 2H), 1.39 – 1.20 (m, 10H), 0.88 (t, J = 6.8 Hz, 3H). **^{13}C NMR** (75 MHz, $CDCl_3$) δ (ppm) 160.6 (d, J = 245.4 Hz), 131.3 (d, J = 16.4 Hz), 130.7 (d, J = 6.0 Hz), 128.0 (d, J = 3.4 Hz), 121.1 (d, J = 9.6 Hz), 118.9 (d, J = 24.5 Hz), 82.8 (d, J = 3.1 Hz), 77.4, 32.0, 30.1 (d, J = 1.0 Hz), 29.5, 29.4, 29.4, 29.1 (d, J = 2.0 Hz), 22.8, 14.2. **^{19}F NMR** (282 MHz, $CDCl_3$) δ (ppm) -118.5 (dd, J = 10.3 Hz, 7.5 Hz). **HRMS** (DCI-CH_4) *m/z*: calcd for $C_{16}H_{22}F$ $[M+H]^+$: 233.1706, found: 233.1698. **FTIR** (cm^{-1}) (neat): 3306, 2955, 2926, 2856, 2110.

1-Ethynyl-2-fluoro-4-octylbenzene (3.8c). The crude terminal free alkyne **3.8c** (73 mg, 96% yield) was used without further purification as a yellow oil. **^{1}H NMR** (300 MHz, $CDCl_3$) δ (ppm) 7.31 (t, J = 7.7 Hz, 1H), 6.90 – 6.77 (m, 2H), 3.20 (s, 1H), 2.53 (ps t, J = 7.7 Hz, 2H), 1.60 – 1.44 (m, 2H), 1.31 – 1.12 (m, 10H), 0.82 (t, J = 6.9, 3H). **^{19}F NMR** (282 MHz, $CDCl_3$) δ (ppm) -111.1. **FTIR** (cm^{-1}) (neat): 3300, 2927, 2856, 2114, 1426.

1-Ethynyl-4-(heptyloxy)benzene (8a). The crude terminal free alkyne **8a** (1.30 mg, 84% yield) was used without further purification as a yellow oil. All analyses agreed with data reported in the literature.[63]

1-(2-(2-Ethoxyethoxy)ethoxy)-4-ethynylbenzene (8b). The crude mixture was purified by flash column chromatography using up to 80% diethyl ether in pentane. The terminal alkyne **8b** (369 mg, 83% yield) was isolated as a yellow oil. **^{1}H NMR** (300 MHz, $CDCl_3$) δ (ppm) 7.43 – 7.40 (m, 2H), 6.87 – 6.84 (m, 2H), 4.14 (t, J = 4.7 Hz, 2H), 3.86 (t, J = 5.0 Hz, 2H), 3.73 – 3.70 (m, 2H), 3.63 – 3.59 (m, 2H), 3.53 (q, J = 7.0 Hz, 2H), 2.99 (s, 1H), 1.22 (t, J = 7.0 Hz, 3H). **^{13}C NMR** (75 MHz, $CDCl_3$) δ (ppm) 159.3, 133.7, 114.7, 114.5, 83.8, 75.9, 71.1, 70.0, 69.8, 67.6, 66.9, 15.3. **HRMS** (DCI-CH_4) *m/z*: calcd for $C_{14}H_{19}O_3$ $[M+H]^+$: 235.1330, found: 235.1334. **FTIR** (cm^{-1}) (neat): 3278, 3253, 2977, 2933, 2873, 2107, 1605, 1506, 1248, 1110, 834.

1-Ethynyl-3-hexylbenzene (13.6). The crude mixture was purified by flash column chromatography using up to 15% diethyl ether in pentane. The terminal alkyne **13.6** (373 mg, 81% yield) was isolated as a yellow oil. **^{1}H NMR** (300 MHz, $CDCl_3$) δ (ppm) 7.35 – 7.27 (m, 2H), 7.27 – 7.12 (m, 2H), 3.04 (s, 1H), 2.57 (t, J = 7.5 Hz, 2H), 1.65 – 1.55 (m, 2H), 1.37 – 1.23 (m, 6H), 0.88 (t, J = 6.6 Hz, 3H). **^{13}C NMR** (75 MHz, $CDCl_3$) δ (ppm) 143.3, 132.3, 129.6, 129.2, 128.4, 122.0, 84.1, 76.7, 35.8, 31.8, 31.4, 29.1, 22.7, 14.2. **HRMS** (DCI-CH_4) *m/z*: calcd for $C_{14}H_{19}$ $[M+H]^+$: 187.1478, found: 187.1478. **FTIR** (cm^{-1}) (neat): 3316, 2961, 2927, 2857, 2107, 1480, 799, 698.

1-Ethynyl-3-nonylbenzene (13.9). The crude mixture was purified by flash column chromatography using up to 20% diethyl ether in pentane. The terminal alkyne **13.9** (420 mg, quantitative yield) was isolated as a yellow oil. **^{1}H NMR** (300 MHz, $CDCl_3$) δ (ppm) 7.33 – 7.29 (m, 2H), 7.25 – 7.14 (m, 2H), 3.05 (s, 1H), 2.58 (t, J = 7.8 Hz, 2H), 1.66 – 1.54 (m, 2H), 1.37 – 1.15 (m, 12H), 0.88 (t, J = 6.7 Hz, 3H). **^{13}C NMR** (75 MHz, $CDCl_3$) δ (ppm) 143.4, 132.3, 129.7, 129.3, 128.4, 122.1, 84.2, 76.9, 35.9, 32.1, 31.5, 29.8, 29.7, 29.6, 29.5, 22.9, 14.4.

1-Ethynyl-3-decylbenzene (13.10). The crude mixture was purified by flash column chromatography using up to 10% diethyl ether in pentane. The terminal alkyne **13.10** (225 mg, 85% yield) was isolated as a yellow oil. All analyses agreed with data reported in the literature.[64]

2-Ethynyl-6-octylnaphthalene (18). The crude mixture was purified by flash column chromatography using 100% pentane. The terminal free alkyne **18** (190 mg, 98% yield) was isolated as a yellow oil. **^{1}H NMR** (300 MHz, $CDCl_3$) δ (ppm) 7.98 (s, 1H), 7.71 (d, J = 8.3 Hz, 2H), 7.58 (s, 1H), 7.49 (dd, J = 8.4, 1.5 Hz, 1H), 7.35 (dd, J = 8.4, 1.6 Hz, 1H), 3.12 (s, 1H), 2.76 (t, J = 7.8 Hz, 2H), 1.70 (quint, J = 7.3 Hz, 2H), 1.42 – 1.18 (m, 10H), 0.88 (t, J = 6.7 Hz, 3H). **^{13}C NMR** (75 MHz, $CDCl_3$) δ (ppm) 142.0, 133.4, 132.2, 131.4, 128.7, 128.4, 127.8, 127. 7, 126.4, 118.5, 84.4, 76.9, 36.3, 32.0, 31.4, 29.6, 29.5, 29.4, 22.8, 14.3. **FTIR** (cm^{-1}) (neat): 3310, 2954, 2925, 2854, 2107, 890, 815, 475.

2-Decyl-5-ethynylthiophene (23.10). The crude terminal free alkyne **23.10** was obtained and used without further purification as a brown oil. **^{1}H NMR** (300 MHz, $CDCl_3$) δ (ppm) 7.09 (d, J = 3.6 Hz, 1H), 6.63 (dt, J = 3.6, 0.9 Hz, 1H), 3.28 (s, 1H), 2.77 (t, J = 7.3 Hz, 2H), 1.65 (dt, J = 14.9, 7.6 Hz, 2H), 1.44 – 1.06 (m, 14H), 0.88 (t, J = 6.7 Hz, 3H).[65]

2-Dodecyl-5-ethynylthiophene (23.12). The crude mixture was purified by flash column chromatography using 100% pentane. The terminal free alkyne **23.12** (131 mg, quantitative yield) was isolated as a yellow oil. **^{1}H NMR** (300 MHz, $CDCl_3$) δ (ppm) 7.09 (d, J = 3.6 Hz, 1H), 6.63 (dt, J = 3.6, 0.9 Hz, 1H), 3.28 (s, 1H), 2.77 (ps t, J = 7.4 Hz, 2H), 1.65 (quint, J = 7.5 Hz, 2H), 1.45 – 1.11 (m, 18H), 0.88 (t, J = 6.7 Hz, 3H). **^{13}C NMR** (75 MHz, $CDCl_3$) δ (ppm) 148.8, 133.3, 124.1, 119.3, 80.5, 77.4, 32.1, 31.7, 30.3, 29.8, 29.8, 29.8, 29.7, 29.5, 29.5, 29.2, 22.8, 14.3. **HRMS** (DCI-CH_4) *m/z*: calcd for $C_{18}H_{29}S$ $[M+H]^+$: 277.1990, found: 277.1985. **FTIR** (cm^{-1}) (neat): 3311, 2924, 2853, 2103, 1463, 801.

General procedure for the synthesis of intermediates 4.6a-4.12a, 4.8b-c, 9a-b, 14.6-14.10, 19, 24.10 and 24.12. A flame-dried flask was charged with a solution of terminal alkyne in THF (0.3 M) under dry argon atmosphere at -78 °C. To the stirred solution, *n*-

butyllithium (1.2 equiv., 2.5M in hexanes) was added dropwise. The solution was stirred for 45 min at the same temperature, (trimethylsilyl)propiolaldehyde (1.0 equiv.) was then added dropwise and the mixture was stirred for 3 h at rt. After treatment with sat. aqueous NH_4Cl solution and addition of water, the aqueous layer was extracted with DCM, the combined organic phases were then dried over $MgSO_4$ and concentrated under reduced pressure. The crude product was purified by flash column chromatography (silica gel) to afford the target silylated PAC.

1-(4-Hexylphenyl)-5-(trimethylsilyl)penta-1,4-diyn-3-ol (4.6a). The crude mixture was purified by flash column chromatography using up to 30% diethyl ether in pentane. The silylated PAC **4.6a** (474 mg, 71% yield) was isolated as a yellow oil. **^{1}H NMR** (300 MHz, $CDCl_3$) δ (ppm) 7.42 – 7.35 (m, 2H), 7.16 – 7.10 (m, 2H), 5.33 (s, 1H), 2.60 (t, J = 7.4 Hz, 2H), 1.66 – 1.52 (m, 2H), 1.37 – 1.22 (m, 6H), 0.87 (t, J = 6.6 Hz, 3H), 0.21 (s, 9H). **^{13}C NMR** (75 MHz, $CDCl_3$) δ (ppm) 144.2, 131.9, 128.6, 119.2, 102.0, 89.9, 85.2, 84.8, 53.3, 36.0, 31.8, 31.3, 29.0, 22.7, 14.2, -0.2. **HRMS** (DCI-CH_4) *m/z*: calcd for $C_{20}H_{29}OSi$ $[M+H]^+$: 313.1987, found: 313.1988. **FTIR** (cm^{-1}) (neat): 3370, 2957, 2928, 2857, 2236, 2183, 1250, 1042, 844, 761.

1-(4-Octylphenyl)-5-(trimethylsilyl)penta-1,4-diyn-3-ol (4.8a). **T**he crude mixture was purified by flash column chromatography using up to 30% diethyl ether in pentane. The silylated PAC **4.8a** (183 mg, 58% yield) was isolated as a yellow oil. **^{1}H NMR** (300 MHz, $CDCl_3$) δ (ppm) 7.38 (d, J = 8.2 Hz, 2H), 7.12 (d, J = 8.2 Hz, 2H), 5.34 (d, J = 7.1 Hz, 1H), 2.59 (t, J = 7.7 Hz, 2H), 2.42 (d, J = 7.3 Hz, OH), 1.58 (quint, J = 7.3 Hz, 2H), 1.39 – 1.09 (m, 10H), 0.87 (t, J = 6.6 Hz, 3H), 0.20 (s, 9H). **^{13}C NMR** (75 MHz, $CDCl_3$) δ (ppm) 144.2, 131.9, 128.6, 119.2, 102.0, 89.7, 85.4, 84.8, 53.2, 36.0, 32.0, 31.3, 29.6, 29.4, 22.8, 14.2, -0.2. **HRMS** (DCI-CH_4) *m/z*: calcd for $C_{22}H_{33}OSi$ $[M+H]^+$: 341.2301, found: 341.2311. **FTIR** (cm^{-1}) (neat): 3368, 3028, 2957, 2926, 2854, 2234, 2179, 1508, 1297, 1250, 1024, 845, 760.

1-(4-Nonylphenyl)-5-(trimethylsilyl)penta-1,4-diyn-3-ol (4.9a). The crude mixture was purified by flash column chromatography using up to 30% diethyl ether in pentane. The silylated PAC **4.9a** (298 mg, 95% yield) was isolated as a brown oil. **^{1}H NMR** (300 MHz, $CDCl_3$) δ (ppm) 7.38 (d, J = 8.2 Hz, 2H), 7.13 (d, J = 8.3 Hz, 2H), 5.33 (br s, 1H), 2.59 (t, J = 7.7 Hz, 2H), 2.25 (br s, OH), 1.67 – 1.46 (m, 2H), 1.39 – 1.13 (m, 12H), 0.88 (t, J = 6.7 Hz, 3H), 0.21 (s, 9H). **^{13}C NMR** (75 MHz, $CDCl_3$) δ (ppm) 144.3, 131.9, 128.6, 119.2, 102.0, 89.8, 85.4, 84.9, 53.3, 36.1, 32.0, 31.4, 29.7, 29.6, 29.5, 29.4, 22.8, 14.3, -0.2. **HRMS** (DCI-CH_4) *m/z*: calcd for $C_{23}H_{35}OSi$ $[M+H]^+$: 355.2457, found: 355.2450. **FTIR** (cm^{-1}) (neat): 3348 (br), 2956, 2925, 2854, 2233, 2179, 1250, 1042, 843, 761.

1-(4-Decylphenyl)-5-(trimethylsilyl)penta-1,4-diyn-3-ol (4.10a). The crude mixture was purified by flash column chromatography using up to 30% diethyl ether in pentane. The silylated PAC **4.10a** (26 mg, 56% yield) was isolated as a brown oil. **^{1}H NMR** (300 MHz, $CDCl_3$) δ (ppm) 7.44 (d, J = 8.2 Hz, 2H), 7.19 (d, J = 8.3 Hz, 2H), 5.42 (s, 1H), 2.61 (t, J = 7.8 Hz, 2H), 2.55 (br s, OH), 1.67 – 1.52 (m, 2H), 1.39 – 1.13 (m, 8H), 0.88 (t, J = 6.7 Hz, 3H), 0.21 (s, 9H).

1-(4-Dodecylphenyl)-5-(trimethylsilyl)penta-1,4-diyn-3-ol (4.12a). The crude mixture was purified by flash column chromatography using up to 30% diethyl ether in pentane. The silylated PAC **4.12a** (183 mg, 58% yield) was isolated as a yellow oil. **^{1}H NMR** (300 MHz, $CDCl_3$) δ (ppm) 7.38 (d, J = 8.2 Hz, 2H), 7.12 (d, J = 8.3 Hz, 2H), 5.33 (d, J = 7.0 Hz, 1H), 2.59 (t, J = 8.0 Hz, 2H), 2.25 (d, J = 7.4 Hz, OH), 1.65 – 1.61 (m, 2H), 1.37 – 1.19 (m, 18H), 0.88 (t, J = 6.7 Hz, 3H), 0.20 (s, 9H). **^{13}C NMR** (75 MHz, $CDCl_3$) δ (ppm) 144.3, 131.9, 128.6, 119.2, 102.0, 85.4, 84.9, 53.3, 36.1, 32.1, 31.4, 29.8, 29.8, 29.7, 29.6, 29.5, 29.4, 22.8, 14.3, -0.2. **HRMS** (DCI-CH_4) *m/z*: calcd for $C_{26}H_{41}OSi$ $[M+H]^+$: 397.2927, found: 397.2918. **FTIR** (cm^{-1}) (neat): 3345 (br), 2923, 2853, 2236, 2176, 1250, 1041, 843, 760.

1-(3-Fluoro-4-octylphenyl)-5-(trimethylsilyl)penta-1,4-diyn-3-ol (4.8b). The crude silylated PAC **4.8b** (68 mg, quantitative yield) was used without further purification as a brown oil. **^{1}H NMR** (300 MHz, $CDCl_3$) δ (ppm) 7.18 – 7.03 (m, 3H), 5.30 (br d, J = 4.8 Hz, 1H), 2.60 (ps t, J = 7.7 Hz, 2H), 2.28 (br d, J = 5.2 Hz, OH), 1.71 – 1.43 (m, 2H), 1.40 – 1.10 (m, 10H), 0.86 (t, J = 6.7 Hz, 3H), 0.19 (s, 9H).

1-(2-fluoro-4-octylphenyl)-5-(trimethylsilyl)penta-1,4-diyn-3-ol (4.8c). The crude mixture was purified by flash column chromatography using 15% diethyl ether in pentane. The silylated PAC **4.8c** (70 mg, 62% yield) was isolated as a brown oil. **^{1}H NMR** (300 MHz, $CDCl_3$) δ (ppm) 7.35 (t, J = 7.7 Hz, 1H), 6.93 – 6.86 (m, 2H), 5.35 (d, J = 7.6 Hz, 1H), 2.59 (ps t, J = 7.7 Hz, 2H), 2.32 (br d, J = 7.6 Hz, OH), 1.67 – 1.49 (m, 2H), 1.39 – 1.11 (m, 10H), 0.88 (t, J = 6.7 Hz, 3H), 0.21 (s, 9H).

1-(4-(Heptyloxy)phenyl)-5-(trimethylsilyl)penta-1,4-diyn-3-ol (9a). The crude mixture was purified by flash column chromatography using up to 20% diethyl ether in pentane. The silylated PAC **9a** (564 mg, 27% yield) was isolated as a brown oil. **^{1}H NMR** (300 MHz, $CDCl_3$) δ (ppm) 7.41 – 7.38 (m, 2H), 6.85 – 6.81(m, 2H), 5.33 (s, 1H), 3.90 (t, J = 6.5 Hz, 2H), 1.76 – 1.61 (m, 6H), 1.45 – 1.26 (m, 5H), 0.87 (t, J = 6.7 Hz, 3H), 0.16 (s, 9H). **^{13}C NMR** (75 MHz, $CDCl_3$) δ (ppm) 159.8, 133.5, 114.6, 114.4, 84.8, 84.6, 68.2, 63.1, 53.4, 37.6, 31.9, 29.3, 29.2, 27.4, 26.1, 22.8, 22.5, 14.2, 14.1. **HRMS** (DCI-CH_4) *m/z*: calcd for $C_{21}H_{31}O_2Si$ $[M+H]^+$: 343.2092, found: 343.2093. **FTIR** (cm^{-1}) (neat): 3357, 2957, 2928, 2851, 2233, 2183, 1613, 1509, 1250, 1026, 843, 760.

1-(4-(2-(2-ethoxyethoxy)ethoxy)phenyl)-5-(trimethylsilyl)penta-1,4-diyn-3-ol (9b). The crude mixture was purified by flash column chromatography using up to 80% diethyl ether in pentane. The silylated PAC **9b** (318 mg, 56% yield) was isolated as a yellow oil. **^{1}H NMR** (300 MHz, $CDCl_3$) δ (ppm) 7.36 – 7.33 (m, 2H), 6.83 – 6.80 (m, 2H), 5.31 (s,1H), 4.10 (t, J = 4.4 Hz, 2H), 3.84 (t, J = 4.4 Hz, 2H), 3.74 – 3.68 (m, 2H), 3.61 – 3.58 (m, 2H), 3.52 (q, J = 7.1 Hz, 2H), 2.3 (br m, OH), 1.19 (t, J = 6.5 Hz, 3H), 0.16 (s, 9H). **^{13}C NMR** (75 MHz, $CDCl_3$) δ (ppm) 159.4, 133.5, 114.7, 114.3, 102.1, 89.7, 84.8, 84.6, 71.1, 70.0, 69.8, 67.6, 66.9, 53.3, 15.3, -0.2.

1-(3-Hexylphenyl)-5-(trimethylsilyl)penta-1,4-diyn-3-ol (14.6). The crude mixture was purified by flash column chromatography using up to 20% diethyl ether in pentane. The silylated PAC **14.6** (373 mg, 81% yield) was isolated as a yellow oil. **^{1}H NMR** (300 MHz, $CDCl_3$) δ (ppm) 7.29 (dt, J = 7.0, 1.6 Hz, 2H), 7.22 (td, J = 7.6, 1.2 Hz, 1H), 7.15 (dt, J = 7.5, 1.7 Hz, 1H), 5.33 (d, J = 7.4 Hz, 1H), 2.57 (t, J = 7.7 Hz, 2H), 2.26 (d, J = 7.4 Hz, 1H, OH), 1.65 – 1.55 (m, 2H), 1.35 – 1.25 (m, 6H), 0.88 (t, J = 6.7 Hz, 3H), 0.21 (s, 9H). **^{13}C NMR** (75 MHz, $CDCl_3$) δ (ppm) 143.2, 132.0, 129.3, 128.4, 128.3, 121.9, 101.9, 89.9, 85.6, 84.9, 53.3, 35.8, 31.8, 31.4, 29.0, 22.7, 14.2, -0.2. **HRMS** (DCI-CH_4) *m/z*: calcd for $C_{20}H_{29}OSi$ $[M+H]^+$: 313.1977, found: 313.1988. **FTIR** (cm^{-1}) (neat): 3364, 2957, 2928, 2857, 2233, 2173, 1250, 1043, 843, 761, 694.

1-(3-Nonylphenyl)-5-(trimethylsilyl)penta-1,4-diyn-3-ol (14.9). The crude mixture was purified by flash column chromatography using up to 20% diethyl ether in pentane. The silylated PAC **14.9** (359 mg, 55% yield) was isolated as a brown oil. **^{1}H NMR** (300 MHz, $CDCl_3$) δ (ppm) 7.34 – 7.25 (m, 2H), 7.25 – 7.12 (m, 2H), 5.33 (d, J = 7.4 Hz, 1H), 2.65 – 2.48 (m, 2H), 2.32 (d, J = 7.5 Hz, OH), 1.64 – 1.54 (m, 2H), 1.34 – 1.22 (m, 12H), 0.88 (t, J = 6.6 Hz, 3H), 0.21 (s, 9H). **^{13}C NMR** (75 MHz, $CDCl_3$) δ (ppm) 143.2, 132.0, 129.3, 128.3, 121.8, 101.9, 89.9, 85.6, 84.9, 77.4, 53.3, 35.8, 32.0, 31.4, 29.7, 29.6, 29.5, 29.4, 22.8, 14.3, -0.2.

1-(3-Decylphenyl)-5-(trimethylsilyl)penta-1,4-diyn-3-ol (14.10). The crude mixture was purified by flash column chromatography using up to 30% diethyl ether in pentane. The silylated PAC **14.10** (201 mg, 62% yield) was isolated as a yellow oil. **^{1}H NMR** (300 MHz, $CDCl_3$) δ (ppm) 7.29 (dt, J = 7.0, 1.6 Hz, 2H), 7.22 (td, J = 7.2, 1.4 Hz, 1H), 7.15 (dt, J = 7.6, 1.7 Hz, 1H), 5.33 (s, 1H), 2.57 (t, J = 7.5 Hz, 2H), 2.26 (bs, 1H, OH), 1.64 – 1.51 (m, 2H), 1.33 – 1.23 (m, 14H), 0.88 (t, J = 6.6 Hz, 3H), 0.21 (s, 9H). **^{13}C NMR** (75 MHz, $CDCl_3$) δ (ppm) 143.2, 132.0, 129.3, 128.3, 121.9, 101.9, 89.8, 85.6, 85.0, 53.3, 35.8, 32.1, 31.4, 29.8, 29.7, 29.6, 29.5, 29.4, 22.8, 14.3, -0.2. **HRMS** (DCI-CH_4) *m/z*: calcd for $C_{24}H_{37}OSi$ $[M+H]^+$: 369.2597, found: 369.2614. **FTIR** (cm^{-1}) (neat): 3332, 2956, 2924, 2854, 2236, 2179, 1250, 1025, 844, 791, 761, 694.

1-(6-Octylnaphthalen-2-yl)-5-(trimethylsilyl)penta-1,4-diyn-3-ol (19). The crude mixture was purified by flash column chromatography using 100% pentane. The silylated naphtyl PAC **19** (273 mg, quantitative yield) was isolated as a yellow solid. **^{1}H NMR** (300 MHz, $CDCl_3$) δ (ppm) 7.96 (s, 1H), 7.71 (d, J = 8.3 Hz, 2H), 7.58 (s, 1H), 7.47 (dd, J = 8.5, 1.6 Hz, 1H), 7.35 (dd, J = 8.4, 1.7 Hz, 1H), 5.39 (d, J = 7.5 Hz, 1H), 2.76 (t, J = 7.7 Hz, 2H), 2.31 (d, J = 7.5 Hz, 1H), 1.69 (quint, J = 7.7 Hz, 2H), 1.46 – 1.16 (m, 10H), 0.87 (t, J = 6.7 Hz, 3H), 0.22 (s, 9H). **^{13}C NMR** (75 MHz, $CDCl_3$) δ (ppm) 142.1, 133.4, 132.0, 131.4, 128. 5, 128.4, 127.8, 127.7, 126.4, 118.4, 101.9, 85.9, 85.2, 53.4, 36.3, 32.0, 31.4, 29.6, 29.5, 29.4, 22.8, 14.3, -0.2. **HRMS** (DCI-CH_4) *m/z*: calcd for $C_{26}H_{34}OSi$ $[M]^+$: 390.2379, found: 390.2373. **FTIR** (cm^{-1}) (neat): 3373 (br), 2957, 2926, 2855, 2227, 2179, 1251, 1042, 845.

1-(5-Decylthiophen-2-yl)-5-(trimethylsilyl)penta-1,4-diyn-3-ol (24.10). The crude mixture was purified by flash column chromatography using 100% pentane. The silylated thienyl PAC **24.10** was used without further purification as a black oil. **^{1}H NMR** (300 MHz, $CDCl_3$) δ (ppm) 7.07 (d, J = 3.6 Hz, 1H), 6.63 (d, J = 3.6 Hz, 1H), 5.32 (br s, 1H), 2.76 (t, J = 7.4 Hz, 2H), 1.75 – 1.52 (m, 2H), 1.42 – 1.18 (m, 14H), 0.88 (t, J = 6.6 Hz, 3H), 0.20 (s, 9H).

1-(5-decylthiophen-2-yl)-5-(trimethylsilyl)penta-1,4-diyn-3-ol (24.12). The crude mixture was purified by flash column chromatography using 100% pentane. The silylated thienyl PAC **24.12** (188 mg, 89% yield) was isolated as a brown oil. **^{1}H NMR** (300 MHz, $CDCl_3$) δ (ppm) 7.11 (d, J = 3.6 Hz, 1H), 6.67 (d, J = 3.6 Hz, 1H), 5.36 (d, J = 7.5 Hz, 1H), 2.80 (ps t, J = 7.5 Hz, 2H), 2.31 (d, J = 7.5 Hz, OH), 1.82 – 1.57 (m, 2H), 1.52 – 1.14 (m, 18H), 0.91 (t, J = 6.7 Hz, 3H), 0.24 (s, 9H). **^{13}C NMR** (75 MHz, $CDCl_3$) δ (ppm) 149.3, 133.2, 124.3, 119.1, 101.6, 90.1, 89.0, 78.7, 53.4, 37.6, 32.1, 31. 7, 30.3, 29.8, 29.8, 29. 7, 29.5, 29. 5, 29.2, 22.8, 14.3, -0.2. **HRMS** (DCI-CH_4) *m/z*: calcd for $C_{24}H_{39}OSSi$ $[M+H]^+$: 403.2491, found: 403.2475. **FTIR** (cm^{-1}) (neat): 3346 (br), 2954, 2923, 2854, 2227, 2179, 1256, 1023, 841, 760.

General procedure for the synthesis of compounds 5.6a-5.12a, 5.8b-c, 10a-b, 15.6-15.10, 20, 25.10 and 25.12 .A solution of silylated PAC in MeOH (0.06 M) containing K_2CO_3 (0.2 equiv.) was stirred at RT for 1h30. DCM and water were added and extraction was realized with DCM (3x). The combined organic layers were dried over $MgSO_4$, filtered and concentrated under reduced pressure. The crude product was purified by flash column chromatography (silica gel) to afford the PAC.

1-(4-Hexylphenyl)penta-1,4-diyn-3-ol (5.6a). The crude mixture was purified by flash column chromatography using up to 30% diethyl ether in pentane. The PAC **5.6a** (258 mg, 71% yield) was isolated as an orange oil. **^{1}H NMR** (300 MHz, $CDCl_3$) δ (ppm) 7.40 – 7.35 (m, 2H), 7.15 – 7.10 (m, 2H), 5.34 (d, J = 2.3 Hz, 1H), 2.61 (d, J = 2.3 Hz, 1H), 2.58 (t, J = 7.9 Hz, 2H), 1.97 (br s, 1H, OH), 1.62 – 1.56 (m, 2H), 1.34 – 1.26 (m, 6H), 0.88 (t, J = 6.7 Hz, 3H). **^{13}C NMR** (75 MHz, $CDCl_3$) δ (ppm) 144.4, 131.9, 128.6, 125.9, 118.9, 85.2, 84.9, 81.1, 73.0, 52.7, 36.1, 31.8, 31.3, 29.0, 22.7, 14.2. **HRMS** (DCI-CH_4) *m/z*: calcd for $C_{17}H_{21}O$ $[M+H]^+$: 241.1592, found: 241.1592. **FTIR** (cm^{-1}) (neat): 3357, 3291, 2961, 2926, 2854, 2246, 2195, 2119, 1508, 1299, 1021, 897, 832, 816, 645, 565, 544.

1-(4-Octylphenyl)penta-1,4-diyn-3-ol (5.8a). The crude mixture was purified by flash column chromatography using up to 20% diethyl ether in pentane. The PAC **5.8a** (104 mg, 72% yield) was isolated as a yellow oil. **^{1}H NMR** (300 MHz, $CDCl_3$) δ (ppm) 7.38 (d, J = 8.1 Hz, 2H), 7.13 (d, J = 8.1 Hz, 2H), 5.34 (d, J = 2.4 Hz, 1H), 2.65 – 2.55 (m, 3H), 2.30 (br s, 1H, OH), 1.59 (quint, J = 7.1 Hz, 2H), 1.35 – 1.15 (m, 10H), 0.87 (t, J = 6.6 Hz, 3H). **^{13}C NMR** (75 MHz, $CDCl_3$) δ (ppm) 144.4, 131.9, 128.6, 118.9, 85.2, 84.9, 81.1, 73.0, 52.7, 36.1, 32.0, 31.3, 29.6, 29.4, 22.8, 14.2. **HRMS** (DCI-CH_4) *m/z*: calcd for $C_{19}H_{25}O$ $[M+H]^+$: 269.1905, found: 269.1910. **FTIR** (cm^{-1}) (neat): 3275, 3189, 2954, 2922, 2851, 2231, 2195, 2123, 1508, 1297, 1023, 889, 840, 825, 707.

1-(4-Nonylphenyl)penta-1,4-diyn-3-ol (5.9a). The crude mixture was purified by flash column chromatography using up to 20% diethyl ether in pentane. The PAC **5.9a** (100 mg, 60% yield) was isolated as a brown oil. **^{1}H NMR** (400 MHz, $CDCl_3$) δ (ppm) 7.38 (d, J = 8.2 Hz, 2H), 7.13 (d, J = 8.2 Hz, 2H), 5.35 (d, J = 4.9 Hz, 1H), 2.74 – 2.51 (m, 3H), 2.45 (br d, J = 7.0 Hz, 1H, OH), 1.65 – 1.50 (m, 2H), 1.40 – 1.20 (m, 12H), 0.88 (t, J = 6.7 Hz, 3H). **^{13}C NMR** (75 MHz, $CDCl_3$) δ (ppm) 144.4, 131.9, 128. 6, 118.9, 85.1, 84.9, 81.1, 72.9, 52.7, 36.0, 32.0, 31.3, 29.7, 29.6, 29.4, 29.4, 22.8, 14.2. **HRMS** (DCI-CH_4) *m/z*: calcd for $C_{20}H_{27}O$ $[M+H]^+$: 283.2062, found 283.2070. **FTIR** (cm^{-1}) (neat): 3291 (br), 2923, 2853, 2227, 2132, 1511, 1296, 1027, 1022, 638.

1-(4-Decylphenyl)penta-1,4-diyn-3-ol (5.10a). The crude mixture was purified by flash column chromatography using up to 20% diethyl ether in pentane. The PAC **5.10a** (16 mg, 79% yield) was isolated as a brown oil. **^{1}H NMR** (400 MHz, $CDCl_3$) δ (ppm) 7.38 (d, J = 8.2 Hz, 2H), 7.13 (d, J = 8.3 Hz, 2H), 5.34 (dd, J = 7.6, 2.3 Hz, 1H), 2.61 (d, J = 2.3 Hz, 1H), 2.59 (t, J = 8.0 Hz, 2H), 2.32 (d, J = 7.6 Hz, 1H, OH), 1.65 – 1.50 (m, 2H), 1.35 – 1.20 (m, 18H), 0.88 (t, J = 6.7 Hz, 3H). **^{13}C NMR** (75 MHz, $CDCl_3$) δ (ppm) 144.4, 131.9, 128.6, 118.9, 85.2, 84.9, 81.0, 73.0, 52.7, 36.1, 32.0, 31.3, 29.7, 29.7, 29.6, 29.5, 29.4, 22.8, 14.3. **HRMS** (DCI-CH_4) *m/z*: calcd for $C_{21}H_{29}O$ $[M+H]^+$: 297.2218, found 297.2223. **FTIR** (cm^{-1}) (neat): 3274, 2921, 2848, 2231, 2123, 1508, 1297, 1022, 707.

1-(4-Dodecylphenyl)penta-1,4-diyn-3-ol (5.12a). The crude mixture was purified by flash column chromatography using up to 20% diethyl ether in pentane. The PAC **5.12a** (81 mg, 66% yield) was isolated as a brown oil. **^{1}H NMR** (400 MHz, $CDCl_3$) δ (ppm) 7.38 (d, J = 8.2 Hz, 2H), 7.13 (d, J = 8.3 Hz, 2H), 5.34 (br s, 1H), 2.65 – 2.55 (m, 3H), 2.33 (br d, J = 6.1 Hz, 1H, OH), 1.65 – 1.50 (m, 2H), 1.35 – 1.20 (m, 18H), 0.88 (t, J = 6.7 Hz, 3H). **^{13}C NMR** (75 MHz, $CDCl_3$) δ (ppm) 144.4, 131.9, 128.6, 118.9, 85.2, 84.9, 81.1, 73.0, 52.7, 36.1, 32.1, 31.3, 29.8, 29.8, 29.7, 29.6, 29.5, 29.4, 22.8, 14.3. **HRMS** (DCI-CH_4) *m/z*: calcd for $C_{23}H_{33}O$ $[M+H]^+$: 325.2531, found: 325.2540. **FTIR** (cm^{-1}) (neat): 3268 (br), 2954, 2918, 2849, 2240, 2113, 1469, 1296, 1026.

1-(3-Fluoro-4-octylphenyl)penta-1,4-diyn-3-ol (5.8b). The crude mixture was purified by flash column chromatography using 20% diethyl ether in pentane. The PAC **5.8b** (13.6 mg, 50% yield) was isolated as a yellow oil. **^{1}H NMR** (300 MHz, $CDCl_3$) δ (ppm) 7.17 (dd, J = 7.7, 1.4 Hz, 1H), 7.15 – 7.07 (m, 2H), 5.33 (dd, J = 7.6, 2.3 Hz, 1H), 2.62 (d, J = 2.3 Hz, 1H), 2.61 (t, J = 7.5 Hz, 2H), 2.32 (d, J = 7.7 Hz, 1H), 1.64 – 1.52 (m, 2H), 1.37 – 1.21 (m, 10H), 0.88 (t, J = 6.6 Hz, 3H). **^{13}C NMR** (75 MHz, $CDCl_3$) δ (ppm) 160.6 (d, J = 245.5 Hz), 131.5 (d, J = 16.3 Hz), 130.7 (d, J = 6.0 Hz), 127.7 (d, J = 3.4 Hz), 120.7 (d, J = 9.6 Hz), 118.6 (d, J = 24.5 Hz), 85.6, 83.9, 80.8, 73.2, 52.7, 32.0, 30.1 (d, J = 1.0 Hz), 29.5, 29.4, 29.4, 29.1 (d, J = 2.1 Hz), 22.8, 14.2. **^{19}F NMR** (282 MHz, $CDCl_3$) δ (ppm) -118.4 (dd, J = 10.0, 7.3 Hz). **HRMS** (DCI-CH_4) *m/z*: calcd for $C_{19}H_{24}FO$ $[M+H]^+$: 287.1811, found: 287.1818. **FTIR** (cm^{-1}) (neat): 3361 (br) 3303, 2954, 2925, 2855, 2246, 2127, 1500, 1170, 1028.

1-(2-Fluoro-4-octylphenyl)penta-1,4-diyn-3-ol (5.8c). The crude mixture was purified by flash column chromatography using 20% diethyl ether in pentane. The PAC **5.8c** (31.5 mg, 56% yield) was isolated as a yellow oil. **^{1}H NMR** (300 MHz, $CDCl_3$) δ (ppm) 7.34 (t, J = 7.7 Hz, 1H), 6.95 – 6.85 (m, 2H), 5.37 (dd, J = 7.7, 2.3 Hz, 1H), 2.62 (d, J = 2.2 Hz, 1H), 2.59 (t, J = 7.9 Hz, 2H), 2.45 – 2.30 (br s, 1H, OH), 1.65 – 1.50 (m, 2H), 1.40 – 1.20 (m, 10H), 0.88 (t, J = 7.0 Hz, 3H). **^{13}C NMR** (75 MHz, $CDCl_3$) δ (ppm) 163.1 (d, J = 252.2 Hz), 147.2 (d, J = 7.4 Hz), 133.5 (d, J = 1.7 Hz), 124.3 (d, J = 3.2 Hz), 115.5 (d, J = 20.3 Hz), 107.5 (d, J = 15.7 Hz), 89.9 (d, J = 3.2 Hz), 80.8, 78.7, 73.2, 52.8, 35.9 (d, J = 1.6 Hz), 32.0, 31.0, 29.5, 29.3, 29.3, 22.8, 14.2. **^{19}F NMR** (282 MHz, $CDCl_3$) δ (ppm) -110.50 (dd, J = 10.4, 7.8 Hz). **HRMS** (DCI-CH_4) *m/z*: calcd for $C_{19}H_{24}FO$ $[M+H]^+$: 287.1811, found: 287.1803. **FTIR** (cm^{-1}) (neat): 3364 (br), 3310, 3275, 2954, 2922, 2855, 2236, 2205, 2129, 1423, 1019.

1-(4-(Heptyloxy)phenyl)penta-1,4-diyn-3-ol (10a). The crude mixture was purified by flash column chromatography using up to 30% diethyl ether in pentane. The PAC **10a** (183 mg, 41% yield) was isolated as a brown oil. **^{1}H NMR** (300 MHz, $CDCl_3$) δ (ppm) 7.42 – 7.36 (m, 2H), 6.86 – 6.80(m, 2H), 5.33 (dd, J = 7.0, 2.3 Hz, 1H), 3.95 (t, J = 6.6 Hz, 2H), 2.61 (d, J = 2.3 Hz, 1H), 2.31 (d, J = 7.44 Hz,

1H), 1.85 – 1.70 (m, 2H), 1.50 – 1.25 (m, 8H), 0.89 (t, *J* = 6.7 Hz, 3H). **^{13}C NMR** (75 MHz, $CDCl_3$) δ (ppm) 159.9, 133.5, 114.6, 113.6, 85.1, 84.2, 81.2, 72.9, 68.2, 52.8, 31.9, 29.3, 29.2, 26.1, 22.7, 14.2. **HRMS** (DCI-CH_4) *m/z*: calcd for $C_{18}H_{22}O_2$ $[M]^+$: 270.1612, found: 270.1620. **FTIR** (cm^{-1}) (neat): 3297, 2958, 2923, 2857, 2236, 2027, 1605, 1508, 1286, 1244, 1172, 1018, 830, 643.

1-(4-(2-(2-Ethoxyethoxy)ethoxy)phenyl)penta-1,4-diyn-3-ol (10b). The crude mixture was purified by flash column chromatography using up to 80% diethyl ether in pentane. The PEG-ether PAC **10b** (63 mg, 28% yield) was isolated as a yellow oil. **^{1}H NMR** (300 MHz, $CDCl_3$) δ (ppm) 7.37 (d, *J* = 9.0 Hz, 1H), 6.84 (d, *J* = 9.0 Hz, 1H), 5.33 (br s, 1H), 4.13 (dd, *J* = 5.5, 4.2 Hz, 2H), 3.86 (dd, *J* = 5.6, 4.2 Hz,, 2H), 3.74 – 3.67 (m, 2H), 3.65 – 3.58 (m, 2H), 3.53 (q, *J* = 7.1 Hz, 2H), 2.86 – 2.64 (m, 1H), 2.60 (d, *J* = 2.3 Hz, 1H), 1.21 (t, *J* = 7.0 Hz, 3H). **^{13}C NMR** (75 MHz, $CDCl_3$) δ (ppm) 159.4, 133.5, 114.7, 114.1, 84.8, 84.5, 81.3, 72.8, 71.0, 69.9, 69.7, 67.6, 66.9, 52.6, 15.3. **HRMS** (DCI-CH_4) *m/z*: calcd for $C_{17}H_{21}O_4$ $[M+H]^+$: 289.1430, found: 289.1440. **FTIR** (cm^{-1}) (neat): 3310, 2977, 2930, 2870, 2230, 2119, 1605, 1508, 1286, 1246, 1104, 1057, 1024, 832, 538.

1-(3-Hexylphenyl)penta-1,4-diyn-3-ol (15.6). The crude mixture was purified by flash column chromatography using up to 30% diethyl ether in pentane. The PAC **15.6** (94 mg, 36% yield) was isolated as a yellow oil.**^{1}H NMR** (300 MHz, $CDCl_3$) δ (ppm) 7.32 – 7.26 (m, 2H), 7.22 (td, *J* = 7.3, 1.0 Hz, 1H), 7.16 (dt, *J* = 7.5, 1.7 Hz, 1H), 5.34 (d, *J* = 2.3 Hz, 1H), 2.61 (d, *J* = 2.3 Hz, 1H), 2.57 (t, *J* = 7.5 Hz, 2H), 2.31 (br s, 1H, 1H, OH), 1.65 – 1.50 (m, 2H), 1.35 – 1.25 (m, 6H), 0.88 (t, *J* = 6.7 Hz, 3H). **^{13}C NMR** (75 MHz, $CDCl_3$) δ (ppm) 143.3, 132.0, 129.4, 129.3, 128.4, 121.6, 85.2, 85.1, 81.0, 73.0, 52.7, 35.8, 31.8, 31.4, 29.0, 22.7, 14.2. **HRMS** (DCI-CH_4) *m/z*: calcd for $C_{17}H_{21}O$ $[M+H]^+$: 241.1590, found: 241.1592. **FTIR** (cm^{-1}) (neat): 3373, 3284, 2961, 2926, 2857, 2243, 2198, 2122, 1492, 1302, 1013, 790, 692, 638.

1-(3-Nonylphenyl)penta-1,4-diyn-3-ol (15.9). The crude mixture was purified by flash column chromatography using up to 30% diethyl ether in pentane. The PAC **15.9** (80 mg, 29% yield) was isolated as a yellow oil. **^{1}H NMR** (300 MHz, $CDCl_3$) δ (ppm) 7.32 – 7.26 (m, 2H), 7.22 (td, *J* = 7.3, 1.0 Hz, 1H), 7.16 (dt, *J* = 7.6, 1.7 Hz, 1H), 5.34 (dd, *J* = 7.5, 2.3 Hz, 1H), 2.61 (d, *J* = 2.3 Hz, 1H), 2.57 (t, *J* = 7.5 Hz, 2H), 2.41 (d, *J* = 7.6 Hz, 1H, OH), 1.65 – 1.50 (m, 2H), 1.40 – 1.10 (m, 10H), 0.88 (t, *J* = 6.7 Hz, 3H). **^{13}C NMR** (75 MHz, $CDCl_3$) δ (ppm) 143.3, 132.0, 129.4, 129.3, 128.4, 121.6, 85.2, 85.1, 81.0, 73.0, 52.7, 35.8, 32.0, 31.4, 29.7, 29.6, 29.5, 29.4, 22.8, 14.3. **HRMS** (DCI-CH_4) *m/z*: calcd for $C_{20}H_{27}O$ $[M+H]^+$: 283.2062, found 283.2059. **FTIR** (cm^{-1}) (neat): 3309, 3290, 2961, 2925, 2853, 2233, 2195, 2119, 1463, 1292, 1036, 792, 697.

1-(3-Decylphenyl)penta-1,4-diyn-3-ol (15.10). The crude mixture was purified by flash column chromatography using up to 30% diethyl ether in pentane. The PAC **15.10** (89 mg, 55% yield) was isolated as an orange oil. **^{1}H NMR** (300 MHz, $CDCl_3$) δ (ppm) 7.32 – 7.26 (m, 2H), 7.22 (td, *J* = 7.3, 1.0 Hz, 1H), 7.16 (dt, *J* = 7.5, 1.7 Hz, 1H), 5.34 (br s, 1H), 2.62 (d, *J* = 2.3 Hz, 1H), 2.57 (t, *J* = 7.5 Hz, 2H), 2.30 (br s, 1H, 1H, OH), 1.65 – 1.50 (m, 2H), 1.40 – 1.20 (m, 14H), 0.88 (t, *J* = 6.5 Hz, 3H). **^{13}C NMR** (75 MHz, $CDCl_3$) δ (ppm) 143.3, 132.0, 129.5, 129.3, 128.4, 121.6, 85.2, 85.1, 81.0, 73.0, 52.7, 35.8, 32.1, 31.4, 29.8, 29.7, 29.6, 29.5, 29.4, 22.8, 14.3. **HRMS** (DCI-CH_4) *m/z*: calcd for $C_{21}H_{29}O$ $[M+H]^+$: 297.2213, found: 297.2218. **FTIR** (cm^{-1}) (neat): 3398, 3303, 2922, 2853, 2233, 2192, 2122, 1306, 1014, 790, 693, 657, 637.

1-(6-Octylnaphthalen-2-yl)penta-1,4-diyn-3-ol (20). The crude mixture was purified by flash column chromatography using 20% Diethyl ether in pentane. The naphtyl PAC **20** (80 mg, 37% yield) was isolated as a yellow solid. **^{1}H NMR** (300 MHz, $CDCl_3$) δ (ppm) 7.96 (d, *J* = 1.1 Hz, 1H), 7.71 (d, *J* = 8.3 Hz, 2H), 7.58 (d, *J* = 1.0 Hz, 1H), 7.46 (dd, *J* = 8.4, 1.6 Hz, 1H), 7.35 (dd, *J* = 8.4, 1.6 Hz, 1H), 5.40 (dd, *J* = 7.6, 2.3 Hz, 1H), 2.76 (t, *J* = 7.7 Hz, 2H), 2.64 (d, *J* = 2.3 Hz, 1H), 2.37 (dd, *J* = 7.6, 1.7 Hz, 1H, OH), 1.70 – 1.60 (m, 2H), 1.45 – 1.20 (m, 10H), 0.88 (t, *J* = 6.7 Hz, 3H). **^{13}C NMR** (75 MHz, $CDCl_3$) δ (ppm) 142.2, 133.5, 132.1, 131.4, 128.4, 128.4, 127.8, 127.7, 126.4, 118.1, 85.5, 85.4, 78.7, 73.1, 52.8, 36.3, 32.0, 31.4, 29.6, 29.5, 29.4, 22.8, 14.3. **HRMS** (DCI-CH_4) *m/z*: calcd for $C_{23}H_{26}O$ $[M]^{+\cdot}$: 318.1984, found: 318.1982. **FTIR** (cm^{-1}) (neat): 3385 (br), 3279, 2956, 2919, 2851, 2240, 2119, 1471, 1031, 896, 826, 478.

1-(5-Decylthiophen-2-yl)penta-1,4-diyn-3-ol (25.10). The crude mixture was purified by flash column chromatography using up to 20% diethyl ether in pentane. The thienyl PAC **25.10** (43 mg, 21% yield) was isolated as a brown oil. **^{1}H NMR** (300 MHz, $CDCl_3$) δ (ppm) 7.08 (d, *J* = 3.6 Hz, 1H), 6.64 (dt, *J* = 3.6, 0.8 Hz, 1H), 5.34 (dd, *J* = 7.6, 2.3 Hz, 1H), 2.77 (t, *J* = 7.4 Hz, 2H), 2.61 (d, *J* = 2.3 Hz, 1H), 2.34 (d, *J* = 7.6 Hz, 1H), 1.66 (quint, *J* = 7.5 Hz, 2H), 1.40 – 1.19 (m, 14H), 0.88 (t, *J* = 6.7 Hz, 3H). **^{13}C NMR** (75 MHz, $CDCl_3$) δ (ppm) 149.5, 133.4, 124.3, 118.8, 88.6, 80.8, 79.0, 73.2, 52.8, 32.0, 31.7, 30.3, 29.7, 29.7, 29.5, 29.1, 22.8, 14.3. **HRMS** (DCI-CH_4) *m/z*: calcd for $C_{19}H_{27}OS$ $[M+H]^+$: 303.1783, found: 303.1778. **FTIR** (cm^{-1}) (neat): 3291 (br), 2955, 2924, 2866, 2175.

1-(5-Dodecylthiophen-2-yl)penta-1,4-diyn-3-ol (25.12). The crude mixture was purified by flash column chromatography using 20% diethyl ether in pentane. The thienyl PAC **25.12** (89 mg, 58% yield) was isolated as a yellow solid. **^{1}H NMR** (300 MHz, $CDCl_3$) δ (ppm) 7.08 (d, *J* = 3.6 Hz, 1H), 6.64 (d, *J* = 3.6 Hz, 1H), 5.34 (dd, *J* = 7.7, 2.3 Hz, 1H), 2.77 (t, *J* = 7.5 Hz, 2H), 2.61 (d, *J* = 2.3 Hz, 1H), 2.30 (d, *J* = 7.7 Hz, 1H), 1.65 (quint, *J* = 7.4 Hz, 2H), 1.28 (d, *J* = 14.2 Hz, 18H), 0.88 (t, *J* = 6.7 Hz, 3H). **^{13}C NMR** (75 MHz, $CDCl_3$) δ (ppm) 149.5, 133.4, 124.3, 118.8, 88.6, 80.7, 78.9, 73.2, 52.8, 32.1, 31.7, 30.3, 29.8, 29.8, 29.7, 29.5, 29.5, 29.2, 22.8, 14.3. **HRMS** (DCI-CH_4) *m/z*: calcd for $C_{21}H_{31}OS$ $[M+H]^+$: 331.2096, found: 331.2091. **FTIR** (cm^{-1}) (neat): 3276, 3209 (br), 2955, 2913, 2849, 2230, 2179, 2124, 1469, 1021, 801.

Route B:

General procedure for the synthesis of intermediates 27a-e, 35 and 47. A Schlenk flask charged with Na_2PdCl_4 (1 mol%), 2-(di-*tert*-butylphosphino)-*N*-phenylindole (PIntB, 2 mol%), CuI (2 mol%), aryl halide (1.0 equiv.), H_2O (0.2 mL/mmol) and TMEDA (1.8 mL/mmol) was evacuated and backfilled with argon three times. The reaction mixture was heated to 70°C and the propargylic alcohol (2.0 equiv.) was added. The reaction mixture was then heated to 80°C until consumption of the starting material monitored by TLC. Then the reaction mixture was cooled to rt, water was added and the mixture was extracted with EtOAc (x3). The combined organic extracts were washed with brine, dried over $MgSO_4$, and concentrated under reduced pressure. The residue was purified by flash column chromatography (silica gel).

3-(4-Octylphenyl)prop-2-yn-1-ol (27a). The crude mixture was purified by flash column chromatography using up to 10% diethyl ether in pentane. The propargylic alcohol **27a** (100 mg, 61% yield) was isolated as a yellow oil. All analyses agreed with data reported in the literature.[66]

3-(3-Fluoro-4-octylphenyl)prop-2-yn-1-ol (27b). The crude mixture was purified by flash column chromatography using up to 20% diethyl ether in pentane. The propargylic alcohol **27b** (241 mg, 66% yield) was isolated as a yellow oil. **^{1}H NMR** (300 MHz, $CDCl_3$) δ (ppm) 7.16 – 7.02 (m, 3H), 4.48 (d, *J* = 6.2 Hz, 2H), 2.61 (td, *J* = 7.7, 1.1 Hz, 2H), 1.66 – 1.50 (m, 3H), 1.40 – 1.10 (m, 10H), 0.88 (t, *J* = 7.2 Hz, 3H).**^{13}C NMR** (125 MHz, $CDCl_3$) δ (ppm) 160.4 (d, *J* = 245.1 Hz), 130.8 (d, *J* = 16.2 Hz), 130.5 (d, *J* = 6.3 Hz), 127.3 (d, *J* = 3.7 Hz), 121.4 (d, *J* = 9.7 Hz), 118.3 (d, *J* = 24.1 Hz), 87.3, 84.8 (d, *J* = 3.3 Hz), 51.6, 31.9, 30.0 (d, *J* = 0.8 Hz), 29.4, 29.3, 29.2, 28.9 (d, *J* = 2.0 Hz), 22.7, 14.1. **^{19}F NMR** (282 MHz, $CDCl_3$) δ (ppm) -118.6 (dd, *J* = 10.2, 5.8 Hz). **HRMS** (DCI-CH_4) *m/z*: calcd for $C_{17}H_{24}FO$ $[M+H]^+$: 263.1811, found: 263.1801.

3-(3,5-Difluoro-4-octylphenyl)prop-2-yn-1-ol (27c). The crude mixture was purified by flash column chromatography using up to 20% diethyl ether in pentane. The propargylic alcohol **27c** (210 mg, 76% yield) was isolated as a yellow oil. **^{1}H NMR** (300 MHz, $CDCl_3$) δ (ppm) 6.96 – 6.86 (m, 2H), 4.48 (d, *J* = 6.2 Hz, 2H), 2.63 (td, *J* = 7.7, 1.1 Hz, 2H), 1.66 (td, *J* = 6.1, 2.5 Hz, 1H), 1.61 – 1.48 (m, 2H), 1.38 – 1.15 (m, 10H), 0.91 – 0.82 (m, 3H). **^{19}F NMR** (282 MHz, $CDCl_3$) δ (ppm) -115.7 (d, *J* = 6.9 Hz). **HRMS** (DCI-CH_4) *m/z*: calcd for $C_{17}H_{23}F_2O$ $[M+H]^+$: 281.1717, found: 281.1709.

3-(4-Octyl-3-(trifluoromethoxy)phenyl)prop-2-yn-1-ol (27d). The crude mixture was purified by flash column chromatography using up to 20% diethyl ether in pentane. The propargylic alcohol **27d** (108 mg, 50% yield) was isolated as a yellow oil. **^{1}H NMR** (300 MHz, $CDCl_3$) δ (ppm) 7.31 – 7.23 (m, 2H), 7.18 (d, J = 8.0 Hz, 1H), 4.49 (d, J = 3.9 Hz, 2H), 2.63 (t, J = 7.7, 2H), 2.00 – 1.90 (m, 1H), 1.57 (quint, J = 7.1 Hz, 2H), 1.40 – 1.15 (m, 10H), 0.88 (t, J = 7.2 Hz, 3H).**^{13}C NMR** (125 MHz, $CDCl_3$) δ (ppm) 147.2 (q, J = 1.6 Hz), 136.2, 130.6, 129.9, 123.5 (q, J = 1.6 Hz), 121.4, 120.6 (q, J = 257.6 Hz), 87.7, 84.4, 51.5, 31.9, 29.8, 29.8, 29.7, 29.4, 29.3, 29.2, 22.6, 14. **^{19}F NMR** (282 MHz, $CDCl_3$) δ (ppm) -57.1. **HRMS** (DCI-CH_4) *m/z*: calcd for $C_{18}H_{24}F_3O_2$ $[M+H]^+$: 329.1728, found: 329.1738.

3-(3,5-Difluoro-4-(7,7,7-trifluoroheptyl)phenyl)prop-2-yn-1-ol (27e). The crude mixture was purified by flash column chromatography using up to 30% diethyl ether in pentane. The propargylic alcohol **27e** (71 mg, 68% yield) was isolated as a yellow oil. **^{1}H NMR** (300 MHz, $CDCl_3$) δ (ppm) 7.00 – 6.95 (m, 2H), 4.51 (s, 2H), 2.65 (t, J = 7.5 Hz, 2H), 2.15 – 1.95 (m, 2H), 1.65 – 1.47 (m, 4H), 1.45 – 1.30 (m, 4H).**^{13}C NMR** (75 MHz, $CDCl_3$) δ (ppm) 161.1 (dd, J = 246.7, 10.3 Hz), 127.2 (q, J = 276.4 Hz), 121.7 (t, J = 12.4 Hz), 119.2 (t, J = 20.9 Hz), 115.2 – 114.8 (m, 2C), 88.5, 83.9 (t, J = 4.1 Hz), 51.5, 33.7 (q, J = 28.3 Hz), 29.0, 28.7, 28.4, 22.2 (t, J = 2.2 Hz), 21.8 (q, J = 2.9 Hz). **^{19}F NMR** (282 MHz, $CDCl_3$) δ (ppm) -66.4, -115.7. **HRMS** (DCI-CH_4) *m/z*: calcd for $C_{16}H_{18}F_5O$ $[M+H]^+$: 321.1278, found: 321.1282.

3-(5-Decylfuran-2-yl)prop-2-yn-1-ol (35). The crude mixture was purified by flash column chromatography using up to 20% diethyl ether in pentane. The propargylic alcohol **35** (30 mg, 25%) was isolated as a yellow oil. **^{1}H NMR** (400 MHz, $CDCl_3$) δ (ppm) 6.51 (d, J = 3.3 Hz, 1H), 5.97 (dt, J = 3.3, 0.9 Hz, 1H), 4.50 (d, J = 6.2 Hz, 2H), 2.60 (t, J = 7.6 Hz, 2H), 1.62 (q, J = 6.2 Hz, 2H), 1.30 (bs, 14H), 0.88 (t, J = 6.8 Hz, 3H).**^{13}C NMR** (100 MHz, $CDCl_3$): δ (ppm) 158.7, 134.4, 116.8, 106.2, 91.4, 77.2, 51.6, 32.1, 29.7, 29.7, 29.5, 29.3, 28.4, 28.0, 22.8, 14.3. **HRMS** (DCI-CH_4): calcd for $C_{17}H_{27}O_2$ $[M+H]^+$: 262.1933 *m/z*, found: 262.1933 *m/z*. **FTIR** (cm^{-1}) (neat): 3450, 2925, 2854, 1714, 1079, 736, 703.

3-(4-(8-(Triisopropylsilyl)oct-7-yn-1-yl)phenyl)prop-2-yn-1-ol (47). The crude mixture was purified by flash column chromatography using up to 30% diethyl ether in pentane. The propargylic alcohol **47** (264 mg, 62% yield) was isolated as a yellow oil. **^{1}H NMR** (300 MHz, $CDCl_3$) δ (ppm) 7.35 (d, J = 8.2 Hz, 2H), 7.12 (d, J = 8.2 Hz, 2H), 4.49 (d, J = 5.8 Hz, 2H), 2.59 (t, J = 7.7 Hz, 2H), 2.24 (t, J = 6.6 Hz, 2H), 1.71 – 1.17 (m, 11H), 1.09 – 1.01 (m, 18H). **^{13}C NMR** (75 MHz, $CDCl_3$) δ (ppm) 143.7, 131.8, 128.6, 119.8, 109.3, 86.7, 86.1, 80.3, 51.9, 35.9, 31.2, 28.8, 28.8, 28.6, 19.9, 18.8, 11.4. **HRMS** (DCI-CH_4) *m/z*: calcd for $C_{26}H_{41}OSi$ $[M+H]^+$: 397.2927, found: 397.2936.

3-(4-(Oct-7-yn-1-yl)phenyl)prop-2-yn-1-ol (48). To a solution of TIPS-protected propargylic alcohol **47** (217 mg, 0.54 mmol) in anhydrous THF (2.7 mL) at 0 °C under nitrogen was added TBAF solution (2 equiv., 1.09 ml, 1 M solution in THF). The reaction mixture was allowed to warm up to RT overnight. After evaporation of the solvent, the residue was dissolved in diethyl ether, washed with water and brine. The organic layer was dried over $MgSO_4$, filtered and concentrated under reduced pressure. The residue was purified by flash column chromatography (silica gel) using up to 30% diethyl ether in pentane. The propargylic alcohol **48** (103 mg, 79% yield) was isolated as a yellow oil. **^{1}H NMR** (300 MHz, $CDCl_3$) δ (ppm) 7.37 – 7.32 (m, 2H), 7.14 – 7.09 (m, 2H), 4.49 (d, J = 6.1 Hz, 2H), 2.60 (t, J = 7.7 Hz, 2H), 2.17 (td, J = 6.9, 2.6 Hz, 2H), 1.94 (t, J = 2.6 Hz, 1H), 1.72 – 1.24 (m, 9H). **^{13}C NMR** (75 MHz, $CDCl_3$) δ (ppm) 143.6, 131.8, 128.6, 119.8, 86.7, 86.0, 84.8, 68.3, 51.9, 35.9, 31.2, 28.8, 28.7, 28.5, 18.5. **HRMS** (DCI-CH_4) *m/z*: calcd for $C_{17}H_{21}O$ $[M+H]^+$: 241.1592, found: 241.1582.

General procedure for the synthesis of intermediates 31a-c. A two-neck round bottom flask charged with $Pd(OAc)_2$ (5 mol%), PPh_3 (15 mol%), CuI (5 mol%) and aryl halide (1.0 equiv.), was evacuated and backfilled with argon three times. Et_3N (0.2 M) was added and the reaction mixture was stirred at room temperature for 10 minutes before the propargylic alcohol (2.0 equiv.) was added. The reaction mixture was then heated to 65°C until consumption of the starting material as monitored by TLC. Then the reaction mixture was cooled to rt, a saturated aqueous solution of NH_4Cl was added. The mixture was extracted with Et_2O (x3). The combined organic extracts were washed with brine, dried over $MgSO_4$, and concentrated under reduced pressure. The residue was purified by flash column chromatography (silica gel).

3-(3-Fluoro-4-(heptyloxy)phenyl)prop-2-yn-1-ol (31a). The crude mixture was purified by flash column chromatography using up to 30% diethyl ether in pentane. The propargylic alcohol **31a** (241 mg, 66% yield) was isolated as a yellow oil. **^{1}H NMR** (300 MHz, $CDCl_3$) δ (ppm) 7.17 – 7.15 (m, 1H), 7.13 (q, J = 1.9 Hz, 1H), 6.86 (t, J = 8.6 Hz, 1H), 4.47 (bs, 2H), 4.02 (t, J = 6.6 Hz, 2H), 1.90 – 1.70 (m, 3H), 1.54 – 1.27 (m, 8H), 0.95-0.90 (m, 3H).**^{13}C NMR** (75 MHz, $CDCl_3$) δ (ppm) 151.9 (d, J = 246.7 Hz), 147.9 (d, J = 10.8 Hz), 128.3 (d, J = 3.8 Hz), 119.4 (d, J = 19.5 Hz), 114.8 (d, J = 8.5 Hz), 114.3 (d, J = 3.0 Hz), 86.5, 84.7 (d, J = 2.9 Hz), 69.4, 52.5, 31.8, 29.1, 29.0, 25.9, 23.2, 14.1. **^{19}F NMR** (282 MHz, $CDCl_3$) δ (ppm) -134.2. **HRMS** (DCI-CH_4) *m/z*: calcd for $C_{16}H_{22}FO_2$ $[M+H]^+$: 265.1604, found: 265.1614.

3-(3-fluoro-4-((6,6,6-trifluorohexyl)oxy)phenyl)prop-2-yn-1-ol (31b). The crude mixture was purified by flash column chromatography using up to 40% diethyl ether in pentane. The propargylic alcohol **31b** (100 mg, 60% yield) was isolated as a yellow oil. **^{1}H NMR** (300 MHz, $CDCl_3$) δ (ppm) 7.21 – 7.18 (m, 1H), 7.18 – 7.14 (m, 1H), 6.89 (t, J = 8.4 Hz, 1H), 4.50 (bs, 2H), 4.06 (t, J = 6.3 Hz, 2H), 2.25-2.03 (m, 2H), 1.87 (quint, J = 6.6 Hz, 2H), 1.71 – 1.54 (m, 4H).**^{13}C NMR** (75 MHz, $CDCl_3$) δ (ppm) 151.9 (d, J = 246.7 Hz), 147.7 (d, J = 10.8 Hz), 128.3 (d, J = 3.8 Hz), 127.1 (q, J = 274.5 Hz), 119.4 (d, J = 20.3 Hz), 114.8 (d, J = 8.5 Hz), 114.3 (d, J = 3.0 Hz), 86.5, 84.7 (d, J = 2.9 Hz), 68.9, 51.6, 33.6 (q, J = 28.5 Hz), 28.8, 25.2, 21.7 (q, J = 3.0 Hz). **^{19}F NMR** (282 MHz, $CDCl_3$) δ (ppm) -66.5, -134.7. **HRMS** (DCI-CH_4) *m/z*: calcd for $C_{15}H_{17}F_4O_2$ $[M+H]^+$: 305.1165, found: 305.1172.

3-(4-(1,1-Difluorooctyl)phenyl)prop-2-yn-1-ol (31c). The crude mixture was purified by flash column chromatography using up to 30% diethyl ether in pentane. The propargylic alcohol **31c** (110 mg, 80% yield) was isolated as a brown oil. **^{1}H NMR** (300 MHz, $CDCl_3$) δ (ppm) 7.50 – 7.36 (m, 4H), 4.51 (bs, 2H), 2.55 – 2.27 (m, 1H), 2.18 – 1.98 (m, 2H), 1.45 – 1.34 (m, 2H), 1.32 – 1.15 (m, 6H), 0.91 – 0.81 (m, 3H).**^{13}C NMR** (75 MHz, $CDCl_3$) δ (ppm) 137.6 (t, J = 27.0 Hz), 131.7, 125.1 (t, J = 6.2 Hz), 123.9 (t, J = 2.3 Hz), 122.9 (t, J = 240.8 Hz), 88.4, 84.9, 51.5, 39.0 (t, J = 27.0 Hz), 31.7, 29.2, 29.0, 22.6, 22.4 (t, J = 3.8 Hz), 14.1. **^{19}F NMR** (282 MHz, $CDCl_3$) δ (ppm) -95.7. **HRMS** (DCI-CH_4) *m/z*: calcd for $C_{17}H_{22}F_2O$ $[M]^+$: 280.1639, found: 280.1647.

3-(5-Decylfuran-2-yl)prop-2-yn-1-ol (39). To a solution of 3-iodo-5-decylfuran (60 mg, 0.179 mmol) in Et_3N (1.70 mL), were added $Pd(PPh_3)_2Cl_2$ (0.018 mmol, 12.5 mg), CuI (0.018 mmol, 3.4 mg) and propargylic alcohol (0.537 mmol, 30 µL) and the mixture was stirred at 50°C under argon overnight. The reaction mixture was quenched with aqueous NH_4Cl solution and extracted with EtOAc. The combined organic layers were washed with brine, dried over $MgSO_4$, and concentrated under reduced pressure. The residue was purified by flash column chromatography (silica gel) using up to 50% *tert*-butyl-methyl ether in hexane. The propargylic alcohol **39** (38mg, 80%) was isolated as a yellow oil. **^{1}H NMR** (400 MHz, $CDCl_3$) δ (ppm) 7.47 (s, 1H), 6.02 (s, 1H), 4.45 (d, J = 6.1 Hz, 2H), 2.57 (t, J = 7.6 Hz, 2H), 1.65 – 1.58 (m, 2H), 1.35 – 1.20 (m, 14H), 0.88 (t, J = 7.2 Hz, 3H).**^{13}C NMR** (100 MHz, $CDCl_3$): δ (ppm) 157.3, 144.4, 107.6, 107.2, 88.7, 77.9, 51.9, 32.0, 29.9, 29.7, 29.7, 29.4, 29.2, 27.9, 27.9, 22.8, 14.3. **HRMS** (DCI-CH_4) *m/z*: calcd for $C_{17}H_{26}O_2$ $[M]^+$: 262.1933, found: 262.1933. **FTIR** (cm^{-1}) (neat): 2924, 2853, 2251, 903, 721.

General procedure for the synthesis of intermediates 28a-e, 32a-c, 36, 40, 49. To a solution of alkynol (1.0 equiv.) in DCM (0.3 M) at 0°C was added Dess-Martin reagent (1.2 equiv.) in portions. The resulting solution was stirred at RT for 2h. After completion, the

reaction was quenched by addition of a saturated aqueous $NaHCO_3$ solution and 10% $Na_2S_2O_3$ aqueous solution. The resulting solution was extracted with DCM. Combined organic layers were washed with brine and dried over $MgSO_4$, filtered and concentrated under reduced pressure and otherwise stated used without further purification.

3-(4-octylphenyl)propiolaldehyde (28a). The aldehyde 28a (38 mg, quantitative yield) was isolated as a yellow oil. All analyses agreed with data reported in the literature.[67]

3-(3-Fluoro-4-octylphenyl)propiolaldehyde (28b). The aldehyde **28b** (230 mg, 82% yield) was isolated as a yellow oil. **^{1}H NMR** (300 MHz, $CDCl_3$) δ (ppm) 9.41 (s, 1H), 7.32 (dd, J = 7.8, 1.6 Hz, 1H), 7 7.27 – 7.18 (m, 2H), 2.67 (t, J = 7.7 Hz, 2H), 1.66 – 1.52 (m, 2H), 1.40 – 1.20 (m, 10H), 0.88 (t, J = 7.2 Hz, 3H). **^{19}F NMR** (282 MHz, $CDCl_3$) δ (ppm) -118.6 (t, J = 8.5 Hz). **FTIR** (cm^{-1}) (neat): 3312, 2955, 2927, 2856, 2242, 2197, 1665, 1615, 1562, 1384, 1287, 1008.

3-(3,5-Difluoro-4-octylphenyl)propiolaldehyde (28c). The aldehyde **28c** (210 mg, quantitative yield) was isolated as a yellow oil. **^{1}H NMR** (300 MHz, $CDCl_3$) δ (ppm) 9.34 (s, 1H), 7.09 – 6.94 (m, 2H), 2.61 (t, J = 7.7 Hz, 2H), 1.59 – 1.41 (m, 2H), 1.34 – 1.10 (m, 10H), 0.88 (t, J = 7.2 Hz, 3H). **^{19}F NMR** (282 MHz, $CDCl_3$) δ (ppm) -113.9 (d, J = 6.7 Hz). **HRMS** (DCI-CH_4) *m/z*: calcd for $C_{17}H_{21}F_2O$ $[M+H]^+$: 279.1560, found: 279.1559. **FTIR** (cm^{-1}) (neat): 3083, 3060, 2927, 2856, 2422, 2211, 1666, 1624, 1567, 1417, 1342, 1122, 1031.

3-(4-Octyl-3-(trifluoromethoxy)phenyl)propiolaldehyde (28d). The aldehyde **28d** (53 mg, 85%) was isolated as a yellow oil. **^{1}H NMR** (300 MHz, $CDCl_3$) δ (ppm) 9.41 (s, 1H), 7.47 – 7.42 (m, 2H), 7.30 (d, J = 8.3 Hz, 1H), 2.67 (t, J = 7.7 Hz, 2H), 1.59 (quint, J = 7.2 Hz, 2H), 1.40 – 1.15 (m, 10H), 0.87 (t, J = 7.2 Hz, 3H). **^{19}F NMR** (282 MHz, $CDCl_3$) δ (ppm) -57.1. **HRMS** (DCI-CH_4) *m/z*: calcd for $C_{18}H_{22}F_3O_2$ $[M+H]^+$: 327.1572, found: 327.1576 *m/z*. **FTIR** (cm^{-1}) (neat): 2926, 2855, 2198, 1667, 1565, 1255, 1218, 1167, 1016.

3-(3,5-Difluoro-4-(7,7,7-trifluoroheptyl)phenyl)propiolaldehyde (28e). The crude mixture was purified by flash column chromatography (silica gel) using up to 30% diethyl ether in pentane. The aldehyde **28e** (54 mg, 78% yield) was isolated as a yellow oil. **^{1}H NMR** (300 MHz, $CDCl_3$) δ (ppm) 9.40 (s, 1H), 7.15 – 7.05 (m, 2H), 2.69 (t, J = 7.5 Hz, 2H), 2.15 – 1.95 (m, 2H), 1.69 – 1.48 (m, 4H), 1.47 – 1.32 (m, 4H).**^{13}C NMR** (75 MHz, $CDCl_3$) δ (ppm) 176.3, 161.3 (dd, J = 248.5, 10.0 Hz), 127.2 (q, J = 276.4 Hz), 122.7 (t, J = 21.4 Hz), 118.6 (t, J = 11.6 Hz), 116.1 – 115.7 (m), 92.0 (t, J = 4.0 Hz), 88.6, 33.7 (q, J = 28.4 Hz), 29.0, 28.9, 28.5, 22.6 (t, J = 2.1 Hz), 21.9 (q, J = 2.9 Hz). **^{19}F NMR** (282 MHz, $CDCl_3$) δ (ppm) -66.4, -113.4. **HRMS** (DCI-CH_4) *m/z*: calcd for $C_{16}H_{16}F_5O$ $[M+H]^+$: 319.1121, found: 319.1132.

3-(3-Fluoro-4-(heptyloxy)phenyl)propiolaldehyde (32a). The crude mixture was purified by flash column chromatography (silica gel) using up to 20% diethyl ether in pentane. The aldehyde **32a** (40 mg, 74% yield) was isolated as a yellow oil. **^{1}H NMR** (300 MHz, $CDCl_3$) δ (ppm) 9.42 (s, 1H), 7.44 – 7.37 (m, 1H), 7.35 (dd, J = 11.1, 2.0 Hz, 1H), 6.98 (t, J = 8.4 Hz, 1H), 4.10 (t, J = 6.6 Hz, 2H), 1.93 – 1.80 (m, 2H), 1.56 – 1.30 (m, 8H), 0.97-0.89 (m, 3H).**^{13}C NMR** (75 MHz, $CDCl_3$) δ (ppm) 176.8, 153.5 (d, J = 246.7 Hz), 147.9 (d, J = 10.8 Hz), 130.9 (d, J = 3.8 Hz), 120.8 (d, J = 20.3 Hz), 114.8 (d, J = 8.5 Hz), 114.2 (d, J = 2.3 Hz), 94.8 (d, J = 2.9 Hz), 88.5, 69.4, 31.7, 29.1, 29.0, 25.8, 22.6, 14.1. **^{19}F NMR** (282 MHz, $CDCl_3$) δ (ppm) -132.9. **HRMS** (DCI-CH_4) *m/z*: calcd for $C_{16}H_{20}FO_2$ $[M+H]^+$: 263.1447, found: 263.1452.

3-(3-Fluoro-4-((6,6,6-trifluorohexyl)oxy)phenyl)propiolaldehyde (32b). The crude mixture was purified by flash column chromatography (silica gel) using up to 30% diethyl ether in pentane. The aldehyde **32b** (50 mg, 53% yield) was isolated as a yellow oil. **^{1}H NMR** (300 MHz, $CDCl_3$) δ (ppm) 9.38 (s, 1H), 7.36 (ddd, J = 8.3, 2.0, 1.2 Hz, 1H), 7.31 (dd, J = 11.1, 2.0 Hz, 1H), 6.94 (t, J = 8.4 Hz, 1H), 4.08 (t, J = 6.3 Hz, 2H), 2.22-2.04 (m, 2H), 1.95-1.82 (m, 2H), 1.73-1.57 (m, 4H).**^{13}C NMR** (75 MHz, $CDCl_3$) δ (ppm) 176.5, 152.0 (d, J = 249.0 Hz), 150.4 (d, J = 9.7Hz), 130.8 (d, J = 3.8 Hz), 127.1 (q, J = 274.5 Hz), 120.8 (d, J = 21.0 Hz), 114.2 (d, J = 2.3 Hz), 111.4 (d, J = 8.3 Hz), 94.6 (d, J = 2.9 Hz), 88.5, 68.9, 33.6 (q, J = 28.5 Hz), 28.8, 25.2, 21.7 (q, J = 3.0 Hz). **^{19}F NMR** (282 MHz, $CDCl_3$) δ (ppm) -66.2, -132.9. **HRMS** (DCI-CH_4) *m/z*: calcd for $C_{15}H_{15}F_4O_2$ $[M+H]^+$: 303.1008, found: 303.1021.

3-(4-(1,1-Difluorooctyl)phenyl)propiolaldehyde (32c). The crude mixture was purified by flash column chromatography (silica gel) using up to 30% diethyl ether in pentane. The aldehyde **32c** (60 mg, 55% yield) was isolated as a brown oil. **^{1}H NMR** (300 MHz, $CDCl_3$) δ (ppm) 9.46 (s, 1H), 7.71 – 7.65 (m, 2H), 7.56 – 7.50 (m, 2H), 2.22 – 2.02 (m, 2H), 1.60 (bs, 1H), 1.48 – 1.38 (m, 2H), 1.36 – 1.20 (m, 6H), 0.95 – 0.84 (m, 3H).**^{13}C NMR** (75 MHz, $CDCl_3$) δ (ppm) 176.6, 140.4 (t, J = 27.0 Hz), 133.3, 125.5 (t, J = 6.2 Hz), 122.6 (t, J = 240.8 Hz), 120.8 (t, J = 1.5 Hz), 93.7, 88.8, 38.9 (t, J = 27.0 Hz), 31.6, 29.1, 29.0, 22.6, 22.4 (t, J = 3.8 Hz), 14.1. **^{19}F NMR** (282 MHz, $CDCl_3$) δ (ppm) -96.4. **HRMS** (DCI-CH_4) *m/z*: calcd for $C_{17}H_{21}F_2O$ $[M+H]^+$: 279.1560, found: 279.1647.

3-(5-Decylfuran-2-yl)propiolaldehyde (36). The crude mixture was purified by flash column chromatography (silica gel) using up to 10% diethyl ether in pentane. The aldehyde **36** (43mg, 73%) was isolated as a colorless oil. **^{1}H NMR** (400 MHz, $CDCl_3$) δ (ppm) 9.39 (s, 1H), 6.96 (d, J = 3.4 Hz, 1H), 6.13 (dt, J = 3.4, 0.8 Hz, 1H), 2.66 (t, J = 7.6 Hz, 2H), 1.66 (quint, J = 7.5 Hz, 2H), 1.35 – 1.20 (m, 14H), 0.88 (t, J = 7.0 Hz, 3H).**^{13}C NMR** (100 MHz, $CDCl_3$): δ (ppm) 175.5, 163.1, 132.7, 124.7, 108.1, 95.3, 86.9, 32.0, 29.7, 29.6, 29.5, 29.4, 29.2, 28.7, 27.8, 22.8, 14.8. **HRMS** (DCI-CH_4) *m/z*: calcd for $C_{17}H_{25}O_2$ $[M+H]^+$: 261.1855, found: 261.1859. **FTIR** (cm^{-1}) (neat): 2196, 1718, 1662, 1465, 1022, 804, 721.

3-(5-Decylfuran-2-yl) propioaldehyde (40). The crude mixture was purified by flash column chromatography (silica gel) using up to 30% *tert*-butyl-methyl ether in hexane. The aldehyde **40** (46mg, 92%) was isolated as a brown oil. **^{1}H NMR** (400 MHz, $CDCl_3$) δ (ppm) 9.35 (s, 1H), 7.73 (d, J = 0.8 Hz, 1H), 6.14 (q, J = 0.9 Hz, 1H), 2.61 (td, J = 7.6, 0.9 Hz, 2H), 1.61 (quint, J = 7.2 Hz, 2H), 1.38 – 1.20 (m, 14H), 0.88 (t, J = 6.8 Hz, 3H).**^{13}C NMR** (100 MHz, $CDCl_3$): δ (ppm) 176.6, 158.5, 148.6, 107.4, 105.2, 91.5, 88.9, 32.0, 29.7, 29.7, 29.5, 29.4, 29.2, 27.8, 27.7, 22.8, 14.3. **HRMS** (DCI-CH_4) *m/z*: calcd for $C_{17}H_{25}O_2$ $[M+H]^+$: 261.1855, found: 261.1868. **FTIR** (cm^{-1}) (neat): 2196, 1718, 1662, 1465, 1022, 804, 721.

3-(4-(Oct-7-yn-1-yl)phenyl)propiolaldehyde (49). The aldehyde **49** (60 mg, 92%) was isolated as a yellow oil. **^{1}H NMR** (300 MHz, $CDCl_3$) δ (ppm) 9.47 (s, 1H), 7.62 – 7.55 (m, 2H), 7.32 – 7.20 (m, 2H), 2.71 (t, J = 7.7 Hz, 2H), 2.24 (td, J = 6.8, 2.6 Hz, 2H), 2.01 (t, J = 2.6 Hz, 1H), 1.80 – 1.24 (m, 9H). **^{13}C NMR** (75 MHz, $CDCl_3$) δ (ppm). 176.9, 147.0, 133.5, 129.0, 116.7, 96.0, 88.6, 84.6, 68.3, 36.1, 31.0, 28.7, 28.5, 28.4, 18.4. **HRMS** (DCI-CH_4) *m/z*: calcd for $C_{17}H_{19}O$ $[M+H]^+$: 239.1436, found: 239.1425.

General procedure for the synthesis of intermediates 5.8a-b, 29c-e, 33a-c, 37, 41, 46. To a solution of alkynal in dry THF (0.1 M) under N_2 at 0°C was added ethynyl magnesium bromide (0.5 M solution in hexane, 1.2 equiv.). The resulting solution was stirred at 0°C for 1h and allowed to warm to rt. After completion of the reaction, monitored by TLC, a saturated aqueous NH_4Cl solution was added to quench the reaction. The resulting mixture was extracted with diethyl ether. Combined organic layers were washed with brine and dried over $MgSO_4$, filtered and concentrated under reduced pressure. The residue was purified by flash column chromatography (silica gel).

1-(4-Octylphenyl)penta-1,4-diyn-3-ol (5.8a). The crude mixture was purified by flash column chromatography using up to 20% diethyl ether in pentane. The PAC **5.8a** (28 mg, 70% yield) was isolated as a yellow oil. All analyses agreed with the previously obtained product.

1-(3-Fluoro-4-octylphenyl)penta-1,4-diyn-3-ol (5.8b). The crude mixture was purified by flash column chromatography using up to 20% diethyl ether in pentane. The PAC **5.8b** (19 mg, 69% yield) was isolated as a yellow oil. All analyses agreed with the previously obtained product.

1-(3,5-Difluoro-4-octylphenyl)penta-1,4-diyn-3-ol (29c). The crude mixture was purified by flash column chromatography using up to 20% diethyl ether in pentane. The PAC **29c** (69 mg, 48% yield)

was isolated as a yellow oil. **^{1}H NMR** (300 MHz, $CDCl_3$) δ (ppm) 7.00 – 6.89 (m, 2H), 5.33 (d, J = 2.3 Hz, 1H), 2.64 (tt, J = 7.5, 1.4 Hz, 2H), 2.62 (d, J = 2.3 Hz, 1H), 2.55 – 2.40 (br s, 1H, OH), 1.55 (quint, J = 7.3 Hz, 2H), 1.40 – 1.20 (m, 10H), 0.88 (t, J = 6.6 Hz, 3H). **^{13}C NMR** (125 MHz, $CDCl_3$) δ (ppm) 161.2 (dd, J = 246.9, 10.4 Hz), 120.7 (t, J = 12.2 Hz), 120.4 (t, J = 20.7 Hz), 114.7 – 114.4 (m, 2C), 86.5, 82.9 (t, J = 3.8 Hz), 80.5, 73.4, 52.6, 32.0, 29.5, 29.4, 29.4, 29.3, 22.8, 22.5 (t, J = 2.3 Hz), 14.2. **^{19}F NMR** (282 MHz, $CDCl_3$) δ (ppm) -115.4 (d, J = 6.9 Hz). **HRMS** (DCI-CH_4) *m/z*: calcd for $C_{19}H_{23}OF_2$ $[M+H]^+$: 305.1717, found: 305.1711 *m/z*. **FTIR** (cm^{-1}) (neat): 3292, 3277, 2956, 2925, 2855, 2245, 2122, 1631, 1569, 1419, 1020.

1-(4-Octyl-3-(trifluoromethoxy)phenyl)penta-1,4-diyn-3-ol (29d). The crude mixture was purified by flash column chromatography using up to 20% diethyl ether in pentane. The PAC **29d** (46 mg, 80% yield) was isolated as a yellow oil. **^{1}H NMR** (300 MHz, $CDCl_3$) δ (ppm) 7.37 – 7.32 (m, 2H), 7.24 (d, J = 8.3 Hz, 1H), 5.38 (dd, J = 7.6, 2.3 Hz, 1H), 2.68 (t, J = 7.6 Hz, 2H), 2.66 (d, J = 2.3 Hz, 1H), 2.41 (d, J = 7.6 Hz, 1H, OH), 1.67 – 1.55 (m, 2H), 1.40 – 1.25 (m, 10H), 0.88 (t, J = 6.6 Hz, 3H). **^{13}C NMR** (75 MHz, $CDCl_3$) δ (ppm) 147.3 ,137.0, 130.8, 130.3, 123.8, 120.7, 120.6 (q, J = 257.3 Hz), 86.0, 83.6, 80.7, 73.3, 52.6, 32.0, 29.9, 29.5, 29.3, 22.8, 14.2. **^{19}F NMR** (282 MHz, $CDCl_3$) δ (ppm) -57.0. **HRMS** (DCI-CH_4) *m/z*: calcd for $C_{20}H_{24}O_2F_3$ $[M+H]^+$: 353.1728, found: 353.1726 *m/z*. **FTIR** (cm^{-1}) (neat): 3292, 3277, 2956, 2925, 2855, 2245, 2122, 1631, 1569, 1419, 1291, 1160, 1119, 1020.

1-(3,5-Difluoro-4-(7,7,7-trifluoroheptyl)phenyl)penta-1,4-diyn-3-ol (29e). The crude mixture was purified by flash column chromatography using up to 30% diethyl ether in pentane. The PAC **29e** (30 mg, 52% yield) was isolated as a grey wax. **^{1}H NMR** (300 MHz, $CDCl_3$) δ (ppm) 7.05 – 6.90 (m, 2H), 5.32 (d, J = 2.3Hz, 1H), 2.65 (t, J = 7.6 Hz, 2H), 2.63 (d, J = 2.2 Hz, 1H), 2.45 – 2.28 (bs, 1H), 2.15 – 1.95 (m, 2H), 1.70 – 1.45 (m, 4H), 1.45 – 1.30 (m, 4H).**^{13}C NMR** (75 MHz, $CDCl_3$) δ (ppm) 161.2 (dd, J = 246.9, 10.3 Hz), 127.4 (q, J = 276.4 Hz), 120.9 (t, J = 12.1 Hz), 119.9 (t, J = 20.5 Hz), 115.2 – 144.4 (m), 86.7, 82.5 (t, J = 3.8 Hz), 80.4, 73.4, 52.4, 33.7 (q, J = 28.3 Hz), 29.0, 28.8, 28.4, 22.2 (t, J = 2.2 Hz), 21.8 (q, J = 2.9 Hz). **^{19}F NMR** (282 MHz, $CDCl_3$) δ (ppm) -66.4, -115.4. **HRMS** (DCI-CH_4) *m/z*: calcd for $C_{18}H_{18}F_5O$ $[M+H]^+$: 345.1278, found: 345.1277.

1-(3-Fluoro-4-(heptyloxy)phenyl)penta-1,4-diyn-3-ol (33a). The crude mixture was purified by flash column chromatography using up to 20% diethyl ether in pentane. The PAC **33a** (40 mg, 48% yield) was isolated as a yellow oil. **^{1}H NMR** (300 MHz, $CDCl_3$) δ (ppm) 7.22 – 7.18 (m, 1H), 7.18 – 7.14 (m, 1H), 6.87 (t, J = 8.5 Hz, 1H), 5.32 (d, J = 2.3 Hz, 1H), 4.02 (t, J = 6.6 Hz, 2H), 2.61 (d, J = 2.3 Hz, 1H), 2.39 (bs, 1H), 1.90 – 1.75 (m, 2H), 1.55 – 1.20 (m, 8H), 0.95-0.80 (m, 3H).**^{13}C NMR** (75 MHz, $CDCl_3$) δ (ppm) 151.9 (d, J = 246.9 Hz), 148.3 (d, J = 10.7 Hz), 128.6 (d, J = 3.8 Hz), 119.5 (d, J = 19.5 Hz), 114.2 (d, J = 3.0 Hz), 113.9 (d, J = 8.4 Hz), 84.7, 83.7 (d, J = 2.7 Hz), 80.8, 73.0, 69.4, 52.5, 31.8, 29.1, 29.0, 25.9, 22.6, 14.1. **^{19}F NMR** (282 MHz, $CDCl_3$) δ (ppm) -134.1. **HRMS** (DCI-CH_4) *m/z*: calcd for $C_{18}H_{21}FO_2$ $[M]^+$: 288.1526, found: 288.1517.

1-(3-Fluoro-4-((6,6,6-trifluorohexyl)oxy)phenyl)penta-1,4-diyn-3-ol (33b). The crude mixture was purified by flash column chromatography using up to 40% diethyl ether in pentane. The PAC **33b** (40 mg, 33% yield) was isolated as a yellow oil. **^{1}H NMR** (300 MHz, $CDCl_3$) δ (ppm) 7.24 – 7.21 (m, 1H), 7.21 – 7.17 (m, 1H), 6.89 (t, J = 8.6 Hz, 1H), 5.35 (s, 1H), 4.06 (t, J = 6.3 Hz, 2H), 2.64 (t, J = 6.6 Hz, 1H), 2.41 (bs, 1H), 2.27 – 2.00 (m, 2H), 1.95 – 1.80 (m, 2H), 1.75 – 1.56 (m, 4H).**^{13}C NMR** (75 MHz, $CDCl_3$) δ (ppm) 151.9 (d, J = 247.0 Hz), 148.1 (d, J = 10.7 Hz), 127.6 (q, J = 273.8 Hz), 128.6 (d, J = 3.0 Hz), 119.6 (d, J = 20.3 Hz), 114.3 (d, J = 2.3 Hz), 114.1, 84.8, 83.6 (d, J = 2.8 Hz), 80.8, 73.0, 68.9, 52.5, 33.7 (q, J = 28.5 Hz), 28.8, 25.2, 21.7 (q, J = 3.0 Hz). **^{19}F NMR** (282 MHz, $CDCl_3$) δ (ppm) -66.4, -134.0. **HRMS** (DCI-CH_4) *m/z*: calcd for $C_{17}H_{17}F_4O_2$ $[M+H]^+$: 329.1165, found: 329.1169.

1-(4-(1,1-Difluorooctyl)phenyl)penta-1,4-diyn-3-ol (33c). The crude mixture was purified by flash column chromatography using up to 30% diethyl ether in pentane. The PAC **33c** (34 mg, 55% yield) was isolated as a brown oil. **^{1}H NMR** (300 MHz, $CDCl_3$) δ (ppm) 7.54 – 7.48 (m, 2H), 7.44 – 7.38 (m, 2H), 5.36 (d, J = 2.4Hz, 1H), 2.63 (d, J = 2.3Hz, 1H), 2.54 – 2.26 (bs, 1H), 2.22 – 2.00 (m, 2H), 1.48 – 1.36 (m, 2H), 1.36 – 1.20 (m, 6H), 0.95-0.85 (m, 3H).**^{13}C NMR** (75 MHz, $CDCl_3$) δ (ppm) 138.2 (t, J = 27.0 Hz), 132.0, 125.2 (t, J = 6.2 Hz), 123.2 (t, J = 1.8 Hz), 122.9 (t, J = 240.8 Hz), 86.6, 84.0, 81.4, 73.3, 52.6, 39.1 (t, J = 27.0 Hz), 31.7, 29.3, 29.1, 22.7, 22.5 (t, J = 4.5 Hz), 14.2. **^{19}F NMR** (282 MHz, $CDCl_3$) δ (ppm) -95.9. **HRMS** (DCI-CH_4) *m/z*: calcd for $C_{19}H_{23}F_2O$ $[M+H]^+$: 305.1717, found: 305.1730.

1-(5-Decylfuran-2-yl)penta-1,4-diyn-3-ol (37). The crude mixture was purified by flash column chromatography using up to 20% diethyl ether in pentane. The furyl PAC **37** (20 mg, 47%) was isolated as a brown oil. **^{1}H NMR** (400 MHz, $CDCl_3$) δ (ppm) 6.57 (d, J = 3.3 Hz, 1H), 5.98 (dt, J = 3.2, 0.9 Hz, 1H), 5.35 (dd, J = 7.7, 2.3 Hz, 1H), 2.61 (d, J = 2.3 Hz, 1H), 2.60 (t, J = 7.4 Hz, 2H), 2.32 (d, J = 7.9 Hz, 1H), 1.63 (quint, J = 7.6 Hz, 2H), 1.35 – 1.20 (m, 14H), 0.88 (t, J = 6.8 Hz, 3H).**^{13}C NMR** (100 MHz, $CDCl_3$): δ (ppm) 159.1, 133.9, 117.9, 106.5, 89.7, 80.4, 76.0, 73.4, 52.6, 32.0, 29.7, 29.7, 29.5, 29.3, 28.4, 28.0, 22.8, 14.3. **HRMS** (DCI-CH_4) *m/z*: calcd for $C_{19}H_{27}O_2$ $[M+H]^+$: 287.2011, found: 287.2012. **FTIR** (cm^{-1}) (neat): 3300, 2926, 2855, 1710, 1264, 734, 703.

1-(5-Decylfuran-2-yl)penta-1,4-diyn-3-ol (41). The crude mixture was purified by flash column chromatography using up to 20% *tert*-butyl-methyl ether in pentane. The furyl PAC **41** (30 mg, 55%) was isolated as a brown oil. **^{1}H NMR** (400 MHz, $CDCl_3$) δ (ppm) 7.51 (d, J = 0.9 Hz, 1H), 6.04 (q, J = 0.9 Hz, 1H), 5.29 (dd, J = 7.6, 2.3 Hz, 1H), 2.60 (d, J = 2.3 Hz, 1H), 2.57 (td, J = 7.6, 0.9 Hz, 2H), 2.26 (d, J = 7.6 Hz, 1H), 1.60 (quint, J = 7.6 Hz, 2H), 1.35 – 1.20 (m, 14H), 0.88 (t, J = 6.8 Hz, 3H).**^{13}C NMR** (100 MHz, $CDCl_3$): δ (ppm) 157.3, 145.0, 107.5, 106.6, 87.0, 81.0, 73.0, 52.7, 32.0, 29.7, 29.7, 29.5, 29.2, 27.9, 27.9, 22.8, 14.3. **HRMS** (DCI-CH_4) *m/z*: calcd for $C_{19}H_{26}O_2$ $[M]^+$: 286.1933, found: 286.1934. **FTIR** (cm^{-1}) (neat): 3303, 2925, 2854, 2123, 1264, 1158, 1137, 735, 704.

1-(4-(Oct-7-yn-1-yl)phenyl)penta-1,4-diyn-3-ol (46). The crude mixture was purified by flash column chromatography using up to 20% diethyl ether in pentane. The PAC **46** (19 mg, 55% yield) was isolated as a yellow oil. **^{1}H NMR** (300 MHz, $CDCl_3$) δ (ppm) 7.38 (d, J = 8.2 Hz, 2H), 7.13 (d, J = 8.5 Hz, 2H), 5.34 (dd, J = 7.6, 2.3 Hz, 1H), 2.61 (d, J = 2.3 Hz, 1H), 2.60 (t, J = 7.6 Hz, 2H), 2.30 (d, J = 7.6 Hz, 1H), 2.18 (td, J = 6.9, 2.5 Hz, 1H), 1.94 (t, J = 2.6 Hz, 1H), 1.70 – 1.20 (m, 6H). **^{13}C NMR** (125 MHz, $CDCl_3$) δ (ppm) 144.2, 131.9, 128.6, 119.0, 85.1, 85.0, 84.8, 81.1, 73.0, 68.3, 52.8, 35.9, 31.1, 29.9, 28.8, z28.5, 18.5 **HRMS** (DCI-CH_4) *m/z*: calcd for $C_{19}H_{21}O$ $[M+H]^+$: 265.1592, found: 265.1579. **FTIR** (cm^{-1}) (neat): 3277, 3195, 2931, 2852, 2578, 2231, 1509, 1297, 1023.

Access to an enantiomerically enriched PAC derivative:

(*S*)-1-(4-Octylphenyl)penta-1,4-diyn-3-ol ((*S*)-5.8a).

*Reaction between 1-ethynyl-4-octylbenzene (**3.8a**) and TMS-propynal.*

(*R*)-1-(4-Octylphenyl)-5-(trimethylsilyl)penta-1,4-diyn-3-ol (4.8a).

A flame-dried flask was charged with $Zn(OTf)_2$ (4 eq., 3.46 g, 9.51 mmol) and (-)-*N*-methyl ephedrine (4 eq., 1.70 g, 9.51 mmol) and dried under vacuum with stirring for 2h. Anhydrous DCM (4 mL) and freshly distilled Et_3N (4 eq., 1.33 mL, 9.51 mmol) were added and the resulting mixture was stirred at RT for a further 2 h. A solution of 1-ethynyl-4-octylbenzene (**3.8a**) (1 eq., 510 mg, 2.38 mmol) in anhydrous DCM (2 mL) was cannulated. The resulting mixture was stirred at RT for 45 min before dropwise addition of TMS-propynal (1 eq., 300 mg, 2.38 mmol) in anhydrous DCM (2 mL). The reaction mixture was stirred at RT for 12 h before being quenched by addition of aqueous saturated NH_4Cl solution and extracted with DCM (3x). The combined organic layers were then washed with water and brine, dried over $MgSO_4$ and concentrated under reduced pressure. The crude mixture was purified by flash column chromatography on silica

gel eluted with up to 20% diethyl ether in pentane. The silylated alkynylcarbinol (*R*)-**4.8a** was isolated as a yellow oil (573 mg, 74% yield). The characterization data were identical to that of the racemic compound **4.8a** except for optical rotation, $[\alpha]_D^{20}$ = + 4.9 (*c* 0.9, $CHCl_3$).

(*S*)-1-(4-Octylphenyl)penta-1,4-diyn-3-ol ((*S*)-5.8a).

A solution of the silylated alkynylcarbinol (*R*)-**4.8a** (553 mg, 1.62 mmol) in MeOH (29.3 mL) containing K_2CO_3 (0.2 eq., 45 mg, 325 µmol) was stirred at RT for 1h30. DCM and water were added and extraction was realized with DCM (3x). The combined organic layers were dried over $MgSO_4$, filtered and concentrated under reduced pressure. The crude mixture was purified by flash column chromatography on silica gel eluted with up to 20% diethyl ether in pentane. The alkynylcarbinol (*S*)-**5.8a** (272 mg, 62% yield) was isolated as a yellow oil with a 57% enantiomeric excess, as measured by analytical chiral supercritical fluid (Chiralpak IG 3 µm (4.6 x 100 mm) column, 90:10 $ScCO_2$/MeOH, 2 mL/min, 100 bar, 40 °C).

*Reaction between TMS acetylene and 3-(4-octylphenyl)propiolaldehyde (**28a**).*

(*R*)-1-(4-Octylphenyl)-5-(trimethylsilyl)penta-1,4-diyn-3-ol (4.8a).

A flame-dried flask was charged with $Zn(OTf)_2$ (4 eq., 822 mg, 2.24 mmol) and (+)-*N*-methyl ephedrine (4 eq., 405 mg, 2.24 mmol) and dried under vacuum with stirring for 2 h. Anhydrous DCM (2 mL) and freshly distilled Et_3N (4 eq., 315 µL, 2.24 mmol) were added and the resulting mixture was stirred at RT for a further 2 h. TMS acetylene (4 eq., 313 µL, 2.24 mmol) was added. The resulting mixture was stirred at RT for 45 min before dropwise addition of 3-(4-octylphenyl)propiolaldehyde (**28a**) (1 eq., 137 mg, 0.56 mmol) in anhydrous DCM (1.5 mL). The reaction mixture was stirred at RT for 12h before being quenched by addition of aqueous saturated NH_4Cl solution and extracted with DCM (3x). The combined organic layers were then washed with water and brine, dried over $MgSO_4$ and concentrated under reduced pressure. The crude mixture was purified by flash chromatography on silica gel eluted with up to 20% diethyl ether in pentane. The silylated alkynylcarbinol (*R*)-**4.8a** was isolated as a yellow oil (74 mg, 39% yield). The characterization data were identical to that of the racemic compound **4.8a** except for optical rotation, $[\alpha]_D^{20}$ = + 5.4 (*c* 1.8, $CHCl_3$).

(*S*)-1-(4-Octylphenyl)penta-1,4-diyn-3-ol ((*S*)-5.8a).

A solution of the silylated alkynylcarbinol (*R*)-**4.8a** (70 mg, 205 µmol) in MeOH (4 mL) containing K_2CO_3 (0.2 eq., 5.7 mg, 41 µmol) was stirred at RT for 1 h 30. DCM and water were added and extraction was realized with DCM (3x). The combined organic layers were dried over $MgSO_4$, filtered and concentrated under reduced pressure. The crude mixture was purified by flash chromatography on silica gel eluted with up to 20% diethyl ether in pentane. The alkynylcarbinol (*S*)-**5.8a** (41 mg, 67% yield) with an 88% enantiomeric excess, as measured by analytical chiral supercritical fluid (Chiralpak IG 3 µm (4.6 x 100 mm) column, 90:10 $ScCO_2$/MeOH, 2 mL/min, 100 bar, 40 °C).

Biological evaluation

Cell lines and treatments.

HCT-116 (Horizon Discovery) and U2OS (ATCC) cells were grown in DMEM 10% Fetal Bovine Serum (FBS) with penicillin and streptomycin (pen./strep.; Thermo Fisher Scientific) at 37 °C in 5% CO_2 humidified incubator. U2OS cells derivatives, KO for HSD17B11 stably complemented with GFP, HSD17B11-GFP or HSD17B13-GFP, or stably expressing the UPS reporter Ub-G76V-YFP or fluorescent proteins marking mitochondria and/or ER were previously generated and described in ref. 22. Cells were treated in complete growth medium except when stated otherwise. Z-VAD-fmk (Selleckchem) was used at 50 µM and a 1 h pre-incubation was performed. BI-3231 was obtained thanks to the opnMe platfom (https://www.opnme.com/).

Cell viability assays.

Cell viability was analyzed using SulfoRhodamine B assays (SRB) on exponentially growing cells as previously described.[68] Each point was measured in duplicate and IC_{50} were obtained using at least three independent experiments. Error bars represent standard deviations. IC_{50} were computed with the GraphPad Prism software using a non-linear regression to a four-parameter logistic curve (variable slope).

Analysis by SDS-PAGE of proteins modified by PACs in cells.

Sub-confluent 60 mm dishes, seeded one day before with U2OS cells, were treated for 2 h with 2 µM of the indicated molecules. At the end of the treatment, the cells were washed with cold PBS and collected by scrapping in PBS 2% SDS. Extracts were incubated 5 min at 95 °C and passed 10 times through a 25G needle. Measuring the absorbance at 280 nm with a Nanododrop spectrometer (Thermo Fisher Scientific) was used to evaluate protein concentration and 40 µL of extracts containing 10 mg/mL of proteins were prepared in PBS 2% SDS. $CuSO_4$, sodium ascorbate and azido-AlexaFluor647 were added to the extracts to reach 4 mM, 10 mM and 2 µM, respectively, in a 50 µL reaction which was incubated 30 min at 20 °C. 6.5 µL of the reaction was added to 40 µL of loading solution (60 mM Tris-HCl pH 6.8, 10% glycerol, 2% SDS, 0.005% bromophenol blue, 100 mM dithiothreitol), incubated at 95 °C for 5 min and loaded on a SDS-PAGE gel (BioRad 4-15% TGX pre-cast gels). After protein separation, the gel was scanned on an infrared imager (700 nm, Odyssey, LI-COR Biosciences). Total proteins in the gel were visualized using Coomassie (InstantBlue, Sigma-Aldrich), scanned with the Biorad Chemidoc imager.

Click-based imaging.

Cells were seeded on #1.5 glass coverslips (VWR) the day before the experiment. At the end of treatments, cells were washed twice with PBS, fixed 15 min with 2% PFA in PBS and washed three times with PBS. Cells were permeabilised by incubation 5 min in PBS 0.2% Triton X-100 before being washed three times with PBS. Click with AlexaFluor488-azido was performed as described.[69] At the end of the procedure, cells were washed four times with PBS-T, twice with PBS and incubated 15 min in PBS containing 2 µg/mL DAPI (Sigma-Aldrich). The coverslips were washed twice with PBS and mounted with VectaShield (Vector laboratories) on glass slides. Images were acquired on a Zeiss Elyra 7 3D Lattice SIM super-resolution microscope fitted with a 63X objective (PLANAPO NA 1.4, Zeiss) and dual sCMOS cameras (pco.edge). 3D-SIM reconstructions were performed with Zen Black (Zeiss).

Live cell imaging.

Pictures of living cells were acquired using an Olympus IX73 fluorescence microscope fitted with a 20X 0.40 NA objective (LCAChN 0.4NA, Olympus) or a 40X objective (0.75NA UPlanFLN, Olympus), a X-Cite Series 120Q lamp (Lumen dynamics), a DP26 camera (Olympus) and using the adequate filters set. For time series, cells were seeded in glass-bottom dishes (ibidi µSlide) in phenol red-free Leibovitz's L-15 medium containing 10% FBS and pen./strep. For each time point, z-stacks were acquired using a Zeiss Elyra 7 3D Lattice SIM super-resolution microscope fitted with a 63X objective (PLANAPO NA 1.4, Zeiss) and dual sCMOS cameras (pco.edge). 3D-SIM reconstructions were performed with Zen Black (Zeiss) and pictures represent max intensity 3D projections.

Flow cytometry.

U2OS cells stably expressing the Ub-G76V-YFP UPS substrate[22,70] were seeded in 60 mm dishes the day before the experiment. Cells were treated for 4 h in complete medium as indicated. At the end of the treatment, cells were washed with PBS, collected by trypsination and washed with the Cell Staining Buffer (CSB, #420201, Biolegend), before fixation for 15 min at room temperature in 2 % paraformaldehyde in PBS.

After fixation, cells were washed with CSB and analyzed using a Fortessa X20 flow cytometer (Becton Dickinson). A minimum of 32 000 cells were acquired per condition. The data were analyzed and formatted using FlowJo v10.8.1. Untreated cells were used to define a gate to identify the YFP positive cells in the treated conditions.

Immunoblotting.

U2OS cells were treated in complete growth medium as indicated. At the end of treatment, cells were washed with cold PBS before being scrapped in 75-100 µL of SDS Lysis Buffer (120 mM Tris-HCl pH6.8, 20 % glycerol 4 % SDS). Lysis and immunoblotting were performed as described.22 The primary antibodies used were: mouse anti-beta-actin (1/2500, sc-47778, Santa Cruz Biotech), rabbit anti-phosphoSer724-IRE1apha (1/1000, NB100-2323, Novus Biologicals), rabbit anti-phosphoThr980-PERK (1/500, #3179, Cell Signaling Technology), rabbit anti-PERK (1/1000, #5683, Cell Signaling Technology), rabbit anti-ATF6 (1/1000, #65880, Cell Signaling Technology), rabbit anti-HSP70 (1/3000, 10995-1-AP, Proteintech), rabbit anti-PARP-1 (1/1000, #9532, Cell Signaling Technology). The secondary antibodies used were horse-radish peroxidase (HRP)-conjugated goat anti-mouse or anti-rabbit secondary antibodies (Jackson Immunoresearch Laboratories diluted at 1/10000). Signal acquisition was performed with a CCD camera (Chemidoc, BioRad) after incubation with peroxidase chemiluminescent substrates (WesternBright, Advansta). To probe all the markers in each experiment, the same extracts were analyzed on different immunoblots, each one with its loading control (see source data in the SI), and the pictures were grouped in logical order on the figure to facilitate the data analysis.

Molecular graphics and docking studies

Molecular graphics were performed with the UCSF Chimera package.[71] Chimera is developed by the Ressource for Biocomputing, Visualization, and Informatics at the University of California, San Francisco (supported by the NIGMS P41-GM103311).

The protein structures used in this paper were downloaded from the RCSB Protein Database[72] and aligned on a reference structure 1A27 chain A (17ß/1 HSD, HSD17B1, formerly 1A27a)[56] after analysis of Uniprot P14061/DHB1_HUMAN domain.[73] The protein structures, were prepared (structure checks, rotamers, hydrogenation, splitting of chains) using Biovia (www.3dsbiovia.com) Discovery Studio Visualizer 2021 (DSV) and UCSF Chimera.

The new compounds were sketched using ChemAxon Marvin 21 (www.chemaxon.com). All ligands were checked (hybridization, hydrogenation, some geometry optimizations, 3D sketching) and merged in SDF libraries using DSV.

Molecular modeling studies were carried with Molegro Virtual Docker 6 software (www.molexus.com) using the AlphaFold model Q8NBQ5-F1 (formerly AF-Q8NBQ5, 17ß/11 HSD). Using structural alignments, the cofactor NAD+ from structure 1FDV (chain A, formerly 1FDVa, HDS17B1)[54] and estradiol (EST) from structure 1A27a were placed in binding site. A search space volume of 15 Å radius was centered in the binding pocket around ligand EST.

A flexible docking protocol (OPT) was used after training on 1FDVa structure. According to structural study, using 1FDVa, 1YB1a and model AF-Q8NBQ5, 16 residues were defined as flexible: ALA173, ALA174, ASN219, ILE226, ILE285, LEU182, LEU233, LYS282, PHE220, PHE289, PRO229, SER172, THR231, TYR185, VAL179 and VAL287. The residue PHE225 is far from ligand-cofactor interface and was not set flexible. Softened potentials were used with a tolerance of 1 and a strength 0.9. Note that PHE225, TYR185 and SER172 are analogous to the PHE192, TYR155 and SER142 residues known in HDS17B1 class (see ESI). No displaceable water molecules were taken in account at the interface (known as mainly hydrophobic) between cofactor and ligands.

Docking process used 10000 iteration steps, the convergence was reached for all ligands, other parameters were let as default. This protocol is set for 30 to 100 independent runs (depending on the ligand). A final minimization (per run) was parameterized using 4000 steps for lateral chains and 2000 steps for protein backbone. The cofactor was set as NAD+ (see ESI) with partial negative charges on phosphates and positive charge on nicotinamide group. The MolDock Optimizer was used as search algorithm, and was parametrized with a population size of 75, a scaling factor of 0.50 and a grid resolution of 0.3 Å. Clustering of poses (tabu clustering) was set with an RMS threshold of 1.8 Å in order to be more discriminant on the best poses. Templates (pharmacophoric profile) were used with a strength of 500 and a grid resolution of 0.3 Å. Only one atom position is used as template: the oxygen (O17) from estradiol (EST/1A27) as hydrogen donor/acceptor, similarity measure parameters were let at their default values. MolDock and Rerank scores were calculated post-docking and post-minimization.[74]

The protocol was able to reach a RMSD of 0.7 Å for reproduction of crystallographic EST in 1A27a (after reconstruction of SER142). This result cannot be directly compared with 1FDVa and AF-Q8NBQ5 because the aligned structures are slightly staggered, and the best poses followed this shift. Nevertheless, a RMSD of 1.1 Å could be achieved in 1FDVa (pose in the three best combined scores).

In the case of AF-Q8NBQ5, the bottom of binding site includes PHE220 (set as flexible in docking) which is directed upper, crossing the envelop of estradiol from 1A27a. The ASN219-PHE220 of AF-Q8NBQ5 are analogous to GLY186-PRO187 of 1FVDa/1A27a. In consequence, the ligands were compared with two conformations taken as references: estradiol from 1A27a, and best pose (staggered but conform) of the same compound in AF-Q8NBQ5 (**Figure 9A**). Using these results, another control was carried on template's constraint: the parameters allow the needed displacements of **EST** hydroxy function around the pharmacophoric position. When used with ligands, this protocol produces typical pose sets with: i) fluctuations of the chains, covering the conformational space in the cavity, and ii) limited set of fluctuations at warhead level, focused on one or two groups of hydroxy positions (see ESI).

Compound maximum solubility in the injection solution.

(*S*)-**5.8a** maximum solubility in the injection solution (0.9 % NaCl, 10% Kolliphor EL) was determined by the PCBIS facilities (UAR3286, Illkirch) by incubating ~1 mg of molecule in 500 µL of injection solution for 24h at room-temperature (~20 °C) on a rotating shaker and by measuring the molecule concentration in the supernatant obtained after centrifuging at 15 000 g for 5 min. For this, each supernatant was diluted at 1/50 in H_2O:CH_3CN (1:1) and 10 µL were analyzed by HPLC (Shimadzu, 2.6 µm C18 100A 50x4.6 mm Kinetex column, 0.05% TFA-CH_3CN 2 mL/min gradient elution) by monitoring the absorbance at 254 nm of the peak of the molecule of interest. The corresponding concentration was determined using a calibration curve with the pure compounds diluted in H_2O:CH_3CN mixture. The analyses were repeated twice.

Pharmacokinetics analyses in mice.

Pharmacokinetics studies were performed by the PCBIS facilities (UAR3286, Illkirch) on CD-1 mice. All animal protocols used by the PCBIS facilities were reviewed and approved by the agriculture ministry regulating animal research in France (Ethics regional committee for animal experimentation Strasbourg, APAFIS 1341#2015080309399690). Administration were performed to reach 5 mg/kg with each route using 3 mice per time point. Stock solutions at 2.5 g/mL for IV injection, 1.25 mg/mL for SC injection and 0.5 mg/mL for per os and IP routes were used. Mice were sacrificed and blood was collected at 5, 15, 30, 60, 120, 360 and 480 min after injection. The plasma was isolated from each sample by centrifugation 10 000 g at 16 °C for 5 min and frozen at -80 °C before analysis. The samples from the 5 and 15 min time points were diluted at 1/20 in plasma. For analysis, 400 µL of each plasma sample was mixed with 1 mL of CH_3CN, vortexed 5 min, incubated 1 min in a sonicating water bath and centrifuged 15 000 g for 5 min at 16 °C. The supernatant containing the extracted small molecules were analyzed by LC-MS/MS: Shimadzu UHPLC LC-MS 8030, FIA mode, 1 µL injection,

positive electrospray ionization, kinetex 2.6 µm C8 100A 50x2.1 mm Phenomenex column, 0.05% HCOOH to CH_3CN 0.5 mL/min gradient elution, selected m/z: 251.20 ($[M\text{-}OH]^+$), 152.00 and 153.10, retention time = 1.42 min. A calibration curve was generated using each compound diluted in extracted plasma to determine the exact plasma concentration for each time point. The half-life for each compound was determined from the blood concentration time curve using the non-compartmental analysis of PK Solver 2.0.

Toxicity analysis in mice.

(*S*)-**5.8a** toxicity was analyzed by Imavita SAS (Toulouse, France) on Balb/c adult female mice with 6 mice per group using 3 IV injections a week for 3 weeks. Animal housing and care complied with the recommendations of Directive 86/609/EEC and the facilities agreement was obtained from the French Veterinary Authorities. The *in vivo* design and procedures were assessed by Ethical Committee N°CEEA-122 (Imavita ethical project identification N°IMV-ETH-13). 0.4, 1 and 2 mg/mL injection solutions in saline containing 10% Cremophor were prepared and used for 5 mL/kg injections to reach the 2, 5 and 10 mg/kg dosage of each group. Reversible tail swelling was observed in some mice, especially with the highest dosage. When IV injection was not possible (e.g. due to tail swelling), an IP injection at the same dosage was performed. Animals were weighted 3 times a week and observed daily for signs of toxicity. Animals were euthanized by cervical dislocation under isoflurane anesthesia at the end of the toxicity analysis or when ethical limit endpoints were reached.

ASSOCIATED CONTENT

Supporting Information

Preparation of all halo-(hetero)aryl precursors, synthesis of all racemic PAC derivatives according to route A or B, corresponding analytical chromatograms of **5.8a**, **5.8b**, **29c**, **29d**, **33a**, **33b**, **33c**, enantioselective preparation of **5.8a** and corresponding chiral analytical chromatograms of both enantiomers, chromatographic chiral resolution of **5.8a**, **29c** and **33c** and corresponding chiral analytical chromatograms of both enantiomers, synthesis and corresponding analytical chromatograms of the racemic clickable probe **46**, chromatographic chiral resolution of **46** and corresponding chiral analytical chromatograms of both enantiomers, immunoblotting source data of **Figure 7C/D**, structural studies for *in silico* docking, table of optimized docked poses energy, illustration of poses fluctuation with (*S*)-**B** and localization of the CF_2 group of (*S*)-**33c** in the vicinity of the 3-OH group of **EST** (PDF). Molecular Formula Strings of all compounds including the associated biological data (CSV). Molecular modeling structures and docked ligand complexes (PDB).

AUTHOR INFORMATION

Corresponding Authors

Yves Génisson* - *Laboratoire de Synthèse et Physico-Chimie de Molécules d'Intérêt Biologique (SPCMIB), UMR 5068, CNRS, Université Paul Sabatier-Toulouse III, Toulouse, France; orcid.org/0000-0002-3647-4617; Phone: +33 5 61 55 62 99; Email: yves.genisson@univ-tlse3.fr*

Sébastien Britton* - *Institut de Pharmacologie et de Biologie Structurale (IPBS), Université de Toulouse, CNRS, Université Toulouse III - Paul Sabatier (UT3), Toulouse, France*

Remi Chauvin* - *LCC-CNRS, Université de Toulouse, CNRS UPR 8241, UPS, Toulouse, France*

Present Addresses

Pauline Rullière[†]- *Solvionic company, Toulouse, France*

Maroua Bourkhis[¥] - *Laboratory of Physics of Lamellar Materials and Hybrid Nanomaterials, University of Carthage, Faculty of Sciences of Bizerte, Zarzouna, 7021, Bizerte, Tunisia*

Author Contributions

The manuscript was written through contributions of all authors. All authors have given approval to the final version of the manuscript.

Funding Sources

This study received fundings from Toulouse Tech Transfer (TTT Maturation Program), the Toulouse IDEX Transversalité program with the "Fishing Sponge" grant, the "Fondation ARC" with a postdoc fellowship to PR and the PJA 20171206477 grant, "Agence Nationale de la Recherche" with the ANR-17-CE18-0002-01 grant, the Université Toulouse 3-Région Occitanie with a PhD fellowship to MB and the Région Occitanie with the "Prématuration Prostacure" grant.

Notes

The authors declare no competing financial interest.

ACKNOWLEDGMENT

We are grateful to the TRI-IPBS Imaging Core Facility, member of TRI-Genotoul and of the national France-BioImaging Infrastructure supported by the French National Research Agency (ANR-10-INSB-04), for providing access to equipment and storage resources. The analysis by supercritical CO_2 were recorded on Acquity UPC², from Waters, which are part of the "Integrated Screening Platform of Toulouse" (PICT, GenoToul, IBiSA), whereas the enantiopurifications by supercritical fluids were made on Prep80, from Waters, which are part of the "Chemistry Institute of Toulouse" (ICT, UAR2599).

ABBREVIATIONS

BAC, butadiynyl alkynylcarbinol; CuAAC, copper-catalyzed azide-alkyne cycloaddition; DAC, dialkynylcarbinol; DAPI, 4′,6-diamidino-2-phenylindole; DMP, Dess-Martin periodinane; DTT, dithiothreitol; ER, endoplasmic reticulum; KO, knockout; LAC, lipidic alkynylcarbinols; NME, *N*-methyl ephedrine; PAC, phenyl dialkynylcarbinols; PIntB, *N*-phenyl-2-(di-*t*-butylphosphino)indole; SDR, short-chain dehydrogenase/reductase; SDS, sodium dodecyl sulfate; TLC, thin layer chromatography; TMEDA, *N*,*N*,*N*′,*N*′-Tetramethylethylenediamine; TMS, trimethylsilyl; UPR, unfolded protein response; UPS, ubiquitin-proteasome system; WT, wild-type.

REFERENCES

(1) Shun, A. L. K. S.; Tykwinski, R. R. Synthesis of naturally occurring polyynes. *Angew. Chem. Int. Edit* **2006,** *45*, 1034-1057.

(2) Gung, B. W. Total synthesis of polyyne natural products. *Cr. Chim.* **2009,** *12*, 489-505.

(3) Pan, Y. Q.; Lowary, T. L.; Tykwinski, R. R. Naturally occurring and synthetic polyyne glycosides. *Can. J. Chem.* **2009,** *87*, 1565-1582.

(4) Kuklev, D. V.; Dembitsky, V. M. Epoxy acetylenic lipids: Their analogues and derivatives. *Prog. Lipid Res.* **2014,** *56*, 67-91.

(5) Listunov, D.; Maraval, V.; Chauvin, R.; Génisson, Y. Chiral alkynylcarbinols from marine sponges: asymmetric synthesis and biological relevance. *Nat. Prod. Rep.* **2015,** *32*, 49-75.

(6) Dawid, C.; Dunemann, F.; Schwab, W.; Nothnagel, T.; Hofmann, T. Bioactive C-17-Polyacetylenes in Carrots (Daucus carota L.): Current Knowledge and Future Perspectives. *J. Agr. Food Chem.* **2015,** *63*, 9211-9222.

(7) Santos, P.; Busta, L.; Yim, W. C.; Cahoon, E. B.; Kosma, D. K. Structural diversity, biosynthesis, and function of plant falcarin-type polyacetylenic lipids. *J. Exp. Bot.* **2022**, *73*, 2889-2904.

(8) Dembitsky, V. M. Anticancer activity of natural and synthetic acetylenic lipids. *Lipids* **2006,** *41*, 883-924.

(9) Dembitsky, V. M.; Levitsky, D. O. Acetylenic terrestrial anticancer agents. *Nat. Prod. Commun.* **2006,** *1*, 405-429.

(10) Dembitsky, V. M.; Levitsky, D. O.; Gloriozova, T. A.; Poroikov, V. V. Acetylenic aquatic anticancer agents and related compounds. *Nat. Prod. Commun.* **2006,** *1*, 773-811.

(11) Siddiq, A.; Dembitsky, V. Acetylenic anticancer agents. *Anti-Cancer Agent Med. Chem.* **2008,** *8*, 132-170.

(12) El Arfaoui, D.; Listunov, D.; Fabing, I.; Oukessou, M.; Frongia, C.; Lobjois, V.; Samson, A.; Ausseil, F.; Ben-Tama, A.; El Hadrami, E.; Chauvin, R.; Génisson, Y. Identification of Chiral Alkenyl- and Alkynylcarbinols as Pharmacophores for Potent Cytotoxicity. *ChemMedChem* **2013,** *8*, 1779-1786.

(13) Listunov, D.; Fabing, I.; Saffon-Merceron, N.; Gaspard, H.; Volovenko, Y.; Maraval, V.; Chauvin, R.; Génisson, Y. Asymmetric Synthesis and Biological Evaluation of Natural or Bioinspired Cytotoxic C-2-Symmetrical Lipids with Two Terminal Chiral Alkynylcarbinol Pharmacophores. *J. Org. Chem.* **2015,** *80*, 5386-5394.

(14) Listunov, D.; Mazeres, S.; Volovenko, Y.; Joly, E.; Génisson, Y.; Maraval, V.; Chauvin, R. Fluorophore-tagged pharmacophores for antitumor cytotoxicity: Modified chiral lipidic dialkynylcarbinols for cell imaging. *Bioorg. Med. Chem. Lett.* **2015,** *25*, 4652-4656.

(15) Listunov, D.; Billot, C.; Joly, E.; Fabing, I.; Volovenko, Y.; Génisson, Y.; Maraval, V.; Chauvin, R. Extended structural modulation of bio-inspired chiral lipidic alkynylcarbinols as antitumor pharmacophores. *Tetrahedron* **2015,** *71*, 7920-7930.

(16) Listunov, D.; Saffon-Merceron, N.; Joly, E.; Fabing, I.; Génisson, Y.; Maraval, V.; Chauvin, R. Ethynylogation approach in pharmacophore design: from alkynyl-to butadiynyl-carbinols vs antitumoral cytotoxicity. *Tetrahedron* **2016,** *72*, 6697-6704.

(17) Bourkhis, M.; Gaspard, H.; Rullière, P.; de Almeida, D. K. C.; Listunov, D.; Joly, E.; Abderrahim, R.; de Mattos, M. C.; de Oliveira, M. C. F.; Maraval, V.; Chauvin, R.; Génisson, Y. Skeletal Optimization of Cytotoxic Lipidic Dialkynylcarbinols. *ChemMedChem* **2018,** *13*, 1124-1130.

(18) Listunov, D.; Joly, E.; Duhayon, C.; Saffon-Merceron, N.; Fabing, I.; Génisson, Y.; Maraval, V.; Chauvin, R. Methinylogation Approach in Chiral Pharmacophore Design: from Alkynyl- to Allenyl-carbinol Warheads against Tumor Cells. *ChemMedChem* **2018,** *13*, 1711-1722.

(19) Rullière, P.; Lizeaux, F.; Joly, E.; Ballereau, S.; Gaspard, H.; Maraval, V.; Chauvin, R.; Génisson, Y. Fluorinated analogues of lipidic dialkynylcarbinol pharmacophores: synthesis and cytotoxicity in HCT116 cancer cells, *French-Ukrainian J. Chem.* **2019**, *7*, 1-9.

(20) de Almeida, D. K. C.; da Silva, M. R.; de Mattos, M. C.; Nunes, F. M.; Ballereau, S.; Génisson, Y.; Maraval, V.; Chauvin, R.; Oliveira, M. C. F. Lipase-catalysed enantioselective kinetic resolution of rac-lipidic alkynylcarbinols and a C-5 synthon thereof via a hydrolysis approach. *Mol. Catal.* **2020,** *488*, article 110926.

(21) Listunov, D.; Joly, E.; Rullière, P.; Gaspard, H.; Bernardes-Génisson, V.; Génisson, Y.; Maraval, V.; Chauvin, R. From Natural to Artificial Antitumor Lipidic Alkynylcarbinols: Asymmetric Synthesis, Enzymatic Resolution, and Refined SARs. *Synthesis-Stuttgart* **2018,** *50*, 3114-3130.

(22) Demange, P.; Joly, E.; Marcoux, J.; Zanon, P. R. A.; Listunov, D.; Rullière, P.; Barthes, C.; Noirot, C.; Izquierdo, J. B.; Rozie, A.; Pradines, K.; Hee, R.; de Brito, M. V.; Marcellin, M.; Serre, R. F.; Bouchez, O.; Burlet-Schiltz, O.; Oliveira, M. C. F.; Ballereau, S.; Bernardes-Génisson, V.; Maraval, V.; Calsou, P.; Hacker, S. M.; Génisson, Y.; Chauvin, R.; Britton, S. SDR enzymes oxidize specific lipidic alkynylcarbinols into cytotoxic protein-reactive species. *Elife* **2022,** *11*, e73913.

(23) HSD17B11 had also been identified as a mediator of (3*S*)-dehydrofalcarinol cytotoxicity in cancer cells: Grant, C. V.; Cai, S.; Risinger, A. L.; Liang, H.; O'Keefe, B. R.; Doench, J. G.; Cichewicz, R. H.; Mooberry, S. L. CRISPR-Cas9 Genome-Wide Knockout Screen Identifies Mechanism of Selective Activity of Dehydrofalcarinol in Mesenchymal Stem-like Triple-Negative Breast Cancer Cells. *J. Nat. Prod.* **2020,** *83*, 3080-3092.

(24) Viedma-Poyatos, A.; Gonzalez-Jimenez, P.; Langlois, O.; Company-Marin, I.; Spickett, C. M.; Perez-Sala, D. Protein Lipoxidation: Basic Concepts and Emerging Roles. *Antioxidants-Basel* **2021**, *10*, 295.

(25) Chauvin, R.; Lepetit, C.; Maraval, V.; Leroyer, L. Variation of aromaticity by twisting or expanding the ring content. *Pure Appl. Chem.* **2010**, *82*, 769-800.

(26) Frantz, D. E.; Fassler, R.; Tomooka, C. S.; Carreira, E. M. The discovery of novel reactivity in the development of C-C bond-forming reactions: In situ generation of zinc acetylides with Zn-II/R_3N. *Accounts Chem. Res.* **2000,** *33*, 373-381.

(27) For an adaptation of this methodology to ynals, see: Li, M.; Zou, C. H.; Duhayon, C.; Chauvin, R. Stereoselective double addition of chiral alkynyl-zincs to cobalt-stabilized acetylenedicarbaldehyde. *Tetrahedron Lett.* **2006,** *47*, 1047-1050.

(28) Purser, S.; Moore, P. R.; Swallow, S.; Gouverneur, V. Fluorine in medicinal chemistry. *Chem. Soc. Rev.* **2008,** *37*, 320-330.

(29) Gillis, E. P.; Eastman, K. J.; Hill, M. D.; Donnelly, D. J.; Meanwell, N. A. Applications of Fluorine in Medicinal Chemistry. *J. Med. Chem.* **2015,** *58*, 8315-8359.

(30) Torborg, C.; Zapf, A.; Beller, M. Palladium catalysts for highly selective Sonogashira reactions of aryl and heteroaryl bromides. *ChemSusChem* **2008,** *1*, 91-96.

(31) Christiansen, E.; Due-Hansen, M. E.; Ulven, T. A Rapid and Efficient Sonogashira Protocol and Improved Synthesis of Free Fatty Acid 1 (FFA1) Receptor Agonists. *J. Org. Chem.* **2010,** *75*, 1301-1304.

(32) Jagodzinska, M.; Huguenot, F.; Candiani, G.; Zanda, M. Assessing the Bioisosterism of the Trifluoromethyl Group with a Protease Probe. *ChemMedChem* **2009,** *4*, 49-51.

(33) Meanwell, N. A. Fluorine and Fluorinated Motifs in the Design and Application of Bioisosteres for Drug Design. *J. Med. Chem.* **2018,** *61*, 5822-5880.

(34) Zheng, X. K.; Zheng, X. Q.; Zhang, C.; Zhang, Q. Y.; Jiang, Y.; Tu, P. F. Cytotoxic polyacetylenes isolated from the roots and rhizomes of Notopterygium incisum. *Chinese Chem. Lett.* **2019,** *30*, 428-430.

(35) Sromek, A. W.; Rubina, M.; Gevorgyan, V. 1,2-Halogen migration in haloallenyl ketones: Regiodivergent synthesis of halofurans. *J. Am. Chem. Soc.* **2005,** *127*, 10500-10501.

(36) Heydenreuter, W.; Kunold, E.; Sieber, S. A. Alkynol natural products target ALDH2 in cancer cells by irreversible binding to the active site. *Chem. Commun.* **2015,** *51*, 15784-15787.

(37) Nickel, S.; Serwa, R. A.; Kaschani, F.; Ninck, S.; Zweerink, S.; Tate, E. W.; Kaiser, M. Chemoproteomic Evaluation of the Polyacetylene Callyspongynic Acid. *Chem. Eur. J.* **2015,** *21*, 10721-10728.

(38) Harano, K.; Minami, K.; Noiri, E.; Okamoto, K.; Nakamura, E. Protein-coated nanocapsules via multilevel surface modification. Controlled preparation and microscopic analysis at nanometer resolution. *Chem. Commun.* **2013,** *49*, 3525-3527.

(39) Kovalerchik, D.; Zovko, A.; Haag, P.; Sierakowiak, A.; Viktorsson, K.; Lewensohn, R.; Ilan, M.; Carmeli, S. Cytotoxic Alkylynols of the Sponge Cribrochalina vasculum: Structure, Synthetic Analogs and SAR Studies. *Ma.r Drugs* **2022**, *20*, 265.

(40) Lee, K. N.; Lee, J. W.; Ngai, M. Y. Synthesis of Trifluoromethoxylated (Hetero)Arenes via OCF_3 Migration. *Synlett* **2016,** *27*, 313-319.

(41) Satoh, Y.; Satoh, M.; Isobe, K.; Mohri, K.; Yoshida, Y.; Fujimoto, Y. Studies on Panax acetylenes: Absolute structure of a new Panax acetylene, and inhibitory effects of related acetylenes on the growth of L-1210 cells. *Chem. Pharm. Bull.* **2007,** *55*, 561-564.

(42) Chou, T. C.; Dong, H. J.; Zhang, X. G.; Lei, X. G.; Hartung, J.; Zhang, Y. D.; Lee, J. H.; Wilson, R. M.; Danishefsky, S. J. Multifaceted cytoprotection by synthetic polyacetylenes inspired by the ginseng-derived natural product, panaxytriol. *Proc. Natl. Acad. Sci. USA* **2011,** *108*, 14336-14341.

(43) Horiguchi, Y.; Araki, M.; Motojima, K., 17 beta-Hydroxysteroid dehydrogenase type 13 is a liver-specific lipid droplet-associated protein. *Biochem. Bioph. Res. Commun.* **2008,** *370*, 235-238.

(44) Thamm, S.; Willwacher, M. K.; Aspnes, G. E.; Bretschneider, T.; Brown, N. F.; Buschbom-Helmke, S.; Veser, T.; Gargano, E. M.; Grabowski, D.; Hoenke, C.; Matera, D.; Mueck, K.; Peters, S.; Reindl, S.; Riether, D.; Schmid, M.; Tautermann, C. S.; Teitelbaum, A. M.; Trunkle, C.; Winter, M.; Fox, T.; Wortmann, L. Discovery of a Novel Potent and Selective HSD17B13 Inhibitor, BI-3231, a Well-Characterized Chemical Probe Available for Open Science. *J. Med. Chem.* **2023**, *66*, 2832-2850

(45) Horiguchi, Y.; Araki, M.; Motojima, K. Identification and characterization of the ER/lipid droplet-targeting sequence in 17 beta-hydroxysteroid dehydrogenase type 11. *Arch. Biochem. Biophys.* **2008,** *479*, 121-130.

(46) Szegezdi, E.; Logue, S. E.; Gorman, A. M.; Samali, A. Mediators of endoplasmic reticulum stress-induced apoptosis. *Embo. Rep.* **2006,** *7*, 880-885.

(47) Preissler, S.; Ron, D. Early Events in the Endoplasmic Reticulum Unfolded Protein Response. *CSH Perspect. Biol.* **2019,** 11: a033894.

(48) Menendez-Benito, V.; Verhoef, L. G. G. C.; Masucci, M. G.; Dantuma, N. P. Endoplasmic reticulum stress compromises the ubiquitin-proteasome system. *Hum. Mol. Genet.* **2005,** *14*, 2787-2799.

(49) Manasanch, E. E.; Orlowski, R. Z. Proteasome inhibitors in cancer therapy. *Nat. Rev. Clin. Oncol.* **2017,** *14*, 417-433.

(50) Dantuma, N. P.; Lindsten, K.; Glas, R.; Jellne, M.; Masucci, M. G. Short-lived green fluorescent proteins for quantifying ubiquitin/proteasome-dependent proteolysis in living cells. *Nat. Biotechnol.* **2000,** *18*, 538-543.

(51) Lukacik, P., Bunkoczi, G., Kavanagh, K., Ng, S., von Delft, F., Bray, J., Edwards, A., Arrowsmith, C., Sundstrom, M., Oppermann, U. Structural Genomics Consortium (SGC), Crystal structure of human 17-beta-hydroxysteroid dehydrogenase type XI. Released: 2004-12-28 (https://www.rcsb.org/structure/1YB1).

(52) Jumper, J.; Evans, R.; Pritzel, A.; Green, T.; Figurnov, M.; Ronneberger, O.; Tunyasuvunakool, K.; Bates, R.; Zidek, A.; Potapenko, A.; Bridgland, A.; Meyer, C.; Kohl, S. A. A.; Ballard, A. J.; Cowie, A.; Romera-Paredes, B.; Nikolov, S.; Jain, R.; Adler, J.; Back, T.; Petersen, S.; Reiman, D.; Clancy, E.; Zielinski, M.; Steinegger, M.; Pacholska, M.; Berghammer, T.; Bodenstein, S.; Silver, D.; Vinyals, O.; Senior, A. W.; Kavukcuoglu, K.; Kohli, P.; Hassabis, D. Highly accurate protein structure prediction with AlphaFold. *Nature* **2021**, *596*, 583-589.

(53) Estradiol 17-beta-dehydrogenase 11 - AlphaFold structure prediction, last updated in AlphaFold DB version 2022-11-01 (https://alphafold.ebi.ac.uk/entry/Q8NBQ5).

(54) Mazza, C.; Breton, R.; Housset, D.; Fontecilla-Camps, J. C. Unusual Charge Stabilization of $NADP^+$ in 17ß-Hydroxysteroid Dehydrogenase. *J. Biol. Chem.* **1998**, *273*, 8145-8152.

(55) Chai, Z. L.; Brereton, P.; Suzuki, T.; Sasano, H.; Obeyesekere, V.; Escher, G.; Saffery, R.; Fuller, P.; Enriquez, C.; Krozowski, Z. 17 beta-hydroxysteroid dehydrogenase type XI localizes to human steroidogenic cells. *Endocrinology* **2003,** *144*, 2084-2091.

(56) Mazza, C., Breton, R., Housset, D., Fontecilla-Camps, J.-C. Human 17-beta-hydroxysteroid-dehydrogenase type 1 c-terminal deletion mutant complexed with estradiol and NADP+. PhD Thesis. (https://www.rcsb.org/structure/1A27).

(57) Abul-Husn, N. S.; Cheng, X.; Li, A. H.; Xin, Y.; Schurmann, C.; Stevis, P.; Liu, Y.; Kozlitina, J.; Stender, S.; Wood, G. C.; Stepanchick, A. N.; Still, M. D.; McCarthy, S.; O'Dushlaine, C.; Packer, J. S.; Balasubramanian, S.; Gosalia, N.; Esopi, D.; Kim, S. Y.; Mukherjee, S.; Lopez, A. E.; Fuller, E. D.; Penn, J.; Chu, X.; Luo, J. Z.; Mirshahi, U. L.; Carey, D. J.; Still, C. D.; Feldman, M. D.; Small, A.; Damrauer, S. M.; Rader, D. J.; Zambrowicz, B.; Olson, W.; Murphy, A. J.; Borecki, I. B.; Shuldiner, A. R.; Reid, J. G.; Overton, J. D.; Yancopoulos, G. D.; Hobbs, H. H.; Cohen, J. C.; Gottesman, O.; Teslovich, T. M.; Baras, A.; Mirshahi, T.; Gromada, J.; Dewey, F. E. A Protein-Truncating HSD17B13 Variant and Protection from Chronic Liver Disease. *New Engl. J. Med.* **2018,** *378*, 1096-1106.

(58) Liston, D. R.; Davis, M. Clinically Relevant Concentrations of Anticancer Drugs: A Guide for Nonclinical Studies. *Clin. Cancer Res.* **2017,** *23*, 3489-3498.

(59) Teicher, B. A.; Tomaszewski, J. E. Proteasome inhibitors Commentary. *Biochem. Pharmacol.* **2015,** *96*, 1-9.

(60) Saleh, M.; Baumgarten, M.; Mavrinskiy, A.; Schafer, T.; Mullen, K. Triphenylene-Based Polymers for Blue Polymeric Light Emitting Diodes. *Macromolecules* **2010,** *43*, 137-143.

(61) Sang Hun, J.; Hyunjin, K.; Min Ji, H.; Eun Bin, J.; Hui Jun, Y.; Dong Hoon, L.; Yun-Hi K.; Chan Eon P.; Yong-Jin Y.; Soon-Ki K.; Sang-Gyeong, L., Solution Processable Symmetric 4-Alkylethynylbenzene End-Capped Anthracene Derivatives. *Bull. Korean Chem. Soc.* **2012,** *33*, 541-548.

(62) Bromby, A. D.; Keller, S. N.; Bozek, K. J. A.; Williams, V. E.; Sutherland, T. C. Pi-Extended Ethynyl 21,23-Dithiaporphyrins: A Synthesis and Comparative Study of Electrochemical, Optical, and Self-Assembling Properties. *J. Org. Chem.* **2015,** *80*, 9401-9409.

(63) Dawood, K. M.; Hassaneen, H. M.; Abdelhadi, H. A.; Ahmed, M. S. M.; Mohamed, M. A. M. Synthesis of Unsymmetrical Aryl-Ethynylated Benzenes via Regiocontrolled Sonogashira Reaction of 1,3,5-Tribromobenzene. *J. Brazil Chem. Soc.* **2014,** *25*, 1688-1695.

(64) Chen, X. C.; Nishinaga, S.; Okuda, Y.; Zhao, J. J.; Xu, J.; Mori, H.; Nishihara, Y. A divergent synthesis of 3,10-dialkylpicenes. *Org. Chem. Front.* **2015,** *2*, 536-541.

(65) Partially described in the literature, see: Van Breemen, A. J. J. M.; Herwig, P. T.; Chlon, C. H. T.; Sweelssen, J.; Schoo, H. F. M.; Setayesh, S.; Hardeman, W. M.; Martin, C. A.; De Leeuw, D. M.; Valeton, J. J. P.; Bastiaansen, C. W. M.; Broer, D. J.; Popa-Merticaru, A. R.; Meskers, S. C. J. Large area liquid crystal monodomain field-effect transistors. *J. Am. Chem. Soc.* **2006,** *128*, 2336-2345.

(66) Baek, D. J.; MacRitchie, N.; Anthony, N. G.; Mackay, S. P.; Pyne, S.; Pyne, N. J.; Bittman, R. Structure-Activity Relationships

and Molecular Modeling of Sphingosine Kinase Inhibitors. *J. Med. Chem.* **2013,** *56*, 9310-9327.

(67) Milgrom, L. R.; Yahioglu, G. 5,10,15,20-Meso-Tetraarylethynylporphyrins. *Tetrahedron Lett.* **1995,** *36*, 9061-9064.

(68) Vichai, V.; Kirtikara, K. Sulforhodamine B colorimetric assay for cytotoxicity screening. *Nat. Protoc.* **2006,** *1*, 1112-1116.

(69) Rozie, A.; Santos, C.; Fabing, I.; Calsou, P.; Britton, S.; Génisson, Y.; Ballereau, S. Alkyne-Tagged Analogue of Jaspine B: New Tool for Identifying Jaspine B Mode of Action. *ChemBioChem* **2018,** *19*, 2438-2442.

(70) Dantuma, N. P.; Lindsten, K.; Glas, R.; Jellne, M.; Masucci, M. G. Short-lived green fluorescent proteins for quantifying ubiquitin/proteasome-dependent proteolysis in living cells. *Nat. Biotechnol.* **2000,** *18*, 538-43.

(71) Pettersen, E. F.; Goddard, T. D.; Huang, C. C.; Couch, G. S.; Greenblatt, D. M.; Meng, E. C.; Ferrin, T. E. J. UCSF Chimera - a visualization system for *exploratory* research and analysis. *J. Comput. Chem.* **2004**, *25*, 1605-1612.

(72) Berman, H. M.; Westbrook, J.; Feng, Z.; Gilliland, G.; Bhat, T. N.; Weissig, N.; Shindyalov, I.; Bourne, P. E. The Protein Data Bank. *Nucleic. Acids Res.* **2000**, *28*, 235-242.

(73) The UniProt Consortium. UniProt: the Universal Protein Knowledgebase in 2023. *Nucleic Acids Res.* **2023**, *51*(D1), D523-D531.

(74) Thomsen, R.; Christensen, M. H. J. MolDock: a new technique for high-accuracy molecular docking. *Med. Chem.* **2006**, *49*, 3315-3321.

Table of Contents Graphic